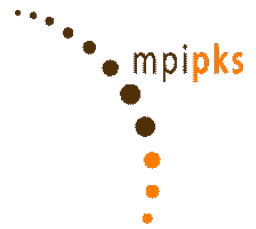# Hydrodynamics in solid state transport, from microscopic to mesoscopic scales

Dissertation

zur Erlangung des akademischen Grades
Doctor rerum naturalium (Dr. rer. nat.)
vorgelegt dem Bereich Mathematik und Naturwissenchaften
der Technischen Universität Dresden

von Piotr Witkowski, M. Sc.

geboren am 1 Februar 1991 in Gleiwitz, Polen

Contents

Acknowledgements

I would like to express my gratitude to two exceptional scientists who supervised me during the preparation of this work: Prof. Roderich Moessner and Dr. Piotr Surówka.

I am grateful to Piotr for many things: for giving me opportunity to join his group in MPI-PKS; for giving me numerous ideas and suggestions on possible research topics while, at the same time, leaving me the freedom to work on what I found the most interesting; for the patience and effort invested in our collaboration, results of which are presented here; and for his help in preparation of this thesis. Finally, and perhaps most importantly, Piotr – being himself a researcher with an enormously broad spectrum of interests – showed me that one can (and should!) focus on working with the problems that one finds interesting rather than on what is considered a fashionable topic at the moment.

Roderich I would especially like thank for accepting us, a group of scientists of high-energy physics origin, to his group and giving us not only the opportunity to work on the fascinating physics of condensed matter systems but also freedom in choosing the topics we research and the methods we apply to them. Roderich's helpful advice made it possible for me to cross the boundary between the fields of high energy and solid state physics, and also taught how to conduct research and present it. Finally, as the head of the condensed matter division he had a lot of understanding, which really helped me to go through the tougher periods of my stay, for which I am very grateful.

Since science is always a team effort, I would like to thank all the people with whom I had the pleasure to collaborate. Among them especially Francisco Peña-Benitez should be mentioned, discussions with whom made me understand the topics included here but also physics in general far better than I could ever do it on my own. Apart from being a great scientist, Fran was also an irreplaceable companion for discussions in the coffee breaks and during scientific trips. I believe I should also acknowledge him as an ambassador of the Italian coffee drinking tradition, thanks to whom I abandoned overly diluted americano in favor of the aromatic espresso.

I would also like to thank Carlos Hoyos for a very fruitful collaboration and hosting me in Oviedo; Nicolás Morales-Durán for the effort he invested in our common work when he visited the Institute as a summer student and Egor Kiselev for the most useful discussions that helped me understand many condensed matter-related aspects and gave me some of the ideas presented here. I sincerely hope that our previous cooperation was just the beginning. Special thanks I would like direct to Prof. Jörg Schmalian, for being always open for discussions and ideas as well as for inviting me for to visit his group. Also, I want to thank my former collaborators from Munich – Prof. Johanna Erdmenger and the members of her group: Mario, Ann-Kathrin, Max, Eugenio and Daniel.

Scientific activity is, however, much more than only direct collaborations – it is the interaction with other scientists, often from different fields, that allows us to identify new problems or find unusual solutions. In the course of my education I had the privilege to discuss with many great scientists: Pavel Alekseev, Nick Poovuttikul, Sergej Moroz, Kristan Jensen, Sebastián Mantilla Serrano, Jakub Jankowski, Pawel Moskal. Further, I would like to thank Paul McClarty, the coordinator of the IMPRS doctoral program in our Institute, for the great effort he invested in organizing countless seminars and scientific events that allowed me to come in contact with many interesting ideas and fascinating people. Finally, I would like to express my

CHAPTER 1

Introduction

Hydrodynamics is one of the oldest and most successful theories of physics. It was developed to describe very common phenomena – motion of fluids like water or air. Despite the fact that the mathematical nature of the theory remains obscure – the existence and smoothness of solutions of the governing equations are still not established [1] – the theory has shown remarkable flexibility and was successfully applied (with various modifications) to describe phenomena on all length scales considered in physics. The applicability of hydrodynamics thus ranges from modeling cosmological evolution [2, 3] and astronomical objects like accretion discs [4] to the description of events in nuclear and high energy physics [5–7], possibly even on the sub-femtometer scale [8]. Even on everyday scales, the use of hydrodynamics is not limited to describing traditional liquids – see for example recent advances in describing so-called active matter (like ensembles of microorganisms) [9].

Given this wide area of applications one may be puzzled: what makes hydrodynamics such a universal language to describe a wide variety of physical phenomena? To answer that question one may start with analyzing the physical origin of the Navier-Stokes equations. By construction, they mathematically encode the *conservation laws* of the system, which in that case are – known from classical mechanics – energy, momentum and particle number [10]. Following this way of thinking, hydrodynamics can be treated as an *effective theory* based on the conservation laws that the system of interest admits. Since the symmetries and the conservation laws that they encode are among the most important organizing principles of physics in the XXth century, it is not surprising that such theories can be directly applied to so many problems of different nature.

From the perspective of a condensed matter theorist it is now natural to ask a different question: if hydrodynamics is such a universal language, can it be used to treat solid state systems? The answer is of course yes. One example of such a treatment is the description of superfluid states [11] where Goldstone bosons of a broken global symmetry can be collectively described by an ideal hydrodynamics. Also, many-body interacting quantum systems were shown to obey hydrodynamic equations, exemplified by a cold-atomic system (unitary Fermi gas) [12]. Another example, maybe closer to the traditional understanding of condensed matter as a field dealing with the physics of crystalline matter, is the hydrodynamics of spin waves [13].

There is, however, yet another, broad class of situations in which the applicability of hydrodynamics can lead to interesting observable consequences for condensed matter systems – namely when it follows from the conservation of momentum. In that case the flow of charge carriers through a sample can be described by a set of Navier-Stokes equations of 'traditional' hydrodynamics (or their relativistic analogues). The first observation that this hydrodynamic behavior of electrons in a conductor may lead to counter-intuitive and very distinctive effects for transport was published by Gurzhi in his insightful papers [14, 15]. The general idea is that the hydrodynamic flow is more efficient in transporting charge through an elongated, 2-dimensional device than a non-interacting ballistic flow. Since the electron-electron interaction mean free path gets shorter with growing temperature, the observable effect is that the resistivity of such a device initially *decreases* with temperature. Of course, further increasing temperature amplifies effects like the breaking of momentum conservation, i.e electron-phonon collisions, that ultimately lead to the rise of resistivity. As a result, the thermal dependence of the resistivity

of an ultra-pure conducting sample should have a distinct minimum, marking the hydrodynamic transport regime. The first experimental confirmation of this so-called Gurzhi effect was achieved by de Jong and Molenkamp in a GaAs sample [16], around 30 years after the theoretical prediction. The reason why the hydrodynamic regime has been experimentally elusive for such a long time is the extremely high degree of purity of the sample that is needed for its unambiguous detection, which only became available in the 90s.

As technology advanced, more pure materials became available, and so the hydrodynamic regime was experimentally accessible in more systems. This motivated a recent growth of interest in electronic hydrodynamics, both from the theoretical and the experimental side. The theory predicted, among others, locally negative electric resistance[17], which was later observed in graphene [18], and strong modification of magneto-transport properties [19–23], which was also observed in graphene [24]. Apart from that, more detailed studies of the Ghurzhi effect allowed to conclude that the higher-than-ballistic conduction is a universal feature of the hydrodynamic transport, present not only in symmetric, elongated devices but also in constrictions [25]. Also this effect was already experimentally demonstrated [26]. The signatures of hydrodynamics have also been observed in thermal transport experiments where a breakdown of the Wiedemann-Franz law was measured [27].

The possibility of measuring new mesoscopic effects was an inspiration for the research presented the first part of this Thesis (see Chapter 4). It is devoted to the study of transport described by the non-relativistic Navier-Stokes equations that are valid for Fermi-liquid type of systems. The first question addressed concerns the AC response of the electronic fluid contained in an elongated narrow channel. The results are published in [28]. The key findings are: high frequency driving leads to the formation of a *boundary layer* at the edges of the sample, where the dissipation of energy takes place, and the presence of a *Drude-like peak* in the imaginary part of conductivity as a function of voltage frequency. Unlike the Drude model of conductivity, in the hydrodynamic regime the frequency-position of the peak depends not only on the microscopic parameters (viscosity) but also on the *physical dimension of the sample*, which is a clear manifestation of the mesoscopic nature of the hydrodynamic transport. The dependence of the peak position on the sample size could be used to determine the viscosity coefficient. The development of the boundary layer, on the other hand, was established to be responsible for a change in the scaling behavior of the absolute value of conductivity with the sample width: in the slow driving regime the scaling is quadratic, while for the boundary layer flow the conductance is almost independent of the channel width.

In condensed matter systems it is not unusual to work with systems in which discrete symmetries, i.e. time reversal symmetry and/or parity are broken. Such systems offer new interesting avenues to study the effects of discrete symmetry breaking on the hydrodynamic transport. In general, under these circumstances one may expect the so-called *odd transport* phenomena. The way in which 'odd' is understood means that the response is transverse to the applied source. The most basic example of such a transport phenomenon is the well known Hall effect in a magnetic field. One of the most striking features of the odd transport is that it may be dissipation-less, as in the case of Hall effect. In the quantum regime, odd transport can have further, non-trivial properties: for example, the Hall effect gets quantized in either integer or fractional fashion [29, 30]. The physics of the Hall conductivity is exceedingly rich and involves various fields: from classical electro-magnetism to strongly interacting quantum systems. There is, however, much more to the odd transport than just single conductivity. Another odd transport coefficient appearing in most of hydrodynamic theories is the *Hall viscosity*, which can be thought of as an analogue of the Hall conductivity for the shear stress. It can also be present in classical fluids as well as quantum systems [19, 31, 32]. Recently, it has also been shown that the presence of the Hall viscosity for an electronic fluid can strongly influence the charge transport in the hydrodynamic regime [24, 33, 34].

This was the general motivation for the studies presented in Chapters 5 and 6 and published in [35] – the second group of original results contributing to this thesis. The concrete aim is to understand odd transport properties of an example of a *strongly interacting* quantum system subject to an external magnetic field by using a string-theory inspired method: the *holographic duality (AdS/CFT)*. This method was previously successfully applied to study properties of the strongly coupled quantum systems, like the famous computation of the viscosity of the quark gluon plasma [36, 37] or the analysis of physics near quantum critical points [38–40]. In the model under consideration it is shown that the Hall viscosity is generated by coupling the electromagnetic field to matter in a non-minimal, parity-breaking way. It also turns out that the states with non-zero Hall viscosity are characterized by the presence of a non-zero charge density proportional to the value of the magnetic field even *at zero chemical potential*. The analysis indicates that the presented model is much more likely to capture the universal behavior of the Hall viscosity than the one of the Hall conductivity. The key premise for that statement is the fact, that the expression for the Hall viscosity can be derived exactly for any values of thermodynamic parameters and symmetry-breaking coupling constants, while there is no similar description of the Hall conductivity, which can only be obtained perturbatively in the couplings. Another interesting observation is that the hydrodynamic description is valid even for magnetic fields that are large compared to the temperature – which lies outside of the traditionally understood hydrodynamic regime. However, the origin of this robustness of hydrodynamics is not yet well understood. Finally, no obvious mechanism of quantization of the Hall viscosity (nor other odd transport coefficients) is found. Further studies are needed to determine whether this is a general feature of the interacting system or some particularity of the studied model that obstructs such quantization.

This work is organized as follows: the second Chapter introduces the modern approach to hydrodynamics as an effective theory – a treatment that will be (sometimes implicitly) applied throughout the text. Next, Chapter 3 discusses the idea of using the hydrodynamic theory to describe phenomena in solid state physics and presents an overview of the current state of this field. Following that three chapters provide the core of this thesis and contain the original results: Chapter 4 focuses on an analysis of mesoscopic hydrodynamic effects in charge transport in Fermi liquids while Chapters 5 and 6 are dedicated to the odd transport. First, Chapter 6 presents analysis of hydrodynamics in the absence of parity and time reversal invariance induced by an external magnetic field and then, Chapter 6 presents a holographic computation of the transport coefficients for a strongly coupled system. The technical details of the (somehow involved) computations of Chapter 6 are presented in a series of Appendices.

The results presented in Chapters 5 and 6 are independent of the content of Chapter 4, so that part of the Thesis can be safely skipped by the Readers only interested in the odd transport phenomena.

CHAPTER 2

Hydrodynamics – a universal theory of transport

The aim of this chapter is to introduce hydrodynamics on a technical level. There are many approaches to introducing it but here the most effective and universal one will be adopted – basing on an effective theory approach [41]. The main advantages of this approach are general applicability and independence from microscopic details of the system. Because of these features hydrodynamics can be used to describe multiple phenomena on starkly different length scales – from collisions of galaxies to collisions of nuclei in particle physics experiments. The next section is devoted to that effective theory approach to hydrodynamics.

Notational remark. In the text the following conventions were used: small Latin indices like a, i, j will be used as *spatial* indices – either in non-relativistic description or as spatial parts of relativistic objects. Small Greek indices μ, ν ... will denote *relativistic* space-time objects. Time-like dimension is always $\mu = 0$. Einstein summation convention is always used – the repeated indices, like T_i^i denote sum. The Greek indices are raised and lowered with the use of Minkowski metric of the form

$$g_{\mu\nu} = \mathrm{diag}(-1, 1, 1).$$

For the non-relativistic objects with Latin indices the Cartesian metric δ_{ij} is used. Capital Latin letters will be introduced as indices in Chapter 5 to describe higher-dimensional space of holographic duality. Also, partial derivatives with respect to space-time variables will be in the text denoted by ∇ symbol, even when the space-time is flat. On the contrary, partial derivatives in different context (i.e. in the thermodynamic relations) will be denoted with ∂. With this notations one can obtain curved space-time equations from the relativistic ones by simply using a covariant derivative whenever ∇ is used.

1. Hydrodynamics as a theory of conserved quantities

To understand the versatility of hydrodynamics it is useful to summarize how such a theory is constructed from first principles. There are two basic ingredients necessary for this construction: notions of *conserved quantities* and *local equilibrium*.

Usually, conserved quantities can be inferred from the symmetries of the system. According to the Nöther theorem, symmetries imply existence of conserved currents $\mathcal{J}^\mu$, fulfilling equations of the following form

$$(2.1) \qquad \nabla_\mu \mathcal{J}^\mu = 0.$$

If the symmetry group has multiple generators, more conservation laws can be written. An important example of such situation is the translational symmetry of the theory in space and time generated by a space-time vector β^μ

$$(2.2) \qquad \tilde{x}^\nu = x^\nu + \beta^\nu.$$

The associated conserved quantity is the *stress energy tensor* $T^{\mu\nu}$

$$(2.3) \qquad \nabla_\mu T^{\mu\nu} = 0.$$

The set above describes independent conservation of each spatial momentum density (equations $\nabla_\mu T^{\mu i} = 0$) and energy density ($\nabla_\mu T^{\mu 0} = 0$). As the set of generators of symmetry transformations forms a relativistic vector β^μ, the set of conserved currents is described by a symmetric

rank 2 tensor. For a general symmetry this may not be the case, and conservation equations assume the following form

$$(2.4) \qquad\qquad\qquad \nabla_\mu \mathcal{J}^\mu_\Pi = 0$$

where Π is some index enumerating the conserved quantities – it does not need to have specific transformation properties under space-time transformations.

The set of conservation equations (2.4) will ultimately serve as an equation of motion for the system. It's important to stress that although the Nöther theorem dictates an explicit form of the conserved currents $\mathcal{J}^\mu_\Pi$ in terms of the microscopic variables, this form will be unimportant in the hydrodynamic construction; indeed the crucial point of hydrodynamics is expressing the conserved quantity in terms of the *effective degrees of freedom*.

But what are the effective degrees of freedom? The systematic way of obtaining those is based on the notion of *local equilibrium*, which generalizes the well-known thermodynamic equilibrium. One of the greatest achievements of XIXth century physics was to reduce the description of a complex system to a small set of macroscopic parameters describing the state of the system – the state parameters like pressure, temperature or density.

Upon constructing the hydrodynamic description of a given system, the first step is to identify what parameters describe its equilibrium state. These parameters will be then promoted to local fields – and these fields will be the effective degrees of freedom in the hydrodynamic theory. For a reason that will become clear later, in the context of hydrodynamics these effective degrees of freedom are sometimes called *slow variables*.

Typical examples of slow variables are the thermodynamic parameters of state: pressure p, temperature T or chemical potential μ. It also worth stressing here that velocity v^μ can also be thought of as a parameter of state for the system – the reason being that the presence of matter allows one to identify a special reference frame, namely the *rest-frame* of the system. Then describing the equilibrium state in a coordinate co-variant way requires giving a relation between observer's frame and the rest-frame of the system – which is nothing but a velocity vector.

There is a very important assumption being done in the procedure of identifying slow variables with 'localized' equilibrium parameters – namely that there is a (fast) mechanism ensuring that the system thermalizes. Such a mechanism is provided by an interaction that is compatible with the conservation laws. Fast means that the interactions in the system are frequent enough to ensure that the local thermalization happens much faster than the phenomena that will be studied in the hydrodynamic theory. If one takes the classical system described by hydrodynamics – e.g. a container with water, that means that inter-particle collisions are much more frequent than frequency of any force acting on a fluid. It also means that non-interacting theories cannot be described by hydrodynamics, while strongly interacting ones are in principle well described. This general statement will later manifest itself in a concrete example of dependence of the fluid viscosity on the strength of interactions.

Hydrodynamics can also be used to describe systems in which the there exists some mechanism dissipating the conserved quantities, provided that this non-conservation is weak. By weak it means that the characteristic timescale of dissipation (for example, scattering time of momentum-relaxing scattering) is much longer than the timescale describing the process responsible for the local equilibration (for example an inter-particle momentum-conserving interaction). In general, if there are multiple interaction mechanisms in the system, the criterion for the validity of the hydrodynamic description is that the one that provides local thermalization must be the fastest.

Once the slow variables are chosen and the local equilibration is examined one may proceed with constructing the equation of the hydrodynamic theory. This is done by means of *gradient expansion*: the conserved quantities are expressed as functions of gradients of slow degrees of freedom. The order of derivatives organizes the expansion: the higher order of expansion, the

higher order of derivatives involved. In principle there is many terms that one can construct even at low order of derivative expansion. However, the symmetries of the system can be used again – now, to restrict the amount of possible terms by requiring that the obtained equations are covariant.

There is another subtlety in the hydrodynamic construction: some quantities do not have absolutely defined order in derivatives in which they should enter the description. This is usually the case with quantities that can play the role of *external forces* as well as *degrees of freedom* in the system. A good example is the electromagnetic force: on one hand it can be treated as an external parameter, influencing the thermodynamic equilibrium of the system, on the other – as a dynamical field coupled to charge current. Which approach should be taken depends on the physical situation that is to be described – two examples of these so-called *power counting schemes* will be presented in Chapters 3 and 5. It should be noted that using different power-counting schemes leads to different theories – describing distinct physical situations. So, the choice of the concrete scheme is dictated by the physics of the system under consideration.

Upon constructing the gradient expansion, the coefficients of different terms are some undetermined numbers called the *transport coefficients*. These are in general functions of microscopic quantities, like coupling constant of the interaction responsible for local thermalization, but can also depend on the state of the system via parameters like temperature or chemical potential. The equations expressing conserved quantities in terms of gradients of slow variables are called *constitutive relations* of the system.

The functional form of transport coefficients *cannot be inferred from hydrodynamics alone* – their computation requires knowledge of some microscopic description of the system. An example of such a computation is presented in Chapter 5. Indeed, one of the great advantages of hydrodynamics as an effective theory is that it reduces a complicated structure of the microscopic theory to a small set of transport coefficients. The price for that simplification is, however, the need of introducing free parameters whose values remain undetermined.

One may ask: why should physical quantities be expanded in gradients of fields in the first place? The answer gets clearer when the expansion is presented in Fourier space. Let's take as an example some conserved current $\mathcal{J}^\mu$ expanded in terms of velocity u^ν and it's gradients

$$(2.5) \qquad \mathcal{J}^\mu = A^\mu_\nu u^\nu + B^{\mu\nu}_\rho \nabla_\nu u^\rho + ...$$

where A, B are some, general transport coefficients. The Fourier expansion is then

$$(2.6) \qquad \tilde{\mathcal{J}}^\mu = A^\mu_\nu \tilde{u}^\nu + i B^{\mu\nu}_\rho k_\nu \tilde{u}^\rho + ...$$

The gradient expansion turns into a power expansion in terms of the Fourier momentum k. So, the 0-th order describes the uniform equilibrium, the 1-st order is the slowest-varying correction to the equilibrium and so on – the order of the gradient expansion controls how "fast changing" perturbations to the equilibrium are taken into account.

There is one subtlety connected to the gradient expansion: from a microscopic perspective only the 0th order (in gradients) thermodynamic quantities are well defined, while all the higher terms are somehow arbitrary [42–44]. From a mathematical perspective one can say that truncating the gradient expansion at some order introduces an extra 'symmetry' of the system: a redefinition of a slow degree of freedom by a term containing derivatives will only modify the conservation equations *in higher orders in derivatives*. So, upon truncating to the original order in derivatives one gets *the same* set of equations for the *modified variable*.

For example, if the equilibrium is described by the temperature T, chemical potential μ and velocity u^μ, at first order in derivatives one can make the following re-definition of the temperature

$$(2.7) \qquad \tilde{T} = T + K u^\nu \nabla_\nu \mu,$$

with K being an arbitrary constant. Then, the definition of the conserved current $\mathcal{J}^\mu$ will also be changed

$$\tilde{\mathcal{J}}^\mu = \mathcal{J}^\mu + (K u^\nu \nabla_\nu \mu) \partial_T \mathcal{J} \tag{2.8}$$

and the conservation equation for the modified current reads

$$\nabla_\mu \tilde{\mathcal{J}}^\mu = \nabla_\mu \mathcal{J}^\mu + \nabla_\mu (K u^\nu \nabla_\nu \mu) \partial_T \mathcal{J}. \tag{2.9}$$

Upon truncating the equations to the 1st order in derivatives one gets

$$\nabla_\mu \tilde{\mathcal{J}}^\mu = \nabla_\mu \mathcal{J}^\mu \tag{2.10}$$

so the redefinition (2.7) is a symmetry of the equations of motion.

To fix this extra redefinition freedom one must demand some condition to hold to all orders in the gradient expansion – a procedure that goes by the name of the *frame choice*. Some popular frame conditions are *the Landau frame* [10]

$$u_\nu \mathcal{J}^\nu = -n, \tag{2.11}$$

$$u_\nu T^{\nu\mu} = -\epsilon u^\mu, \tag{2.12}$$

or another frame, sometimes referred to as 'historic' [42]

$$\mathcal{J}^\mu = n u^\mu. \tag{2.13}$$

A natural question arising is the one of the convergence of the gradient expansion. On one hand it can be naively expected that including higher order terms allows the hydrodynamic theory to describe more realistic situations by taking shorter-wavelength physics into account. On the other hand – it is well known that many expansions used in physics (like perturbative series in quantum theory) are not convergent in a traditional mathematical way. In last ten years there has been a lot of progress on the issue of the convergence of hydrodynamics. It is now understood that although the expansion is not convergent in a 'power series' sense there exist methods to re-sum the hydrodynamic series. Reference [43] provides an excellent overview of that matter. The recent and very important results on these re-summation procedures were published in the following references [45, 46]. In particular the latter of the two provides a very interesting insight that the gradient expansion is indeed convergent but only if some conditions on the choice of effective degrees of freedom are obeyed.

Apart from the issue of convergence, the gradient expansion has yet another problematic feature: additional derivatives included in higher orders terms may in principle change the mathematical character of the equations by increasing the number of the boundary conditions needed to form a mathematically well-posed differential equations problem. In particular, the standard initial value problem may get ill-posed at some order of the gradient expansion.

Indeed, it turns out that even constructing a second-order relativistic hydrodynamics is a non-trivial task, as the equations obtained directly from the above-presented procedure violate the *relativistic causality* and allow superluminal propagation of modes. This issue can be resolved by using a proper regularization procedure [43]. Luckily, the problematic nature of relativistic hydrodynamics will not manifest itself in the computations presented in this Thesis, so a deeper discussion of these issues is omitted here.

2. A basic example – diffusion

To summarize the presented construction of a hydrodynamic theory let us analyze a theory of a single scalar conserved quantity. This quantity could be for example concentration of some chemical in water. Let us take a non-relativistic set-up. The first ingredient is the conservation equation

$$\nabla_t \rho = \nabla_i J^i \tag{2.14}$$

with ρ being the scalar quantity and J^i – the current describing the transport of this density. Having only this single quantity it is enough to have a single, scalar state parameter, the chemical potential μ. Let's assume that local equilibration is assured somehow, for example by inter-particle interactions between the chemical and water particles. Then, the constitutive relations to first order in derivatives are

$$(2.15) \qquad \rho(t, x) = C_1 \mu(t, x) + \mathcal{O}(\nabla^2),$$

$$(2.16) \qquad J_i(t, x) = D_1 \nabla_i \mu(t, x) + \mathcal{O}(\nabla^2).$$

The first relation at zero-th order can be thought of as a consequence of the fact that the density and the chemical potential are thermodynamically conjugated variables. There is also no 1-st order in derivatives term as there is no way of constructing a scalar object from the spatial gradient of a scalar. For the same reason there is no 0th order term in the second equation for the current. Now (2.15, 2.16) can be inserted into (2.14) to yield

$$(2.17) \qquad C_1 \nabla_t \mu(t, x) = D_1 \nabla^i \nabla_i \mu(t, x)$$

which is a diffusion equation for the chemical potential. Using the first constitutive relation (2.15) one can cast it in a traditional form for the density

$$(2.18) \qquad \nabla_t \rho(t, x) = D \nabla^i \nabla_i \rho(t, x)$$

with $D = D_1 / C_1$ the diffusion constant. It is worth underlining that in this construction the microscopic arguments were not used at all – all that was needed to obtain this equation is the symmetry of the system and a conservation law.

3. Ideal relativistic hydrodynamics

The previous example showed the construction of the simplest hydrodynamic theory – diffusion of a conserved charge. To make contact with more traditional understanding of hydrodynamics it is instructive to present another simple example – a theory of conserved momentum, energy and particle number.

The conservation equations in that case read

$$(2.19) \qquad \nabla_\mu T^{\mu\nu} = 0,$$

with $T^{\mu\nu}$ – the stress-energy tensor and

$$(2.20) \qquad \nabla_\mu J^\mu = 0.$$

The former equation encodes the conservation of energy and momentum, while the latter – the number of particles.

The equilibrium state is described by the *pressure p, energy density ε*, the *chemical potential μ* and the rest-frame velocity u^ν.

For that equilibrium system in a rest-frame the following holds

$$(2.21a) \qquad T^{\mu\nu} = \begin{pmatrix} \varepsilon & 0 \\ 0 & p\delta^{ij} \end{pmatrix}.$$

$$(2.21b) \qquad J^\mu = (n, 0, 0, ...)$$

Above n denotes the density of particles. This, however, cannot be the desired constitutive relation, since it does not involve the velocity and does not have a Lorentz-covariant form. Knowing that in the rest-frame the velocity assumes a concrete form $u^\nu = (1, 0, 0, ...)$, the equation (2.21) can be re-written in the following way

$$(2.22) \qquad T^{\mu\nu} = (\varepsilon + p) u^\mu u^\nu + p\eta^{\mu\nu}, \ J^\mu = n u^\mu.$$

Above $\eta^{\mu\nu}$ is the inverse space-time metric. The expressions above has the right covariance properties, they are therefore the correct constitutive relations for the stress-energy tensor at lowest order in derivatives.

Now, the parameters ε, p, μ, u^ν can be promoted to local fields, and the following set of equations is obtained

$$(2.23) \qquad\qquad\qquad \nabla_\mu(\varepsilon + p)u^\mu u^\nu = -\nabla^\nu p,$$

$$(2.24) \qquad\qquad\qquad \nabla_\mu(nu^\mu) = 0.$$

This is a set of $d + 2$ differential equations for $d + 3$ variables: d independent components of velocity u^i (u^0 is fixed by the normalization condition $u_\nu u^\nu = -1$), ε, p and μ. Therefore this equations need to be supplemented by an *equation of state* of the system.

This equation can be inferred from the thermodynamic properties of the system. Since the local equilibration is one of the assumptions for the hydrodynamic construction, one can safely assume that in any small sub-volume of the system V the equations of thermodynamics hold.

The basic thermodynamical identity is the first law of thermodynamics that links the extensive thermodynamic quantities (E, S, V, N – energy, entropy, volume and the number of particles respectively)

$$(2.25) \qquad\qquad\qquad dE = TdS - pdV + \mu dN.$$

Defining densities as quotient of extensive quantity and volume

$$(2.26) \qquad\qquad\qquad \varepsilon = \frac{E}{V}, \; n = \frac{N}{V}, \; s = \frac{S}{V},$$

and assuming constant volume V, the first law (2.25) can be expressed in terms of these densities as

$$(2.27) \qquad\qquad\qquad d\varepsilon = Tds + \mu dn.$$

Then, inverting (2.26), one can express extensive parameters in (2.25) in terms of the corresponding densities and volume, i.e $E = V\varepsilon$. Now the first law for densities assumes form

$$(2.28) \quad 0 = d(\varepsilon V) - Td(sV) + pdV - \mu d(nV) = dV(\varepsilon - Ts + p - \mu n) + V(d\varepsilon - Tds - \mu dn).$$

Keep in mind that in the expression above, unlike in (2.27), the volume variations are taken into account. By the virtue of the product rule for derivatives, it consists of two parts: first one describes variation due to change of volume

$$dV(\varepsilon - Ts + p - \mu n)$$

and another, that is a variation in constant volume

$$V(d\varepsilon - Tds - \mu dn).$$

Since for a constant-volume variation equation equation (2.27) holds, the first part has to vanish independently, for any value of dV. As a result, the following important identity holds

$$(2.29) \qquad\qquad\qquad \varepsilon - Ts + p - \mu n = 0.$$

Taking a total derivative (in a fixed volume) of the equation above and using (2.27) one obtains

$$(2.30) \qquad\qquad\qquad dp = nd\mu + sdT$$

which has two important consequences: first, the equation of state may be written in a form $p = p(\mu, T)$ with temperature and chemical potential playing the role of parameters of state (also – slow degrees of freedom) and second, that entropy and the density of particles are nothing else but partial derivatives of pressure with respect to these parameters

$$(2.31) \qquad\qquad\qquad n = \partial_\mu p, \; s = \partial_T p.$$

Independent fields are now μ, T and u^i – in that way, the number of degrees of freedom is reduced and matches the number of equations in the system.

Using the thermodynamical identities derived above, one can show a very particular behavior of the entropy in first order of gradient expansion. Projecting equation (2.23) onto the velocity u^ν and using the normalization condition $u^2 = -1$ the following is obtained

$$(2.32) \qquad u^\mu \nabla_\mu \varepsilon + (\varepsilon + p) \nabla_\mu u^\mu = 0.$$

The derivative of energy can be expressed using the first law for densities (2.27)

$$(2.33) \qquad u^\xi \nabla_\xi \varepsilon = T u^\pi \nabla_\pi s + \mu u^\pi \nabla_\pi n$$

if the general variation d is replaced by the co-moving derivative $u^\mu \nabla_\mu$. Making use of this form and using chain-rule in projected equation (2.32) yields

$$(2.34) \qquad T \nabla_\mu (s u^\mu) + \mu \nabla_\mu (n u^\mu) + (\varepsilon + p - Ts - \mu n) \nabla_\mu u^\mu = 0.$$

In the equation above one can identify that one term is proportional to equation (2.29) and another – to the conservation equation (2.24). As a result one gets

$$(2.35) \qquad T \nabla_\mu (s u^\mu) = 0,$$

i.e. a conservation equation for the entropy current $s u^\mu$ defined in analogy with the particle number current $J^\mu = n u^\mu$.

This result means that entropy production is impossible in zeroth order hydrodynamics if the number of particles is conserved – hence the name *ideal fluid equation*. To go away from this idealized picture and include dissipation one needs to goto higher order in derivatives. This theory will be presented in the following chapter, when particular realization of hydrodynamics useful for describing condensed matter systems will be introduced.

4. Hydrodynamics from kinetic equation

Previous sections were devoted to the presentation of the 'effective theory' approach to hydrodynamics – one that abstracts from the microscopic phenomena. It is however also instructive to present in short an alternative approach – one based on the statistical mechanics. The two understandings of hydrodynamics are largely complimentary and allow one to gain understanding of the regions of applicability of the theory and the way that the theory breaks down.

If the system of interest consists of well defined particles (be they Galilean or relativistic) it can be described in terms of classical mechanics. The best known approaches to do that are Newtonian, Lagrangian and Hamiltonian equations of motion. There is however another, equivalent approach: the Liouville equation

$$(2.36) \qquad \partial_t f_{(N)} + \sum_{i=1}^N \frac{\partial H}{\partial p_i} \frac{\partial f_{(n)}}{\partial q_i} - \frac{\partial H}{\partial q_i} \frac{\partial f_{(n)}}{\partial p_i} = \partial_t f_{(n)} + \left\{ H, f_{(n)} \right\} = 0.$$

Above the bracket $\left\{ H, f_{(n)} \right\}$ (Poisson bracket) is a standard, shortened notation for the sum in the second term and H is the (classical) Hamiltonian.

In the Liouvillian description of a system consisting of N particles instead of looking at $d \times N$ equations for the same amount of functions describing positions of the particles (or $2d \times N$ – momenta and positions) one searches for a *distribution function* $f_n(t, q_1, p_1 ... q_n, p_n)$ that is a single, real function on $2dN + 1$ dimensional *phase space* of the system (time t, N canonical positions q_n and their conjugate momenta) This function has an interpretation of a *probability distribution* on the phase-space, telling a probability that the system can be found in a vicinity of any given point on the phase space.

If the particles do not interact, the distribution factorizes into a product of independent distributions

$$(2.37) \qquad f_{(n)} = f_1(t, q_1, x_1) f_2(t, q_2, x_2) ... f_n(t, q_n, x_n),$$

evolving according to single-particle equations of motion

$$\partial_t f_i + \{H_0, f_i\}, \tag{2.38}$$

with H_0 being the single-particle Hamiltonian. Now, one can imagine that if the particles are only weakly interacting, there should be an effective equation of motion in the form of the equation above plus some corrections.

Indeed, there is a procedure to derive an approximate equation for a *single particle distribution function* – a function on $2d + 1$ space describing probability of finding a particle at a given position and given values of momentum. That single particle distribution can be formally defined in terms of $f_{(n)}$ by integrating out all canonical coordinates but one pair:

$$f(t, q, p) = N \int dq_2 dp_2 ... dq_N dp_N. \tag{2.39}$$

The factor N is conventionally inserted to turn f into particle density with integral equal the number of particles $\int dp dq f = N$. The resulting equation has the following form

$$\partial_t f + \{H_0, f\} + \mathcal{C}[f, H_{int}] = 0. \tag{2.40}$$

This equation is called the *Boltzmann kinetic equation*. The term $\mathcal{C}[f, H_{int}]$ is called the *collision integral* and encodes the interactions between particles. Even though this equation is already far simpler than the original (2.36) as it only contains the single particle distribution f, it has still a rather complicated mathematical structure. The complication comes as the term $\mathcal{C}$ includes a convolution of f with so-called *particle scattering rate* yielding an integro-differential system that cannot, in general, be solved.

Even though the equation (2.40) cannot be solved exactly it is a basis for deriving the hydrodynamic equations from a different perspective. The idea is: if the microscopic theory encoded in H_{int} admits some conserved quantities, they must be preserved by collisions. That means that for a conserved quantity $A(p, q)$ one can write

$$\int dp A \mathcal{C}[f, H_{int}] = 0. \tag{2.41}$$

As a result, the following equation holds

$$\int dp A \partial_t f + \{H_0, f\} = 0 \tag{2.42}$$

To express this equation in a more familiar form, one must use a concrete Hamiltonian. To make contact with the previous section, relativistic particles will be treated. With that choice of Hamiltonian, the Boltzmann equation can be posed in a Lorentz-covariant form

$$p^\mu \nabla_\mu f + F^\mu \partial_{p^\mu} f + \mathcal{C}[f] = 0 \tag{2.43}$$

with F^μ – the relativistic force vector – defined by a derivative of the Hamiltonian with respect to position and p^μ being the relativistic momentum that now plays the role of a canonical momentum p. Also, let us take concrete examples of conserved quantities fulfilling (2.41): vector p^μ and tensor $p^\mu p^\nu$. For those one gets

$$\nabla_\mu \langle p^\mu f \rangle = 0, \tag{2.44}$$

$$\nabla_\mu \langle p^\mu p^\nu f \rangle + \langle F^\nu \rangle = 0. \tag{2.45}$$

The equations above have the form of conservation equations for averages, denoted here with the bracket notations

$$\langle A \rangle = \int d\chi(p^\mu) A(p^\mu, x^\mu), \tag{2.46}$$

where $d\chi(p^\mu)$ is a rather complicated, Lorentz-invariant integration measure (see [43] for the concrete definition). Now, one can identify the averages with conserved quantities: particle current and stress-energy

$$(2.47) \qquad \langle p^\mu f \rangle = J^\mu, \ \langle p^\mu p^\nu f \rangle = T^{\mu\nu}$$

and the equations above become just the conservation equations that are also the starting point for the hydrodynamic construction. However, now there is a microscopic definition of conserved quantities in terms of the distribution function f.

To get hydrodynamic equations in terms of velocity, temperature and chemical potential one must solve for the function f. This is impossible for the full equation (2.40), so some approximations must be taken.

One way to simplify the equation (2.40) is expanding it around some 'background' distribution $f^{(0)}$

$$(2.48) \qquad f = f^{(0)} + \delta f, \ \mathcal{C}[f^{(0)}, H_{int}] = 0,$$

the assumption here is that collision integral vanishes on $f^{(0)}$ which is the kinetic definition of an *equilibrium distribution*. Then, the simplest approximation to the collision integral, valid to linear order in δf is

$$(2.49) \qquad \mathcal{C}[f, H_{int}] \approx \frac{\delta f}{\tau}.$$

τ is called *relaxation time*, and for that reason the form above bares the name *relaxation time approximation*. Obviously, it describes how the rate at which the distribution f relaxes to an equilibrium distribution $f^{(0)}$. The Boltzmann equation in the relaxation time approximation is then

$$(2.50) \qquad p^\mu \nabla_\mu f + F^\mu \partial_{p^\mu} f + \frac{\delta f}{\tau} = 0$$

There is an important limit of the equation above, that is particularly simply tractable. If the relaxation time is sent to zero $\tau \to 0$, the equation (2.50) simplifies dramatically

$$(2.51) \qquad \lim_{\tau \to 0} \tau \left(p^\mu \nabla_\mu f + F^\mu \partial_{p^\mu} f \right) + \delta f = \delta f = 0.$$

Then the kinetic equation is solved even by the locally equilibrium distribution

$$f_{(0)} = f_{(0)}(T(x), \ \mu(x), \ u^\mu(x)), \ \delta f = 0.$$

The concrete, functional form of $f_{(0)}(T(x), \ \mu(x), \ u^\mu(x))$ depends on the type of particles under consideration and is either Maxwell, Bose or Fermi-Dirac distribution. Then equations (2.47) can be directly evaluated to yield precisely (2.22), which in terms of effective degrees of freedom again yield ideal fluid equations (2.23, 2.24). The thermodynamic identities that were used in the previous section hold in that case since $f_{(0)}$ is at every point a equilibrium distribution.

From the discussion above it follows clearly, that ideal hydrodynamics (2.23, 2.24) only holds if the system relaxes to thermodynamic equilibrium *infinitely fast*. It turns out, that keeping τ finite one can also derive hydrodynamic equations – including these terms is equivalent to adding first order hydrodynamic corrections.

The idea behind this first order computation is to parametrize both the equilibrium distribution $f^{(0)}$ and δf by local equilibrium parameters $T(x)$, $\mu(x)$, $u^\mu(x)$. Then one solves the Boltzmann equation (2.50) for δf. In the end demanding consistency of this solution with conservation equations (2.44, 2.45) yields hydrodynamic equations for $T(x)$, $\mu(x)$, $u^\mu(x)$ with *transport coefficients fixed in terms of the relaxation time τ*. This is a very involved computation that has been well described in the lecture notes [47] (for the non-relativistic case) and in the reference [48] (for the relativistic case).

The most serious limitation of the approach described above is that it requires the notion of (quasi)particles in the system. These need to obey some version of 'separable' dynamics, be

it classical as here or quantum. That means, that strongly coupled quantum theories are out of reach for this kinetic approach. This assumption was not at all needed in the previous derivation of hydrodynamics.

The main advantage of the kinetic approach, on the other hand, is that the procedure of obtaining hydrodynamic equations of motion gives also explicit prescription for computing the transport coefficients for the system. The fact that kinetic equation reduces to hydrodynamics in some limit allows one to study systems in which hydrodynamics is the description at some ranges of parameter space while it is not the case in the other. One example of such systems are gases, where at low densities inter-particle interactions are too weak to provide mechanism of local thermalization needed for hydrodynamics to work, while increasing density one pushes the system into the hydrodynamic regime. In particular this happens in electron gases – in that case the phenomenon of crossing from non-interacting to hydrodynamic regimes is called 'ballistic to viscous crossover'. It will be discussed in more detail in the next Chapter.

CHAPTER 3

Hydrodynamic transport in solid state physics

As presented in the previous chapter, hydrodynamics can be thought of as an effective theory based on conservation laws. This formulation abstracts from the original understanding of hydrodynamics as a theory of liquids, so nothing stands in the way to apply it to describe phenomena in solid state physics. The following chapter is meant to present the current state of knowledge on this topic. An excellent and much broader review of this field is the reference [49].

1. When could one expect hydrodynamic regime?

The idea that the transport in a crystal can be governed by collective, hydrodynamic movement of electrons is not new. Already in 1963 Gurzhi [14] had a brilliant insight that, in a clean enough semiconductor crystal, electric resistance should have a minimum as a function of the temperature. The reason for that was, in short, that an interaction-based, self-organized flow of the electrons can be more efficient in transporting charge than unorganized ballistic type movement. A sketch of this so-called Gurzhi effect is presented on Fig. 1.
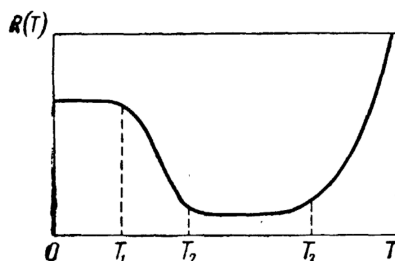
FIGURE 1. A sketch of the so-called Gurzhi effect, from the original paper [14]. The mechanism behind the observed minimum of resistance is the following: at low temperatures all the bulk interactions are negligible and the resistance comes only from scattering of charge carriers at the boundary of the sample. This non-interacting model of transport is sometimes called ballistic (or incoherent ballistic). At the temperature T_1, momentum-conserving interaction becomes frequent enough to dominate transport which leads to *decreasing* of resistance. This is what isunderstood as the hydrodynamic regime of transport where the resistance drops quadratically with the temperature. At the temperature T_2 momentum-relaxation by impurities starts to play a dominant role, yilding another plateau of resistance (the Ohmic regime) and at the temperature T_3 phonon-caused momentum relaxation starts to take over yielding a high-temperature resistance growth $R \sim T^5$.

Despite the idea being proposed in the '60, the experimental exploration of a regime where electronic transport is governed by electron-electron interactions was not possible until almost 30 years later, when Gurzhi effect was observed in 2d electron gases by the Molenkamp group [16]. Around 20 years later the same regime was predicted and observed in graphene [17, 18, 24, 27, 50].

The reason why it took so long to observe this hydrodynamic effects in solid state systems is the specific circumstances under which electrons behave as a fluid. In the view of the previous chapter, two conditions need to be examined: the conservation laws and the thermalization mechanism.

First let us analyze the conservation laws obeyed by the theory of electrons in a crystal. The most basic one is the *conservation of charge.* As electric charge is conserved in all the known processes this is also the most robust conserved quantity present irrespectively of the deformations applied to microscopic system. Another rather universally conserved quantity is the *energy* (implied by the time translation invariance).

The conservation of *momentum*, on the other hand, is a more subtle issue. In general for the momentum to be conserved the microscopic theory needs to be translationally invariant in space. This is of course not the case for a crystal. However, one can make use of the lattice periodicity to define a crystal (quasi)momentum. This quantity is also not always conserved: due to the periodicity of the lattice the state of a particle is described by the momenta lying in a compact subset of the momentum space – the Brillouin zone. The momenta outside of the Brillouin zone can be mapped to the inside. So, if a momentum-conserving scattering process occurs between two particles and the sum of their momenta goes out of the Brillouin zone, the total momentum must be mapped to a momentum on the inside of the zone, and as a result the the total momentum of the particles after collision is not an algebraic sum of their momenta before. This leads to an effective relaxation of momentum occurring when the average particle momentum is *large* compared to the size of the Brillouin zone – the so-called Umklapp process. So, in a periodic system, if the average (momentum) of the electrons is small, the scattering processes are (almost) momentum-conserving. In other words, at low temperatures there should be a notion of effectively conserved electronic momentum. However, the definition of the quasi-momentum relies on a periodicity of the crystal and so a presence of impurities or lattice defects will generically lead to the momentum relaxation. Another source of quasi-momentum relaxation is the scattering of charge carriers on phonons – the quanta of crystal lattice vibration. To sum up, one can say that momentum is a good conserved quantity in very pure crystals (with no defects nor impurities) and at temperatures low enough to make Umklapp processes and phonon scattering negligible. For the case of graphene a detailed discussion of momentum conservation can be found in Section 2 of [42] and references therein.

In the view of the previous chapter, one could say that some hydrodynamic behavior should be always present in the crystalline phase, due to the conservation of charge. As was shown in the example presented in the previous chapter, this leads to a diffusion-type behavior, that is a well-studied phenomenon. On the other hand, when the momentum is conserved, a set of hydrodynamic equations can be derived for this quantity. As it results in a starkly different transport physics, this is what will be further called *hydrodynamic regime*. In other words, the necessary conditions to observe this hydrodynamic regime is high purity of the system and low average energy of charge carriers.

The second crucial assumption for the use of hydrodynamics is the presence of the local equilibration mechanism. In the case of electronic systems such a mechanism is provided by an electron-electron interaction. So, another condition for the hydrodynamic regime is that momentum-conserving interactions are present and relatively strong.

To quantify the two conditions one can use the notions of characteristic length-scales describing interactions. These length-scales are the *mean free paths* (MFP) describing mean distance traveled by a particle before it encounters another particle and interacts with it. Denoting MFP of momentum-conserving interactions as l_{MC} and the shortest of momentum-relaxing ones as

l_{MR}[1] one can write the following condition for the validity of hydrodynamics

$$(3.1) \qquad\qquad l_{MC} << l_{MR}.$$

There is, however, one more relevant length-scale: the physical size of the device L. It is important, as interactions of the charge carriers with the boundaries of the sample can influence the transport significantly. Even if material is very clean and the simple condition above (3.1) holds, but the size of the device is the smallest length scale – the dominant process is carrier-boundary interaction, which leads to ballistic transport behavior. On the other hand, if L is much bigger than than both of the scales the signatures of hydrodynamic effects may be obscured by the presence of momentum relaxation. So, the ideal *hierarchy of scales* to observe hydrodynamic effects in solid state systems is [14, 17, 33, 42]

$$(3.2) \qquad\qquad l_{MC} \ll L < l_{MR}.$$

This equation makes it easier to understand why did it take so much time between the theoretical prediction of Gurzhi and the early experiments of Molenkamp: the reason is that the hydrodynamic regime is only accessible in relatively large samples of very pure materials. Such samples where not accessible until the 90s. One should however be aware that the condition above (3.2) is a bit sketchy in nature and will be discusses in a bit more detail in the section devoted to non-hydrodynamic transport.

2. The hydrodynamic equations for electronic fluid–graphene case

If the conditions discussed in the previous section are fulfilled, one can proceed to derive the equations of motion. To restrict the form of the equations, symmetries of a microscopic system must be taken into account. As this work is motivated by the recent theoretical and experimental works in graphene [17, 18] equations will be based on the symmetries of this microscopic system, which effectively consists of massless fermions [42], at least on the level of low-energy excitations. So, intuitively speaking the hydrodynamic description must be valid for a fluid that can have either positive or negative charge and moreover the fluctuations around charge-neutrality point can consist of both particles and antiparticles at the same time.

For that reason, the general hydrodynamic equations for graphene charge carriers must be relativistic in nature, however the characteristic velocity of the Lorentz group will be the Fermi velocity v_F rather than the speed of light c. As will be shown later, in Section 3, in some limits the relativistic invariance is broken to Galilean one and in turn the equations take a form of modified Navier-Stokes equations.

The starting point of the hydrodynamic construction is the same relativistic theory that was presented as an example in the previous chapter, section 3. Let's recapitulate on the thermodynamics of the system. Following [42] it is convenient to work with the chemical potential μ and temperature T as the parameters of state. Then the pressure p plays the role of the thermodynamic potential

$$(3.3) \qquad\qquad dp = nd\mu + sdT$$

with $n = \partial_\mu p$ – number and $s = \partial_T p$ entropy density respectively. On the dimensional grounds one can infer that the pressure takes a general form, valid in two spatial dimensions

$$(3.4) \qquad\qquad p(\mu, T) = \frac{(k_B T)^3}{(\hbar v_f)^2} \mathcal{F} \left(\frac{\mu}{k_B T} \right)$$

where k_B is the Boltzmann constant, $\hbar$ is the Planck constant and $\mathcal{F}$ is an arbitrary function fulfilling the thermodynamic conditions (i.e that entropy is positive). Taking the total derivative

---

[1]As was mentioned before, the rate of momentum relaxation due to Umklapp and phonon scattering are in general very temperature-dependent, so one can always hope to tune the system to the point where these are not dominant. In turn usually the crucial momentum-relaxation mechanism is the impurity scattering. In what follows the momentum relaxing length-scale will be identified with that impurity scattering process on default.

of the equation above and comparing coefficients, one can find similar expressions for $n(\mu, T)$ and $s(\mu, T)$. Then, using the familiar Gibbs-Duhem relation

$$(3.5) \qquad\qquad \epsilon + p = sT + \mu n$$

where ϵ stands for the energy density, one finds an important thermodynamic property of that system[2]

$$(3.6) \qquad\qquad \epsilon = 2p.$$

As before, the conserved quantities in the case of graphene are be *charge density* n, *energy* and *momentum*. Taking units such that $v_F = 1$ one can write these conservation equations in a compact form

$$(3.7a) \qquad\qquad \nabla_\nu J^\nu = 0,$$

$$(3.7b) \qquad\qquad \nabla_\nu T^{\nu\mu} = 0.$$

The local equilibrium parameters that will be the slow variables are *chemical potential* μ, *temperature* T and *velocity* u^μ. The latter is normalized to unity using Minkowski metric $g_{\mu\nu}$ $u^\mu u^\nu g_{\mu\nu} = u^\mu u_\mu = -1$. This condition can be used to express it in terms of the spatial velocity u^i

$$(3.8) \qquad\qquad u^\mu = \frac{1}{\sqrt{1 - |u|}}(1, u^i).$$

The *zeroth order gradient expansion* of the conserved quantities reads

$$(3.9) \qquad J^\mu = nu^\mu, \qquad\qquad T^{\mu\nu} = (\epsilon + p)u^\mu u^\nu + p\eta^{\mu\nu}.$$

The 0-th order coefficients are fixed by thermodynamics and on physical grounds [42], the same way as it was presented in the example in the previous chapter. Since at this order the equations of motion 'accidentally' conserve the entropy s (see (2.35) in the previous chapter) one needs to go to the next order in the gradient expansion.

In the second order of the gradient expansion, as was stated previously, one must take care of the frame redefinition freedom. Here it is convenient to use the Landau hydrodynamic frame (2.12). If one writes the 1st order gradient expansion schematically as

$$(3.10a) \qquad\qquad J^\mu = nu^\mu + J^\mu_{(1)},$$

$$(3.10b) \qquad\qquad T^{\mu\nu} = (\epsilon + p)u^\mu u^\nu + pg^{\mu\nu} + T^{\mu\nu}_{(1)}$$

the Landau frame conditions (2.12) are equivalent to

$$(3.11) \qquad\qquad u_\mu J^\mu_{(1)} = u_\mu T^{\mu\nu}_{(1)} \equiv 0.$$

Now, defining a projector $P^{\mu\nu}$ on the direction transverse to the velocity

$$(3.12) \qquad\qquad P^{\mu\nu} = g^{\mu\nu} + u^\mu u^\nu$$

one can write the first-order contributions

$$(3.13a) \qquad\qquad J^\mu_{(1)} = -\sigma_Q T P^{\mu\nu} \nabla_\nu \left(\frac{\mu}{T}\right),$$

$$(3.13b) \qquad\qquad T^{\mu\nu}_{(1)} = P^{\mu\rho} P^{\nu\sigma} \left[\eta(\nabla_\rho u_\sigma + \nabla_\sigma u_\rho - g_{\rho\sigma}\nabla_\kappa u^\kappa) + \zeta g_{\rho\sigma}\nabla_\kappa u^\kappa\right].$$

With this gradient expansion it is possible to define an entropy current s^μ which has a no-vanishing divergence $\nabla_\mu s^\mu \geq 0$ [42]. This will also pose some constraints on the transport coefficients from the formulas (3.13). The idea is again, to project the conservation equation for

---

[2]Analogous reasoning could be performed for systems with the same symmetries in different dimensions and only the numerical pre-factor of formula 3.6 would be changed.

stress-energy tensor onto the velocity direction. Repeating the computation from the example in the previous chapter and using properties of the Landau frame one gets the following identity

$$(3.14) \qquad \nabla_\mu(su^\mu) - \mu\nabla_\mu(nu^\mu) + T^{\mu\nu}_{(1)}\nabla_\mu u_\nu = 0.$$

This expression is more problematic than the example case. First, now the second term $\nabla_\mu(nu^\mu)$ is not proportional to any equation of motion. One can use the definition of current to re-write it

$$(3.15) \qquad \nabla_\mu(su^\mu) - \mu\nabla_\nu(J^\nu_{(1)}) + T^{\mu\nu}_{(1)}\nabla_\mu u_\nu = 0.$$

This is, however, still not satisfactory: since μ has arbitrary sign entropy defined by the 0-order current su^μ can decrease in the evolution. The only solution is to assume that the entropy current gets modified in the first order. To see how to do it, let us divide the equation by T and use chain-rule identity on the second term above

$$\frac{\mu}{T}\nabla_\nu(J^\nu_{(1)}) = \nabla_\nu\left(\frac{\mu}{T}J^\nu_{(1)}\right) - J^\nu_{(1)}\nabla_\nu\left(\frac{\mu}{T}\right).$$

With the help of that identity, equation (3.15) can be expressed as

$$(3.16) \qquad \nabla_\nu\left(su^\nu - \frac{\mu}{T}J^\nu_{(1)}\right) = -J^\nu_{(1)}\nabla_\nu - T^{\mu\nu}_{(1)}\nabla_\mu u_\nu.$$

Importance of the result above is that if all the transport coefficients from (3.13) are positive then a current s^ν defined as

$$(3.17) \qquad s^\nu = su^\nu - \frac{\mu}{T}J^\nu_{(1)}$$

has a positive divergence. This means that s^ν is a good 1st order definition of the entropy current that fulfills locally the Second Law of thermodynamics. It also poses the no-negativity constraint on the transport coefficients. Finally, it should be noted that in locally co-moving system of coordinates (in a local rest-frame of the fluid) the definition (3.17) coincides with the standard definition, yielding entropy density just s. It's easy to see that projecting (3.17) on u^μ – the first order term vanishes by the virtue of frame condition (2.12).

The final step to obtain effective theory of transport is to couple the conservation equations (3.7) to the electromagnetic field. In doing so, first one must modify the momentum conservation (3.7b) by adding an electromagnetic force term

$$(3.18) \qquad \nabla_\nu T^{\nu\mu} = F^{\mu\nu}J_\nu.$$

$F^{\mu\nu}$ is the electromagnetic field strength tensor. It turns out, that in order to define an entropy current in this case one must also modify the constitutive relation for the current

$$(3.19) \qquad J^\mu_{(1)} = -\sigma_Q T P^{\mu\nu}\nabla_\nu\left(\frac{\mu}{T} - \frac{1}{T}F_{\nu\rho}u^\rho\right).$$

This modification means that the way the electromagnetic field acts on a hydrodynamic current is formally identical to the way in which the gradient of chemical potential acts. This fact will be used later to define the total *electrochemical potential* in the following Chapter and argue that it is in fact this combined potential that is a relevant observable in electronic experiments.

The complete set of equations for electronic fluid can now be written

$$(3.20a) \qquad \nabla_\mu\left[nu^\mu - \sigma_Q T P^{\mu\nu}\nabla_\nu\left(\frac{\mu}{T} - \frac{1}{T}F_{\nu\rho}u^\rho\right)\right] = 0,$$

$$(3.20b) \qquad \nabla_\nu\left[(\epsilon+p)u^\mu u^\nu - pg^{\mu\nu} + P^{\mu\rho}P^{\nu\sigma}\left(\eta(2\nabla_{(\rho}u_{\sigma)} - g_{\rho\sigma}\nabla_\kappa u^\kappa) + \zeta g_{\rho\sigma}\nabla_\kappa u^\kappa\right)\right] = F^{\mu\nu}J_\nu.$$

In the set of equations above η, ζ and σ_Q are non-negative but otherwise arbitrary transport coefficients that must be determined from the microscopic theory.

Despite the presence of electromagnetic field in this equations the system of equations is valid on assumption that the equilibrium state is not influenced by the electromagnetic field.

This is equivalent to assumption, that the field strength $F_{\mu\nu}$ is first order in derivatives. This assumption can be backed by observation that

$$(3.21) \qquad F_{\mu\nu} = \nabla_\mu A_\nu - \nabla_\nu A_\mu$$

so, it is just taking the vector potential A to be the primary object. This may, however, not be compatible with some physical situations. For example, the presence of a strong magnetic field would break the time reversal symmetry and allow for more terms in the gradient expansion. Then, magnetic field should be treated as a zeroth order object, which enters the thermodynamic description of the system. This case will be treated in Chapter 5, where also transport coefficients will be computed from some model of microscopic theory. In the hydrodynamic jargon one calls the two scenarios *different power counting schemes*.

Although the equations above where derived having graphene in mind, they can be applied to other electronic systems, provided that the symmetries match and there is no extra degrees of freedom (like for example spin coupled to angular momentum). The equations themselves are quite general and valid for wide range of parameters – a virtue that comes at the price of great complication. First, the equations are non-linear so there is no hope of finding a closed-form solutions in most situations. Apart from that, the amount of degrees of freedom is relatively large and can obscure important physical consequences.

3. Fermi liquid limit

To simplify the discussion it is instructive to investigate some limits of a general system (3.20). The most natural one, that will be later basis of computations in the next chapter is the *Fermi liquid* limit

$$(3.22) \qquad \mu \gg k_B T.$$

In that limit the hydrodynamic description simplifies considerably. One strategy [42] to see this is to linearize the equations (3.20) around an equilibrium state

$$(3.23) \qquad \mu = \mu_0 + \delta\mu, \ u^i = \delta u^i, \ T = T_0 + \delta T, p = p_0 + \delta p$$

and then take a limit $T \to 0$. If one assumes that the spatial fluctuations of the chemical potential are small $\delta\mu/\mu_0 \ll 1$ and the flow is static, one gets the following set of equations

$$(3.24a) \qquad \nabla_i u^i = 0,$$

$$(3.24b) \qquad \nabla_i \delta p - \eta \nabla_j \nabla^j u_i = 0.$$

They are the same as non-relativistic, incompressible viscous flow equations [10], i.e. linearized version of the familiar, Galilean invariant hydrodynamics.

3.1. Electronic hydrodynamics from Galilean fluid equations. Another approach to obtaining the hydrodynamic description of the Fermi liquid is constructing the equations from first principles. A crucial observation here is that in the Fermi liquid limit (3.22) thermal effects must be suppressed, as this is formally equivalent to $T \to 0$ limit in which temperature drops from the description of equilibrium state. Since the chemical potential is large, charge fluctuations have a definite sign, so the theory does not need to incorporate particles and antiparticles at the same time. Also, the drift velocities are much less than the Fermi velocity v_f [51] – thanks to that, one can start the construction in a non-relativistic framework.

Then, the starting point equations are the non-relativistic Navier-Stokes equations [17, 52]

$$(3.25a) \qquad \nabla_t(n) + \nabla_i(nu^i) = 0,$$

$$(3.25b) \qquad m\nabla_t(nu^i) + m\nabla_j(nu^i u^j) = \nabla_j T^{ij}_{(1)}(\nabla_j u^i, \eta, ...) - \nabla^i p + F^i.$$

$T_{(1)}^{ij}$ is the first order stress tensor, which is a function of spatial gradients of velocity $\nabla_j u^i$ and first order transport coefficients and F^i denotes external forces applied to fluid.

The first assumption taken in the theory of Fermi liquids is incompressibility, understood as

$$(3.26) \qquad \nabla_t(n) + u^i \nabla_i(n) = 0.$$

This equation means that the density of the carriers is constant along the flow. Having this assumption, equation (3.25b) can be simplified, by dividing out the mass density nm. Now, assuming that $T_{(1)}^{ij}$ is linear in transport coefficients and that system is rotationally, parity and time-translation invariant one obtains that there is only one free coefficient involved

$$(3.27) \qquad T_{(1)}^{ij} = \nu(\nabla_i u^j + \nabla_j u^i), \ \nu = \frac{\eta}{mn}.$$

The coefficient ν is called the *kinematic viscosity*, and measured in the units $[length^2]/[time]$. Since the density of mass is divided out in its definition it can be used to compare viscosities of different fluids, as it intuitively measures the ratio of viscous force to mass of the fluid element.
[3]

Let us study the resulting system in some detail. The equations are non-linear

$$(3.28a) \qquad \nabla_i u^i = 0,$$

$$(3.28b) \qquad \nabla_t u^i + u^j \nabla_j u^i - \nu \nabla^j \nabla_j u^i = \frac{1}{mn}(-\nabla^i p + F^i).$$

There is only a single free parameter ν entering the equations. If this parameter is large enough, one can safely ignore the non-linear effects. To quantify the notion of 'big enough', equation must be expressed in a dimension-less manner. Then, when the fields and variables are non-dimensional, there will be a natural notion of magnitude: quantities may be larger, smaller or of order one. This makes the comparison between the coefficients meaningful.

To proceed with this *non-dimensionalization* one takes the following variable and field re-definitions:

$$(3.29) \qquad x^i = L x^{*i}, \ \nabla_i = L^{-1} \nabla^*_i, \ u^i = U u^{*i}, \ t = \frac{L}{U} t^*, \nabla_t = \frac{U}{L} \nabla^*_t$$

Here L is the length-scale (size of the system) and U is some characteristic velocity – for example average drift velocity in the electronic case. With those substitutions one can re-write (3.28b)

$$(3.30) \qquad \nabla^*_t u^{*i} + u^{*j} \nabla^*_j (u^{*i}) - \frac{1}{Re} \nabla^{*j} \nabla^*_j u^{*i} = -\nabla^{*i} p^* + F^{*i},$$

where Re traditionally denotes the *Reynolds number*

$$(3.31) \qquad Re = \frac{UL}{\nu}$$

and p^*, F^* are non-dimensional pressure and force, whose concrete forms are not important at this moment.

The non-dimensional equation (3.30) has two obvious limiting cases. When $Re \gg 1$, the non-linear terms dominate, yielding complicated theory of *turbulent flows*. When $Re \ll 1$ on the other hand, it reduces to a linear, 2nd order equation that comes under the name of the *creeping flow* or Stokes equation. In this regime, the viscous forces dominate over the inertia yielding (in the time-independent scenario)

$$(3.32) \qquad \nabla^{*j} \nabla^*_j u^{*i} - \nabla^{*i} p^* + F^{*i} = 0$$

which, upon re-introduction of dimensions already reminds (3.24).

---

[3]Despite the assumption of incompressibility, the pressure gradient will be kept separate in the equations. It should be noted that for an incompressible fluid the definition of pressure is somehow arbitrary and could be treated as a part of the general force term, see for example [53]. Indeed, as will be shown later for a Fermi liquid there is no physical distinction between the pressure, chemical potential and electrostatic potential.

The important question then is the magnitude of the kinematic viscosity for graphene. In the Fermi liquid regime, it is given by the following [17, 19, 31]

$$(3.33) \qquad \nu = \frac{1}{4}v_F l_{MC} \sim \frac{\mu^4}{T^2},$$

which, in the hydrodynamic regime, yields approximate numerical value of [18, 26, 27, 54]

$$(3.34) \qquad \nu \approx 0.1 m^2/s.$$

The typical drift velocity in graphene is of order [51]

$$(3.35) \qquad U \approx 10^2 m/s,$$

so for a micrometer-scale device $L \approx 10^{-6}m$ the Reynolds number is

$$(3.36) \qquad Re \approx 10^{-3} \ll 1.$$

As the value of the Reynolds number is much smaller than one, the non-linear terms can be safely ignored.

In fact, if the Reynolds number is so small, one can use the linearized equation even in the time-dependent case. So, the full system of flow equations applicable to Fermi liquid reads [17, 33, 51, 52] (again in dimension-full units)

$$(3.37a) \qquad \nabla_i u^i = 0,$$

$$(3.37b) \qquad \nabla_t u^i = \nu \nabla_j \nabla^j u^i + \frac{1}{nm}(F^i - \nabla^i p).$$

These time-dependent equations will be employed in the next chapter to study the AC response of graphene Fermi liquid.

Finally, it is worth mentioning that in this limit the pressure gradient $\nabla_i p$ is a function of the gradient of chemical potential $\nabla_i \mu$ only. The reason is the following: the general functional form of pressure is given by (3.4). Upon expanding the arbitrary function $\mathcal{F}$ and taking the Fermi liquid limit (3.22), one gets the following expression (restoring the dimension-full constants)

$$(3.38) \qquad p(\mu, T) = a\frac{\mu^3}{(\hbar v_f)^2}\left(1 + b\left(\frac{k_B T}{\mu}\right)^2 + ...\right)$$

where a, b are some expansion coefficients. Acting with a gradient operator on the formula above one gets that thermal gradients are suppressed by the factor of $\frac{k_B T}{\mu}$. Once again it is visible that the thermal effects decouple from the description. As a result, the pressure gradient and the gradient of the chemical potential are proportional one to another.

3.2. What is viscosity in hydrodynamics? As was shown previously, the equations describing the hydrodynamic flow of momentum are, in many cases, dominated by viscous force. It is therefore instructive to gain some intuition on viscous effects by analyzing the origin and effects of viscosity in the conceptually simple, non relativistic system (3.25).

Viscosity in hydrodynamics can be understood as a measure of internal friction in the fluid, i.e. friction between two neighboring layers of fluid that move in the same direction. The traditional way to define this friction is via forces acting on surfaces moving in fluid. This intuition is, however, not so useful in the microscopic context treated here.

Instead, a useful intuition can be obtained by examining the analogies between the Stokes equation (3.37b) and the diffusion equation, treated in chapter 2. Assuming momentarily constant density and absence of external forces one can write (3.37b) as

$$(3.39) \qquad \nabla_t p^i - nm\nu\nabla^j(\nabla_j u^i) = 0$$

with momentum $p^i = nmu^i$. Comparing with the charge diffusion equation which, for charge density ρ, reads

$$(3.40) \qquad \nabla_t \rho = D\nabla_i \nabla^i \rho,$$

one infers that the dynamic (shear) viscosity $nm\nu$ (denoted in most hydrodynamic textbooks with letters μ or η) plays the role of the *diffusion constant for momentum*.

On the other hand, the non-linear term of Navier-Stokes equation (3.25), $u^i\nabla_i u^j$, is responsible for the *parallel transport* of momentum through the flow. So, to sum up: the first zeroth order (ideal) hydrodynamics only describes streaming momentum along the flow while the first order, viscous terms supplement the transport of momentum with diffusive behavior. In our case the diffusive effects are far more important.

Finally, it should be mentioned that although the momentum diffusion (3.39) is governed by the dynamic viscosity $nm\nu$, in the main text usually the kinematic viscosity will be used. The reason why the kinematic viscosity is more useful as a quantity is because it appears in the equations involving velocity directly (3.25). Apart from that, the advantage of the kinematic viscosity ν is that by dividing out the mass one obtains quantity that can be directly compared between fluids of different density.

3.3. Weak momentum relaxation. The equations discussed so far completely neglected the residual microscopic momentum relaxation provided by the mechanisms mentioned in the first Section of this Chapter. It is instructive to incorporate those effects in the equations (3.37) in order to assure that the effects predicted by hydrodynamics could be observed in the real experimental situation.

The momentum-relaxation can be added by a modification of the momentum conservation equation (3.37b), and the full system takes the following form [17, 28, 42]

$$(3.41a) \qquad\qquad \nabla_i u^i = 0,$$

$$(3.41b) \qquad\qquad mn\nabla_t u^i - \nu\nabla_j\nabla^j u^i + \gamma u^i = -\nabla^i p + F^i.$$

The extra term γu^i can be understood intuitively as a force proportional to velocity. From the effective theory perspective it can be also understood as a lowest-order term breaking momentum conservation (as it introduces a preferred rest-frame in which $u^i = 0$). This term is also sometimes called 'Ohmic' as it represents momentum relaxation that is characteristic for standard conductors and introduces effects similar to ones described by the Drude model of electric conduction. It is worth mentioning that for large devices (that can break the assumption (3.2)) the physics described by the equation (3.41b) is the same as predicted by the Drude model, yielding DC conductivity that only depends on the momentum-relaxation coefficient γ [42]. This is an additional argument for the validity of the mentioned extension of hydrodynamics.

The presence of momentum relaxation influences not only the hydrodynamic equations, but also the transport coefficients. As was shown in [19], the kinematic viscosity in the presence of momentum-relaxing interactions is:

$$(3.42) \qquad\qquad \nu = \frac{1}{4}v_F^2\tau, \ \tau = (1/\tau_{MC} + 1/\tau_{MR})$$

where τ_{MC} and τ_{MR} are momentum-conserving and momentum-relaxing relaxation times respectively.

The final important consequence of adding the momentum-relaxing term manifests itself on the level of the full, non-linear system. The equations (3.20) modified by an addition of an analog momentum-relaxing term are much less prone to developing turbulent behavior than the ones with complete momentum conservation[42]. This provides and extra argument for using the linearized equations (3.41b) as the optimal ones to describe the transport in electronic systems.

3.4. Stream function method and Coulomb interaction. The form of equations (3.37a) and (3.41b) allows one more simplification, known in classical hydrodynamics as *the stream function method*. In the classical case of a two-dimensional incompressible flow, this stream function method allows one to reduce the number of independent variables and equations thus simplifying the system. In electronic hydrodynamics it has yet another advantage: it

simplifies the treatment of possibly complicated self interaction of charged electronic fluid.
In a typical situation, if the motion of charges is caused by applying the electric field, the system (3.41) consists of two equations: the Stokes equation in which the force terms are written explicitly

$$(3.43) \qquad \nabla_t u^i - \nu \Delta u^i + \gamma u^i = \frac{e}{m} \nabla^i \chi - \frac{1}{m} \nabla^i \delta\mu,$$

and the continuity equation

$$(3.44) \qquad \nabla_j u^j = 0.$$

The forces in the description above are of two-fold origin: χ is the electric potential and $\delta\mu$ is the local variation of the chemical potential giving rise to effective pressure [34]. m, e are the mass and electric charge of a carrier respectively. In principle, the electric potential above should be not only the external driving potential but also should contain, even at the linearized level, a self-consistent term stemming from variations of a local carrier density [55] that would make the equations non-local.
However, since the electric potential enters in the equations in a special way, this difficulty can be avoided.
. First, electric and chemical potentials are combined into so-called *electrochemical potential*

$$(3.45) \qquad \phi = \chi - \frac{1}{e} \delta\mu.$$

Real life experiments are usually sensitive to the electrochemical potential rather than electric voltage or chemical potential alone[34, 49]. Given equation (3.44), the system is incompressible. This incompressibility condition can be solved introducing a single scalar function describing the components of velocity

$$(3.46) \qquad u^i = \epsilon^{ij} \nabla_j \Psi.$$

Function Ψ is called the *stream function*. For a 2-dimensional, incompressible flow it encodes the same information as the original velocity field. From its definition follow two properties, that make the stream function a very convenient mathematical tool to analyze flow patterns.
First one is almost automatic to obtain from (3.46) since velocity u^i is orthogonal to the gradient $\nabla_i \Psi$ in 2 dimensions it must be proportional to a the vector tangent to a curve along which $\Psi = const$. So, plotting lines with the property $\Psi = const$ is equivalent to plotting the integral lines of u^i (in hydrodynamic context also called streamlines) – i.e. the trajectories of fluid elements. See figures 2, 3.
The other important consequence is the relation between a stream function and the total flux of velocity through a given surface – which in 2 dimensions is just a curve C. This flux H is defined by an integral

$$(3.47) \qquad H = \int_C u^i n_i dl.$$

n_i is the normal vector do the curve $n_i = \epsilon_{ij} \frac{dx^j(l)}{dl}$ and $x^i(l)$ is the parametrization of the curve. Now, using the definition of the stream function and the following identity for the contraction of ϵ symbols

$$\epsilon_{ij}\epsilon_{ik} = \delta_{jk},$$

one obtains

$$(3.48) \qquad H = \int_C \nabla_i \Psi \frac{dx^i(l)}{dl} dl = \int_C \frac{d}{dl} \Psi(x(l)) dl$$
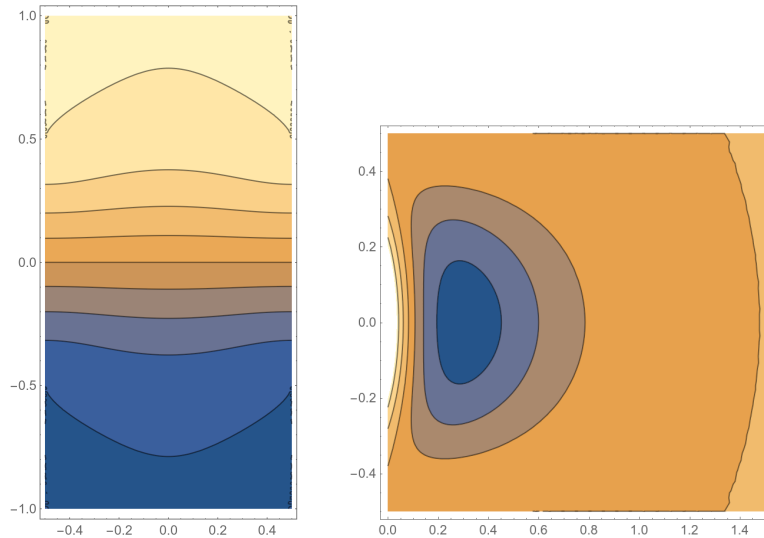
FIGURE 2. Two example stream function plots for flows on rectangular domains. Left: fluid is entering the domain through a part of the boundary on the left and exits on the right via symmetric part. The streamlines penetrate the cavities to some depth indicating that the motion of the fluid happens there. The value of stream function on top and bottom boundaries give the total flow of mass/charge through the sample. Right: flow inside of a cavity, forced by non-zero velocity at the boundary on the left. A close contour of the stream function indicates the presence of a fluid vortex – part of fluid is confined in family of closed trajectories.

which is just an integral of derivative of Ψ along curve. If the curve C connects two points A and B, the consequence is

$$(3.49) \qquad\qquad H = \Psi(B) - \Psi(A).$$

It is independent of curve C. If C is a closed curve, $A = B$, the flux vanishes – nothing less than the statement of incompressibility $\nabla_i u^i = 0$ once again. From a technical viewpoint knowing the values of the stream function of a flow on the boundaries of a device allows one to directly compute the charge flow through this device by simply taking the difference. It also helps to express the boundary conditions for velocity in terms of the stream function.

Having the intuition on what the stream function is, it is interesting to derive the equation governing its evolution. To do that one inserts the definition (3.46) into the Stokes equation forced by the electrochemical potential 3.45

$$(3.50) \qquad\qquad \nabla_t u^i - \nu \Delta u^i + \gamma u^i = \frac{e}{m} \nabla^i \phi.$$

and acts on the resulting equation with a antisymmetrized derivative operator

$$\nabla \times = \epsilon^{ij} \nabla_j,$$

contracting the free index with the vector index of equations. Using the following identities

$$(3.51) \qquad\qquad \epsilon^{ij} \nabla_j \epsilon_i{}^k \nabla_k f(x) = \nabla_j \nabla^j f(x), \ \ \epsilon^{ij} \nabla_j \nabla_i f(x) = 0,$$

valid for all smooth functions f, one arrives to the stream function equation

$$(3.52) \qquad\qquad (\partial_t + \gamma) \Delta \Psi - \nu \Delta^2 \Psi = 0.$$

The equation above is fourth order, but does not explicitly depend on the gradient terms (gradient of the electrochemical potential).
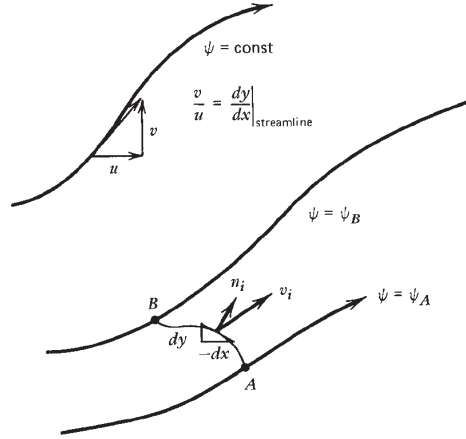
FIGURE 3. The properties of the stream function, picture adopted from [53]: 1)streamlines (lines, to which the velocity field is tangent) are the lines of constant value of Ψ, 2) the total flux of velocity through a curve connecting points A and B is equal to the difference $\Psi(B) - \Psi(A)$.

As a result, the observable potentials have to be computed *a posteriori* from the stream function solution. To do it one uses the Stokes equation (3.50) once more, solving it for $\nabla^i \phi$

$$(3.53) \qquad \nabla^i \phi = \frac{m}{e} \left(\partial_t \epsilon^{ij} \nabla_j \Psi - \nu \Delta \epsilon^{ij} \nabla_j \Psi + \gamma \epsilon^{ij} \nabla_j \Psi \right),$$

which can be done by simple integration as now Ψ is known. This method will be of great use in the following Chapter.

3.5. Boundary conditions for hydrodynamics. The final issue connected with the equations (3.25) is finding the correct boundary condition for the fields. The conditions for the velocity field u^i have to fix two separate quantities: the normal component of velocity $u^i n_i$ and it's tangent component $u_T^i = u^i - n^i(u^j n_j)$.

The conditions one needs to impose on the former are rather intuitive: it describes how fast are the elements of the fluid crossing the boundary of the sample. Therefore, in most cases it will hold

$$(3.54) \qquad u^i n_i |_{bdr} = 0.$$

One obvious exception of from this case is the part of boundary through which the fluid enters the domain and exits it – in case of an electronic device these are the electric contacts. There equation (3.54) needs to be modified

$$(3.55) \qquad u^i n_i |_{contact} = j_{el}$$

with j_{el} denoting the injected electric current density.

In terms of the stream function Ψ, the boundary conditions above (3.54, 3.55) read

$$(3.56) \qquad \Psi|_{bdr} = const, \ \Psi|_{contact} = \int j_{el} dl,$$

where integral is computed along the boundary on the part that is a contact. The fact that the stream function is constant on the boundary (except from source/sink regions) is compatible with the before-discussed properties of Ψ.

The conditions governing the behavior of the tangent component of velocity are a far more complicated issue. The most general boundary condition possible is

$$(3.57) \qquad u_T^i = \xi n^j \nabla_j u_T^i.$$

ξ is a numerical coefficient called the *slip length*. For classical systems a kinetic-theory-based estimation can be done [53] to get

$$(3.58) \qquad\qquad \xi \sim l_{MC},$$

i.e. the slip length is of order of the momentum-conserving mean free path of the particles. Of course, for macroscopic systems this effectively means that slip is negligible and one obtains the so-called *no-slip boundary condition*

$$(3.59) \qquad\qquad u_T^i = 0.$$

This is, however, not so simple for a microscopic system. First of all, the equation (3.58) is based on a classical kinetic theory, so may not be valid for ensembles of quantum particles. Secondly, even though l_{MC} must be much smaller than the size of the sample $l_{MC} << L$ in the hydrodynamic regime it may not be *negligibly small*, i.e. the effects of slip may be important for electronic transport. This will be discussed later in much greater detail – there is a section of the next chapter devoted to the issue of the boundary conditions.

For completeness, let us only state the version of the boundary condition (3.57) for the stream function. It is

$$(3.60) \qquad\qquad n^i \nabla_i \Psi\big|_{bdr} = \xi\, n^j\, \nabla_j n^i \nabla_i \Psi\big|_{bdr}$$

i.e. a relation between the first and second normal derivative of Ψ on the boundary.

4. Fermi vs. Dirac fluid

The Fermi liquid equations presented in the previous Section provide a simple framework to investigate the observable signatures of hydrodynamic transport. They are, however, only an approximation to the full system (3.20) – valid far away from the charge neutrality point. It is very interesting to compare the transport properties in this Fermi liquid regime with the situation at charge neutrality, as it turns out the observable phenomena are starkly different.

The first difference worth noting is the definition of the current. In the Fermi liquid regime the spatial current can be written in terms of velocity

$$(3.61) \qquad\qquad J_{FL}^i = -enu^i.$$

The analogue of that in full theory would be the 'historical' frame condition (2.13 of Chapter 2). At charge neutrality $n = 0$ such condition would render identically vanishing current which makes the equations ill-defined. This is also the reason why the Landau frame choice (2.12 in Chapter 2) is more convenient for a general theory. If one performs a mode analysis of the general theory (3.20), i.e a linearization around a background with given μ_0, T_0 it turns out that at neutrality $\mu_0 = 0$ charge fluctuations decouple from the hydrodynamic theory [42]. Then the hydrodynamic effects can only be seen in the heat transport sector. The thermal transport at charge neutrality shares some qualitative similarities with charge transport in Fermi liquids (i.e some mesoscopic effects that will be discussed in the following Chapter, see [56]) but is experimentally much more challenging to explore.

There is, however, much interest in the hydrodynamics of charge neutral graphene, and the reason is the following: in the Fermi liquid limit charge carrier state density is concentrated in a disc of radius given by the Fermi momentum p_F. This form of momentum distribution poses a strong constrain on the possible electron-electron scattering events, limiting the electronic interactions (this is also the classical stability argument for Fermi liquid [42, 57]). In turn, the Fermi liquid (be it in graphene or other system) consists always of relatively weakly interacting particles – which results in its high viscosity.

The charge neutral case on the other hand lacks these constrains on electron-electron interactions, which opens possibilities of observing strong coupling effects. Indeed, the Renormalization Group based studies of massless fermions in graphene show that the electron-electron interactions are significant [58–60] near to charge neutrality. It is generally known that strongly coupled

theories have much lower value of viscosity than weakly coupled ones [36], which also raises hopes of observing non-linear effects in this regime. The possibility of accessing the strong coupling effects near charge neutrality was a partial motivation for the studies described in Chapter 5.

5. Non hydrodynamic transport and Boltzmann kinetic equation

Finally, it is worth mentioning that the hydrodynamic equations can also be obtained as a limiting case of the Boltzmann kinetic equation. The kinetic theory, at least in classical, tractable formulation is a description, based on a single-particle weakly interacting picture. As mentioned in the introductory chapter, the kinetic equation allows to trace the viscous-to-ballistic crossover, thanks to it's validity in the weakly interacting regime. Such studies were performed in the literature [26, 42], showing for example that the hydrodynamic regime allows more efficient charge transport than the ballistic one (see Fig 4). It also allows one to trace the limits of validity of the hydrodynamic approach by studying the lifetime of hydrodynamic and non-hydrodynamic modes, and the imprint of momentum relaxation on the hydrodynamic conservation equations [61, 62]. The kinetic approach is also very useful in studying magneto-
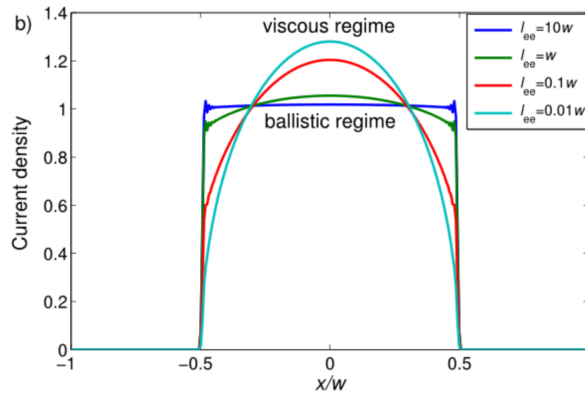
FIGURE 4. Profiles of current flow through a constriction, computed in a kinetic theory model. The parabolic, hydrodynamic flow transports charge more efficiently than the flat ballistic profile. Figure from [26].

transport across the ballistic-to-hydrodynamic crossover[33, 63]. The studies indicate that the hydrodynamic transport behaves much smoother as a function of magnetic field (Fig.5). However the price to pay for this greater generality of kinetic equations is the complication of that description. As the equations of motion in the kinetic formalism are of integro-differential nature, obtaining a solution is always challenging, especially on finite domains. So, if the validity of the hydrodynamic approach is not an issue the hydrodynamic equations offer much simpler way to extract the physical information about the transport phenomena. This is the approach that will be taken in general in this work.
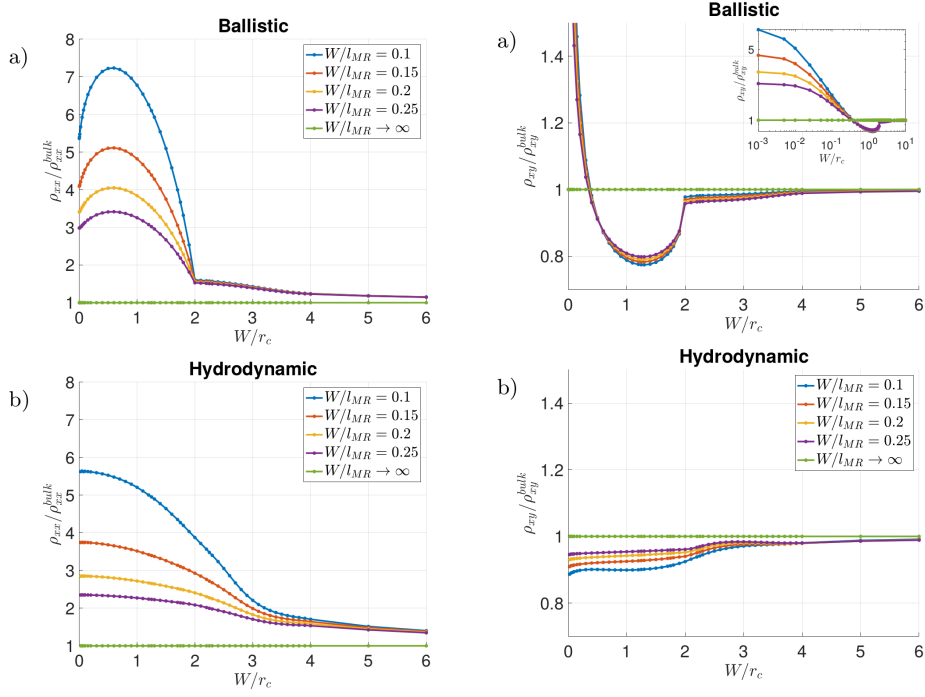
FIGURE 5. Magnetoesistance (left) and Hall resistance (right) as a function of magnetic field expressed (expressed as ratio between the sample size and the cyclotron radius). It can be clearly seen, that in the ballistic regime a sharp crossover happens, when the size of magnetic orbits is less than the size of the sample. Once the interactions start to dominate, this point is not marked by any specific behavior anymore. Image taken from [33]

CHAPTER 4

Mesoscopic phenomena in viscous electronics

This chapter is devoted to study of mesoscopic phenomena in the hydrodynamic electronic transport. Here a 'mesoscopic' effect is understood as one related directly to the shape of the material sample in a qualitative (phenomena present in some samples and absent in others) or quantitative way. Some of the most notable early examples of these where: the locally negative resistance [17, 51] and the negative magneto-resistance [19]. Especially the first of those, presented schematically on Fig. 1, clearly shows how the interaction-organized flow of charge carriers can lead to counter-intuitive results in transport measurements. This type of effects were motivations for the studies presented in the following chapter.
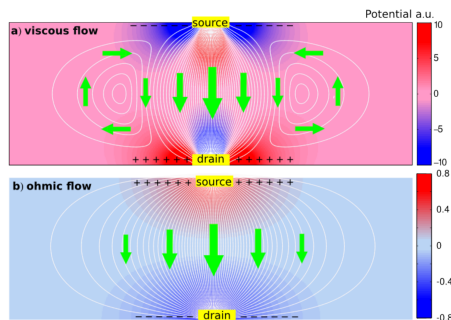
FIGURE 1. Negative local resistance in hydrodynamic flow (top) arises from current eddies. The electrons trapped in such a vortex can locally travel in the opposite direction to the globally applied current – a phenomenon absent in the Ohmic regime dominated by bulk momentum relaxation (bottom). Figure adapted from [17]

The first example is a very simple set-up: elongated, 2-dimensional channel (length much bigger than width) with time-dependent external voltage. This is in spirit a hydrodynamical analog of the Drude model of conductivity.

1. AC driving

Section based on [28]

The mesoscopic effects presented before are spectacular displays of hydrodynamic behavior in an electronic system, but present significant challenges from an experimental point of view. There is a major, technical issue in performing quantitative measurements in such set-ups: varying the physical size of the sample is a complicated procedure, likely to pollute the material (especially in case if ion beam etching) or even physically destroy the system due to multiple cycles of cooling down and heating to room temperatures. The overall complication of such procedure makes it also much harder to collect larger amount of data. One way of circumventing these issues is considering a set-up in which an additional, continuously variable parameter influences the behavior of the fluid. One example of such parameter can be magnetic field, which was investigated in [33]; another, which also belongs to the standard measurements for solid state

systems – is a time dependent electric field, where the extra parameter is the frequency of the applied electric field ω.

The latter set-up is a offers very good perspectives. First of all, as was already mentioned, AC conductivity has been intensively studied in the context of condensed matter, so it is natural to ask how it differs between hydrodynamic regime and the traditionally observed Ohmic transport. It should be also mentioned that, since the Ohmic effects can be easily incorporated in the hydrodynamic description (see Chapter 3), this set-up allows one to study the transition between hydrodynamic and Ohmic transport quite easily. Apart from that, the experimental protocol of such measurement is well-known, so confronting the theoretical computations with measured data should not pose too many problems. Finally, following the intuition of the Drude model, in an AC experiment one can hope to extract an effective momentum-relaxation time scale that should give a direct access to the microscopic property of the fluid – i.e the viscosity. It is therefore instructive to analyze the simplest possible model of such AC measurement.

The starting point for this analysis is the set of equations (3.41) from the previous Chapter. To describe a flow in an elongated, narrow channel the following Ansatze are employed:

$$(4.1) \qquad u^y = u(t, x), \ u^x = 0, \ F^y = -en|E|e^{i\omega t}, \ F^x = 0 \ ,$$

where y is the direction perpendicular and x parallel to the channel, n and $|E|$ stand for density and the intensity of the electric field respectively. Due to the assumptions on the velocity vector, the continuity equation is automatically fulfilled.[1] Mind that charge and mass densities are assumed to be proportional to the particle density n. Finally, a non-hydrodynamic, Ohmic dissipative term is included with coefficient γ. Then the set of equations reduces to a single one

$$(4.2) \qquad \nabla_t u - \nu \nabla_x^2 u + \gamma u = -en|E|e^{i\omega t}.$$

It's convenient to non-dimensionalize. Mind however, that unlike in the example of the previous chapter, there is a well defined time-scale in the problem at hand: the force frequency. For that purpose the following variables are employed

$$(4.3) \qquad u = L\omega u^*, \ t\omega = \tau, \ x/L = \chi \ ,$$

yielding dimensionless velocity u^*, relative width χ, and time τ (measured in radians). No additional 'velocity scale' is needed for the procedure. Using the substitutions above, equation (4.2) becomes

$$(4.4) \qquad \nabla_\tau u^* - \frac{1}{\Omega}\nabla_\chi^2 u^* + \Gamma u^* = \Phi e^{i\tau}$$

with

$$(4.5) \qquad \Phi = \frac{-en|E|}{mn\omega^2 L}, \qquad \Omega = \frac{L^2\omega}{\nu}, \qquad \Gamma = \gamma/\omega.$$

The first parameter encodes the forcing scale, the second is related to the Reynolds number in this set-up while the latter encodes the Ohmic friction coefficient. To simplify the analysis frequency dependence is expressed only in terms of the dimensionless ratio Ω. This introduces new dimensionless parameters

$$(4.6) \qquad \Psi = \Phi\Omega^2 = \frac{-enEL^3}{mn\nu^2}, \qquad \Sigma = \Gamma\Omega = \frac{L^2\gamma}{\nu}.$$

The velocity function depends on the spatial coordinate and time. Now the system can be solved analytically, and a general solution (for static initial condition $u(\tau = 0)$) assumes form of an infinite series. However, the interesting 'late-time', periodic part can be extracted in a closed form by the use of the following substitution:

$$(4.7) \qquad u^* = \exp(i\tau)\mathcal{U}(\chi).$$

---

[1]Also, given this Ansatz, the non-linear terms of equations (3.25) vanish, which further suppresses the possibility of encountering the non-linear effects in this set-up.

The above Ansatz gives the following solution to Eq.(4.4):

$$(4.8) \qquad u^* = e^{i\tau} \frac{\Psi}{\Omega(i\Omega + \Sigma)} \left(1 - \frac{\cosh(\sqrt{i\Omega + \Sigma}\chi)}{\cosh(\sqrt{i\Omega + \Sigma}/2)} \right).$$

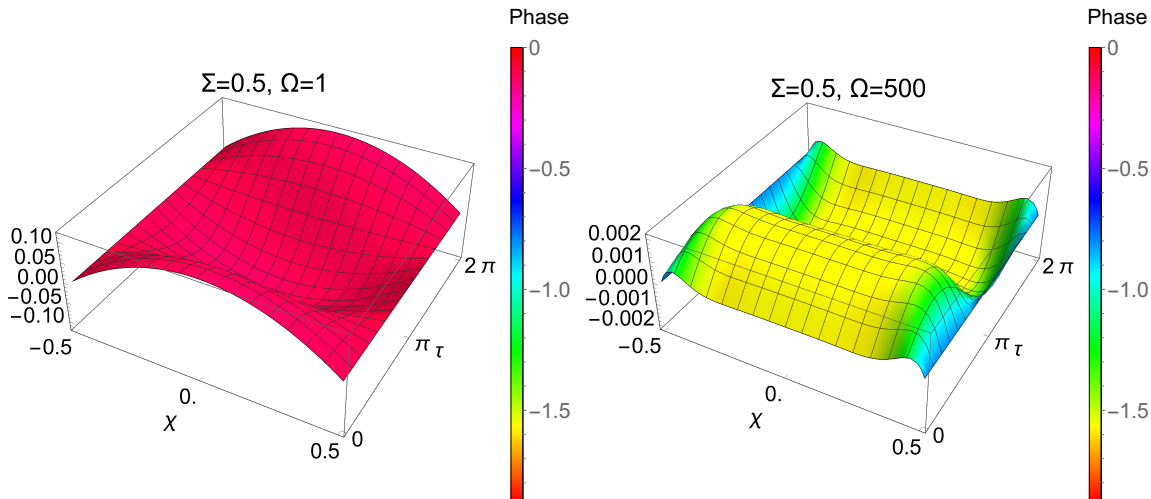The physical (dimensional) velocity u can be recovered from the solution using the following

FIGURE 2. Spatiotemporal flow profiles $u^*(\chi, \tau)$ (z-axis) for different driving frequencies. The color represents the phase difference between the driving and the fluid velocity.

substitution $u = \frac{\nu}{L}\Omega u^*$.

The first interesting feature of this solution is its asymptotic behavior for small and large frequencies. For the former, the velocity profile retains the same phase as the field that drives it, while the amplitude is parabolic as in the steady case. However, for large frequencies, the fluid ceases to be in phase with the rapidly oscillating force. In this case the solution acquires Stokes boundary-layer behavior. The fluid in the middle oscillates uniformly, and with an 'inductive' phase relation to the drive, while close to the boundary it is dominated by viscous effects. The velocity amplitude is plotted in Fig. 2. For slow forcing, the maximal velocity is reached in the middle of channel. Fast forcing induces the maximal velocity some distance from the channel center; the phase shift is visible, with the flow turning first near the boundaries and only then in the middle. The phase shift is also spatially dependent in the fast driving limit, reaching almost $\pi/2$ in the middle of the channel, which means that the flow in the bulk of the sample is reactive and energy is not deposited there. Te phase shift rapidly decreases (albeit not to zero) towards the boundaries of the sample and that is where the dissipation takes place.

This transition between 'parabolic' and 'boundary layer' type of flow is strictly connected with the nature of the viscous force originating from microscopic inter-particle interactions and exemplifies how momentum relaxation occurs in the viscous regime. One can build the following intuition on the emergence of the boundary layer: viscous force, which arises from a gradient in the velocity field, is only able to transport signal at some finite rate. If the forcing is slow enough, the speed of viscous signal suffices to slow down the fluid elements inside of the channel gradually, therefore building a parabolic profile with almost constant gradient. As the forcing gets faster, the regime that can be efficiently influenced by the viscous force gets smaller, and at some point is smaller than a half of the channel width. At that moment the flow can be divided into two parts: one, near to the boundaries, in which the viscous force influences the motion of fluid elements and another, in the bulk of the channel, where the influence of the viscous force

does not reach. As the forcing becomes faster, the region influenced by the viscous force – the boundary layer – shrinks.

This provides important insight in the nature of viscous dissipation: the total momentum of the electronic fluid is lost due to interaction between the fluid and the boundary of the sample – the viscous force can produce interesting effects only if the velocity is somehow restricted in some region. If the boundary condition allowed for a finite *slip velocity* at the boundary the effect of viscous flows would be obscured. Therefore the issue of correct boundary conditions for an electronic flow is crucial – it will be discussed in a greater detail later in this Chapter. Other examples on the finite 'range' of viscous effects were presented in a static situation in [49].

1.1. Conductance. The charge current k is constructed from the velocity in the following way $k = -enu$ and it reads

$$(4.9) \qquad k = \frac{-en\nu}{L} \Re \left[e^{i\tau} \frac{\Psi}{i\Omega + \Sigma} \left(1 - \frac{\cosh(\sqrt{i\Omega + \Sigma}\chi)}{\cosh(\sqrt{i\Omega + \Sigma}/2)} \right) \right]$$

$$\equiv \frac{-en\nu}{L} \Psi \Re \left[e^{i\tau} j(\chi, \Omega, \Sigma) \right] .$$

This is a local expression. Conductance is encoded in its integral over the sample width

$$(4.10) \qquad \sigma = C \left[\frac{1}{\Sigma + i\Omega} - \frac{2 \tanh\left(\frac{1}{2}\sqrt{\Sigma + i\Omega} \right)}{(\Sigma + i\Omega)^{3/2}} \right] ,$$

with $C = \frac{e^2 nL^2}{m\nu}$, a dimensional constant. In order to identify the effect of driving on conductance, given the above solution, we have two possibilities: There are two interesting scenarios which one can imagine for such a mesoscopic transport experiment 1) fix the driving frequency ω and measure the conductivity for different sample sizes L, 2) vary the driving frequency at fixed sample size. These two experimental protocols yield different results and reveal different properties of the system that are described below.

1.1.1. *Scaling with the channel width.* As all the dimensionless parameters (Ω, Σ, Ψ) are functions of width L, changing this value also can induce transition between two flow profiles form Fig. 2. It can also be understood in the following way: the thickness of the boundary layer only depends on viscosity and forcing frequency. If the channel is narrow, comparable with width of the boundary layer for given frequency, the flow will have 'quasistatic', parabolic shape. If the same forcing frequency is used in much wider channel, it will drive a boundary layer type of flow with a distinct velocity plateau in the middle. To quantitatively describe this behavior, it is instructive to perform the following rescaling procedure. First, conductance for some width L^* and fixed ω is defined as a reference. Then width is rescaled $L = \beta L^*$. The dimensionless parameters (4.10) have the following scaling with β:

$$(4.11) \qquad \Omega = \beta^2 \Omega^*, \ \Sigma = \beta^2 \Sigma^*, \ C = \beta^2 C^* ,$$

whence the conductance

$$(4.12) \qquad \sigma = C^* \left[\frac{1}{\Sigma^* + i\Omega^*} - \frac{2 \tanh\left(\frac{\beta}{2}\sqrt{\Sigma^* + i\Omega^*} \right)}{\beta(\Sigma^* + i\Omega^*)^{3/2}} \right] .$$

Above the asterisks denote reference values of parameters.

The behavior of conductance is plotted for several parameter values in Fig. 3. On a logarithmic scale a clear crossover is visible: initially the absolute value of conductance scales quadratically with β to later saturate. The crossover occurs at the point when the boundary layers develop in the flow profile. Note that Ohmic friction does not have a significant impact on the quantitative behavior.
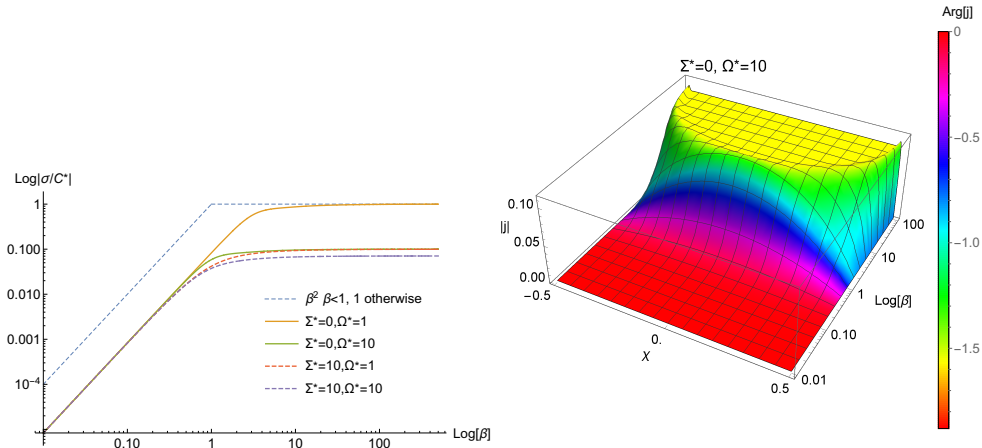
FIGURE 3. Top: Scaling of the optical conductance for various values of the reference parameters Σ^*, Ω^*. C^* is set to 1. For β smaller than the annular crossover value the scaling is $\sigma \sim \beta^2$. Bottom: local conductivity j as a function of the width scaling β. The cross-over to annular flow happens approximately for the same value as the scaling change of the total conductance.

1.1.2. *Frequency dependence and floating Drude peak.* Analysis of the frequency dependence of conductance is much more straightforward, as whole frequency dependence of (4.10) comes by it's Ω dependence. It is therefore enough to analyze the Ω dependence of our result. This analysis is presented on Fig. 4. As can be seen on the left panel, the shape of the curve in log-normal coordinates resembles the well known Drude form, with imaginary part having a visible maximum at some frequency (the so-called Drude peak). However, in the standard Drude model the position of the peak depends only on the microscopic relaxation time, whereas here the peak occurs at constant value of $\Omega \approx 9.89$, which means that in the hydrodynamic regime a *mesoscopic* viscous relaxation time τ_{visc}

$$(4.13) \qquad \tau_{visc} \approx \frac{L^2}{9.89\nu}$$

is encoded in the Drude peak. Interestingly, this relaxation time depends on L, which means that it's position will depend on the size of the sample. Another interesting observation is that viscous Drude peak survives the addition of the Ohmic dissipation as a single maximum. This happens despite Ohmic term providing a competing relaxation time (that is responsible for classical Drude peak). Also in that case where momentum relaxation is broken, a single peak is observed and it's location depends on both Ohmic coefficient γ and width L.
The scaling behavior of conductance for large $\omega >> \tau_{visc}$ is $\sigma \sim \omega^{-1}$, much like in standard Drude model.

1.2. Experimental implications. Pulsating flows have been experimentally investigated for three-dimensional ducts. In these experiments the local velocity measurements identified the boundary layers in the flow [64], to which at high-frequency the effects of viscosity are confined. The presented analysis suggests a very simple experimental set-up for the purpose of electronic hydrodynamics, which consists of a longitudinal sample of e.g. monolayer graphene positioned between voltage probes. On top of that we require an external drive. Our considerations are based on experiments in graphene or delafossites, in which the current technology allows to reach sample sizes around 0.01 of the electron mean free path, for $L \approx 10^{-6}m$. In the case of delafosite metals this can be achieved from flux-grown single crystals by focused ion beam etching [54]. Bilayer graphene devices are prepared crystals of hexagonal boron nitride using lithography and subsequent etching processes [18]. The estimates for kinematic viscosity are
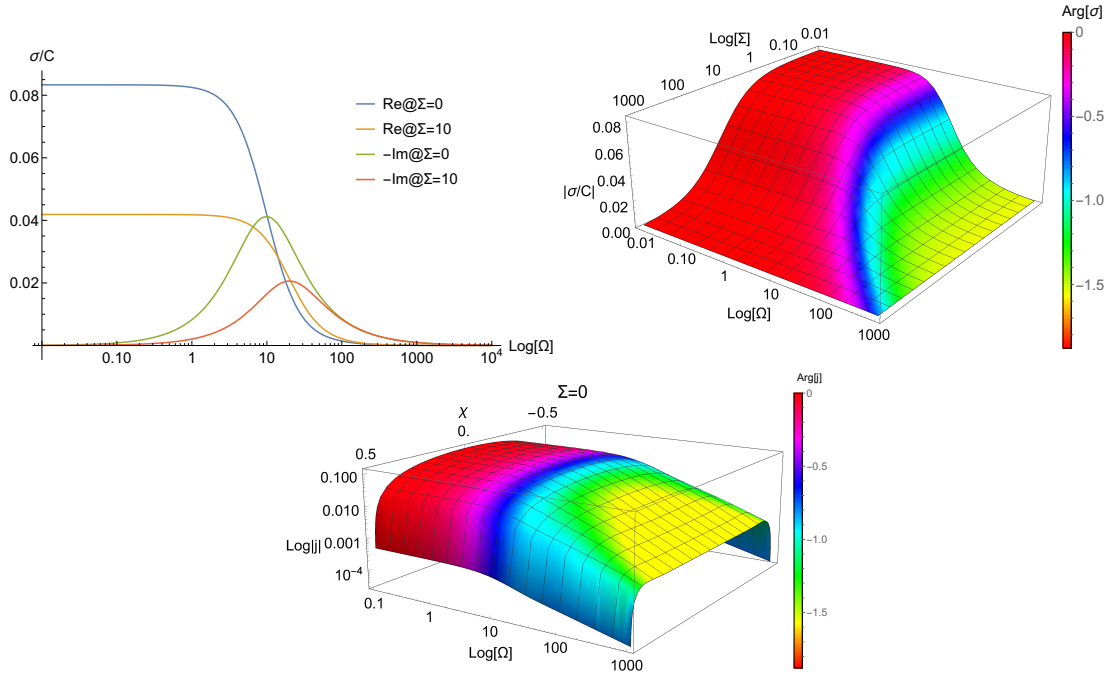
FIGURE 4. Top: Real and imaginary parts of conductance for various choices of the parameter Σ. The behavior resembles Drude conductivity and is stable against small Ohmic perturbations. The position of the Drude peak is $\Omega \approx 9.89$ at $\Sigma = 0$. The Drude peak separates two different scaling regimes, low frequency ($\sigma \sim \omega^0$) and high frequency ($\sigma \sim \omega^{-1}$). Middle: Conductivity plotted in the $\Sigma - \Omega$ plane. The hydrodynamic behavior is stable for $\Sigma < 10$. Bottom: local conductivity $j(\Sigma = 0)$ as a function of the relative channel width χ and Ω. Color encodes a local phase shift with respect to forcing, resistive at small Ω, tuning reactive (inductive) at large Ω.

around $\nu = 0.1 m^2/s$ [18, 21, 26, 27, 54]. The boundary layer requires high frequencies $\Omega \gg 1$. Given the above estimates for ν and L we deduce the boundary-layer to have emerged at $\Omega = 100$, around 100 GHz, i.e. in the high-frequency microwave/far infrared part of the electromagnetic spectrum. Numerical evaluation of the solution (4.8) suggests that the layer actually starts to emerge at $\Omega \approx 80$. Of course one may worry if this lies in the range of applicability of hydrodynamic description. However, comparing the time scales: momentum-conserving collision rate $\gamma_{MC} \approx 8 \times 10^{-14} s$ [17] and forcing frequency time scale $100 GHz$ ($\approx 10^{-11} s$) leads us to the conclusion, that we are still deep in the regime, where momentum-conserving interactions are dominating enough to facilitate the use of collective (i.e hydrodynamic) description. Standard estimates for the width of the boundary layer give

$$(4.14) \qquad \delta \sim \sqrt{\frac{\nu}{\omega}},$$

which, for the values of viscosity measured for graphene or delafossite metals, results in the layer thickness of order $10^{-7} m$. The parameter Σ produced by Ohmic friction can reach the numerical values up to 10, based on the experimental estimates [18, 21, 54].

The results presented before, concerning the width scaling and frequency dependence of the conductance, have proven that a standard 'global' AC measurement can provide sharp signatures of hydrodynamic behavior in solid state systems. Recently however a new, fascinating avenue of experimental activity have been opened, thanks to local current density measurements based on

single electron transistors [50]. Utilizing this technique could allow for observing not only the global signatures of hydrodynamic flow but also the development of the boundary layer itself.

The above analysis focuses on periodic solutions. The real experiment however would involve applying periodic driving to ensemble of electrons with zero average velocity. It is therefore interesting how this periodic steady state reached in such an experiment. To answer that one must solve a initial problem: equation (4.4) on a domain $\chi \in [-1/2; 1/2]$, $\tau \geq 0$, with conditions on the behavior of functions at the boundaries of spatial domain at every time and initial (steady) state. The analytical solution consists of the periodic part (4.8) and an infinite series of functions of complex frequency which correspond to exponentially dumped modes. The slowest-relaxing mode has a lifetime given by

$$(4.15) \qquad\qquad t_{rel} = \frac{\nu\pi^2}{L^2} \approx 10^{-12}s,$$

with the last number estimated using previously mentioned parameters. The non-periodic behavior is therefore experimentally irrelevant.

The presented results show that the hydrodynamic AC transport starkly differs from the previously studied regimes: ballistic and Ohmic. Even in the simplest set-up the observable effects despite staying in close analogy to results observed in Ohmic regime, show unmistakable signatures of hydrodynamic origin, manly due to the way the mesoscopic parameters of the system enter the description. In the next section, further study of this mesoscopic dependencies is presented, focusing this time on another important issue: the boundary condition and the way it manifests itself in the observables.

2. Boundary condition. Slip length, slip control and measurement

Section based on [65]

One of the important aspects of hydrodynamics as an effective transport theory is the fact that the solutions of the transport equations strongly depend on the boundary conditions. The previous section showed an example of effect – the boundary layer – that crucially depends on the conditions that the electronic fluid obeys at the edges of the sample. As was already mentioned, the effective momentum dissipation in the viscous flow occurs due to the boundaries forcing the fluid to stop. Therefore it is important to analyze if the previously-assumed 'no-slip' boundary conditions, that do not allow any velocity parallel to the boundary are physically realized ones. From the mathematical point of view, there is some freedom in choosing the boundary condition for viscous hydrodynamics. It is known, that hydrodynamics admits a one parameter family of consistent boundary conditions (the so-called *Maxwell boundary conditions*) which reads

$$(4.16) \qquad\qquad u_T^i\big|_B = \xi\, n^j\, \nabla_j u_T^i\big|_B \ .$$

The parameter ξ is called the *slip length*. This boundary condition involves the tangent velocity u^t at the boundary of flow domain and its normal (with respect to *inward* pointing vector n_j) derivative.

In many every-day uses of hydrodynamics, the slip length is negligibly small, encoded by the no-slip boundary condition that prohibits the fluid from having any tangent velocity at the domain's boundary. However, there are situations, like in liquid helium or microfluidics[66, 67], where slip length cannot be neglected.

If one considers hydrodynamic theory of charge carriers in a solid state system, in principle it is also not obvious which boundary condition is the right one. In fact, some experiments aiming to explore this regime reported failure to observe the Gurzhi effect in a long graphene channel [18], which in light of what was presented in the previous chapter may be caused by a 'slippery' boundary that allows for some non-zero value of velocity. There are also theoretical insights on the dependence of slip length ξ on temperature [68] – all of those circumstances suggest that the issue of boundary conditions in viscous electronics may be non-trivial in a

similar way as it is for liquid helium. In that case the question of determining and correctly treating the boundary condition becomes crucial for both further theoretical developments and possible practical applications of the field.

Whereas the microscopic slip in viscous electronic systems has been investigated in detail [68], there is another aspect of the boundary condition 4.16 associated with the *geometry* of the boundary, studied by Einzel, Panzer and Liu [66]. If the boundary of a channel is not flat but has some curvature, it modifies the boundary condition by replacing the microscopic slip length ξ by an effective parameter ξ_{eff} that is a function of the local curvature. For a mesoscopic sample the curvature can be either mesoscopic (i.e. of order of characteristic system size) or sub-mesoscopic (i.e. much smaller than system size yet bigger than momentum conserving scattering mean free path). This opens new possibilities in the realm of viscous electronics, as the slip can not only be controlled by microscopic properties (like doping, temperature or the way the sample is prepared) but also by carefully shaping the system itself. This chapter is devoted to study of such possibilities in various set-ups, and contains a proposal on how to utilize this slip effects to get access to the microscopic slip parameter. Technically, it will be based on the stream function method introduced in the previous Chapter in Section 3.4. The equation that will be solved here is

$$(4.17) \qquad (\nabla_t + \gamma)\,\Delta\Psi - \nu\Delta^2\Psi = 0,$$

where γ is the Ohmic dissipation coefficient and ν is the viscosity.

. Boundary conditions for the stream function follow partially from (4.16) which reads (n^i is the unit normal to the boundary)

$$(4.18) \qquad n^i\nabla_i\Psi\big|_B = \xi\,n^j\,\nabla_j n^i\nabla_i\Psi\big|_B$$

which is relation between first and second normal derivative of the stream function at the boundary. Since equation (3.52) is fourth order, more conditions are needed. An independent condition describes injecting fluid through the boundary

$$(4.19) \qquad t^i\nabla_i\Psi\big|_B = V_B,$$

where t is the normalized tangent to the boundary and V_B is the velocity of injected fluid on the boundary. Since the condition above is only condition on first derivative along the boundary, it is often used in it's integrated form where it bounds the value of stream function with integral (primitive) of injected velocity profile.

One feature of the stream function method is connected to this set of the boundary conditions: in stream function formulation, the gradient terms (that include external forcing encoded in electric potential) are traded for extra boundary condition that requires knowledge of velocity distribution at the boundary of the sample. So, the logic of solving stream function equations is analogous to performing transport experiment using a *fixed current source*, that applies given current to the sample. In such experiment the voltage drop is measured, and similarly in stream function computation the electrochemical potential is extracted from the solution at the end. With powerful stream-function method at hand, one can proceed to analyze how the boundary condition influences the flow.

2.1. Hindering the boundary slip. The first issue connected to boundary conditions is the question if, and to what extend can they be controlled. As was shown in [68], slip length ξ is a function of temperature and chemical potential. Unfortunately, the small temperature behavior, independently of microscopic boundary reflection model, tends to diverge at $T \to 0$ rather fast at low temperatures. This means that for low temperatures where hydrodynamics is valid, the slip length can be of the same order of magnitude as sample size. In turn, the correct boundary condition may be no-stress rather than no-slip, which would make it harder to observe hydrodynamic signatures, as no-stress condition obscures viscous effects in parallel flow set-ups. This stems from the fact that the viscous force is proportional to the *gradient*

of velocity so, in any set-up where a flow is locally parallel to the boundary, any nonzero slip length will substantially reduce the local resistance. Probably the simplest example of such a situation is a Hagen-Poiseuille flow through a channel with an arbitrary slip length, where the average velocity is *proportional* to the slip length. In particular, the velocity turns infinite in the no-stress limit where the slip length diverges.

This situation can be regularized if one takes into account weak momentum relaxation due to momentum-non-conserving impurities, phonons and Umklapp scattering. In order to do that one adds an Ohmic term proportional to velocity to the Navier-Stokes equation. In that case, however, the conductivity is dominated by the Ohmic rather than the viscous effects for large slip. Experimental results of [18] are in agreement with this hypothesis, as they fail to observe parabolic flow in a parallel channel.

It is therefore interesting to check if artificial slip can be engineered. One simple idea is to introduce obstacles in an infinite channel, similar to the one discussed in the previous section. In the example below it is shown that obstacles of a mesoscopic size, easy to include during device fabrication, can serve the purpose. The mechanism guaranteeing efficiency of that method takes up an idea by Moffatt, [69] who noticed that an arbitrary viscous flow outside of a cavity will drive a vortical flow inside (see also [70–72] for a discussion of this effect in various set-ups). Later Wang [73] constructed a solution for a Stokes flow with no-slip boundary conditions in a channel with perpendicular barriers equally spaced on the channel boundaries. He observed Moffatt vortices appearing inside the cavities below a critical distance between barriers.

Crucially, the induced vortices are typically tiny – the flow velocity around such a vortex is orders of magnitude smaller that in the main driving flow. Thus, in general the fluid inside the cavity flows with a relatively small velocity compared to flow in the middle of the channel, thus mimicking the no-slip boundary.
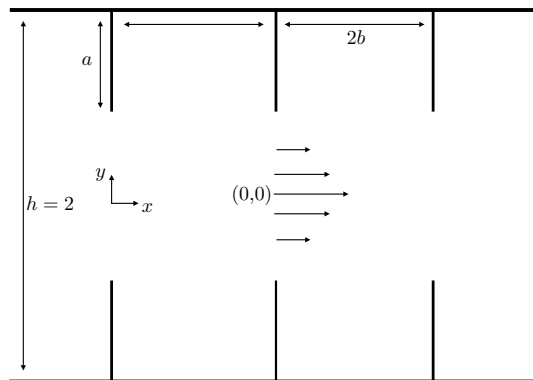
FIGURE 5. Flow geometry with a series of obstacles forming cavities on the boundaries

2.1.1. *Solution in a channel with perpendicular obstacles.* To investigate the idea of mesoscopic obstacles, the solution in a channel with periodic array of walls perpendicular to the sample boundary will be investigated (see Fig 5).

As the system under consideration is two-dimensional, it is convenient to use a stream function formulation of the equations. The most general time-dependent case is governed by the following equation

$$(4.20) \qquad \partial_t \, \Delta \Psi - \nu \Delta^2 \, \Psi + \gamma \Delta \Psi = 0.$$

Here ν is the viscosity and γ the coefficient of the Ohmic term.

Following the procedure developed in [72], an Ansatz for stream function is taken $\Psi(x,y,t) =$

$\hat{\Psi}(x, y) \, e^{i \, \omega \, t}$, from which one obtains an equation for the spatial part of the stream function

$$(4.21) \qquad\qquad\qquad\qquad \Delta^2 \, \hat{\Psi} = \Lambda \, \Delta \, \hat{\Psi},$$

with $\Lambda = \frac{(i\omega+\gamma)(h/2)^2}{\nu}$, a no-dimensional complex parameter. Note that for zero frequency $\omega = 0$, $\Lambda = \Gamma$ reduces smoothly to a DC problem, yielding real stream function. On the mathematical side, the equation above is a non-homogeneous biharmonic equation for the complex function $\hat{\Psi}$. Physics is encoded in the real part of the complete stream function, which is given by

$$(4.22) \qquad\qquad\qquad \mathrm{Re}[\Psi] = \mathrm{Re}[\hat{\Psi}] \cos(\omega \, t) - \mathrm{Im}[\hat{\Psi}] \sin(\omega \, t).$$

Now, equation (4.21) is solved for different values of the slip parameter and in different driving frequency regimes using the method of eigenfunction expansion and point match [73]. Based on the symmetries that the geometry of the channel imposes on the stream function, defining $\alpha = \frac{n\pi}{b}$ and $\beta = n\pi$, the following Ansatz for the spatial function is taken

$$(4.23) \qquad \Psi(x, y) = \frac{\sinh\left(\sqrt{\Lambda}\, y\right) - \sqrt{\Lambda} \cosh\left(\sqrt{\Lambda}\right) y}{\sinh\left(\sqrt{\Lambda}\right) - \sqrt{\Lambda} \cosh\left(\sqrt{\Lambda}\right)} + A_0 \left[y - \frac{\sinh\left(\sqrt{\Lambda}\, y\right)}{\sinh\left(\sqrt{\Lambda}\right)} \right]$$

$$+ \sum_{n=1}^{\infty} A_n \cos(\alpha x) P_n(y) + \sum_{n=1}^{\infty} \left[B_n \sin(\beta y) \, Q_n(x) + x \, C_n \sin(\beta y) \, T_n(x) \right].$$

The first term corresponds to the solution for a flat channel [68] and the second term introduces a possible correction due to the presence of the obstacles. The functions $P_n(y), Q_n(x)$ and $T_n(x)$ are given by

$$P_n(y) = \left[e^{\sqrt{\alpha^2+\Lambda}\,(y-1)} - e^{-\sqrt{\alpha^2+\Lambda}\,(y+1)} \right] - \frac{1 - e^{-2\sqrt{\alpha^2+\Lambda}}}{1 - e^{-2\alpha}} \left[e^{\alpha(y-1)} - e^{-\alpha(y+1)} \right].$$

$$Q_n(x) = e^{\sqrt{\beta^2+\Lambda}\,(x-b)} + e^{-\sqrt{\beta^2+\Lambda}\,(x+b)}, \qquad\qquad T_n(x) = e^{-\beta(x+b)} - e^{\beta(x-b)}.$$

According to the boundary condition (4.19) in it's integrated form, a constant value of the stream function is imposed on the top and bottom walls and on the obstacles, $\psi(x, \pm h/2) = \pm 1$. Additionally, the slip boundary condition is exactly imposed on the top and bottom walls of the channel.

For the boundary condition at $x = b$, N equally-spaced points along this line are chosen and the boundary conditions are imposed numerically there: the series in the stream function is truncated up to N terms, so that the problem reduces to solving a $(3N+1) \times (3N+1)$ resulting linear system. Once the coefficients A_n, B_n and C_n are obtained, the streamlines indicate the direction of the electron flow.

2.1.2. *Artificial no-slip.* Using the above method, flow profiles with arbitrary slip parameters were computed, to identify the range of obstacle lengths and spacings, where the dependence of the flow profile on the value of the slip length is the weakest, and indeed the flow in the center of the channel resembles then a standard no-slip parallel Poiseuille flow. As an additional check, the simulations for a periodically driven AC flow where performed, and confirmed the development of a boundary layer in the high frequency regime. That phenomenon, like the Gurzhi effect, is characteristic of the viscous flow regime [28], but it is absent in parallel flows with no-stress boundary condition.

In order to quantify the behavior of the flow through the finned channel, the following parameters are convenient

$$(4.24) \qquad\qquad\qquad \sigma \equiv \frac{2a}{h} \qquad \text{and} \qquad \beta \equiv \frac{2b}{h},$$

σ being a fraction of the channel in which the fluid is blocked, so that in the middle one can think of a free 'channel' of width $h(1-\sigma)$. β on the other hand measures the aspect ratio of the unit cell.
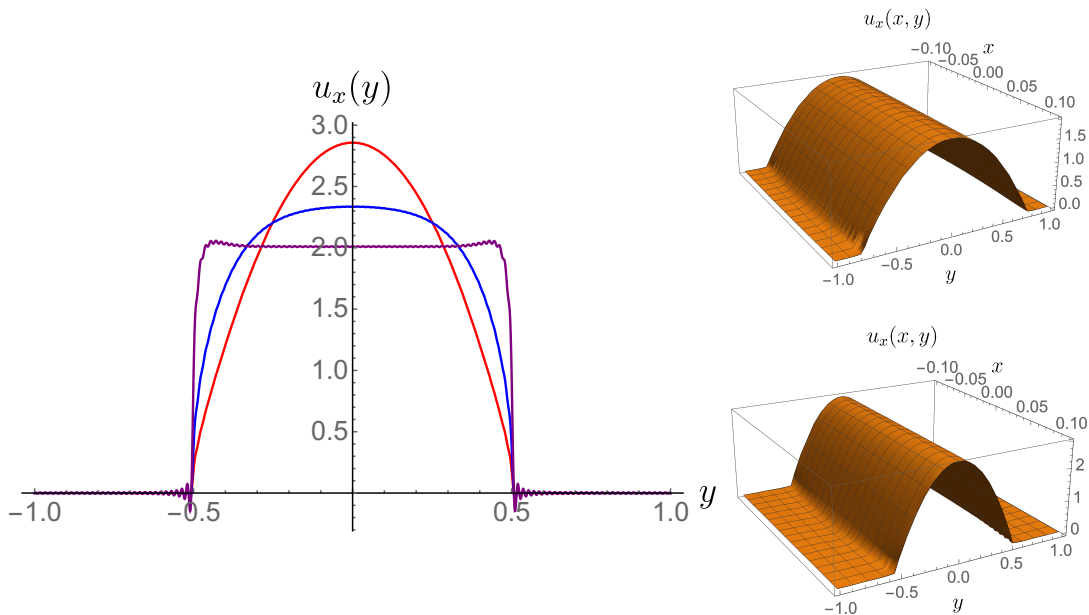
FIGURE 6. **L**eft panel: Flow velocity cuts at the edge of the unit cell, $x = 1/10$, for different Ohmic coefficients. The three plots correspond to no-slip boundary conditions and parameters $\sigma = 1/2$, $\beta = 1/10$ (see text). Red line $\Gamma = 1$ (hydrodynamic), blue line $\Gamma = 100$ (crossover) and purple line $\Gamma = 1000$ (ohmic). **R**ight panel: Profile of the flow velocity along a unit cell for no-stress boundary conditions, both plots correspond to $\beta = 1/10$, while $\sigma = 1/4$ (top) and $\sigma = 1/2$ (bottom).

In Fig. 6 (left panel), the x-component of the velocity along the line $x = 1/10$, for a unit cell with $\beta = 1/10$ and $\sigma = 1/2$, is plotted for different Ohmic coefficients. It can be seen that it looks parabolic for small Ohmic dissipation, resembling hydrodynamic behavior. For higher values of the Ohmic coefficient the flow profile becomes flat. This result is for no-slip boundary condition and is in correspondence with [25].

More interestingly, if the no-stress boundary condition is implemented, the flow through the middle aperture of the channel still resembles a parabolic flow, as can be seen from the right panel of Fig. 6. That shows, that the idea of introducing mesoscopic obstacles emulates sticky boundaries.

To investigate the similarity of the flow with the Poiseuille case in detail, it is convenient to fix the dimensionless Ohmic coefficient $\Gamma = 1$, which places it in an experimentally feasible range[18, 21, 54]. In Fig. 7 the behavior of the velocity profile in the middle of the channel is presented as a function of the parameter β for both no-slip and no-stress boundary conditions. All plots are for fixed $\sigma = 1/2$, and for comparison we also the velocity for the Poiseuille flow on a flat channel of width equals one is plotted.

Given the similarity of the obtained profiles with the parabolic flow, an effective channel in the middle of the sample can be defined. Along this effective central channel, the fluid behaves as if the boundary condition on its walls were no-slip, regardless of the actual boundary conditions on the full finned channel.

How small can the obstacles be made for the flow along the effective channel to be effectively parabolic, is another important question. This is addressed in Fig. 8, which depicts the
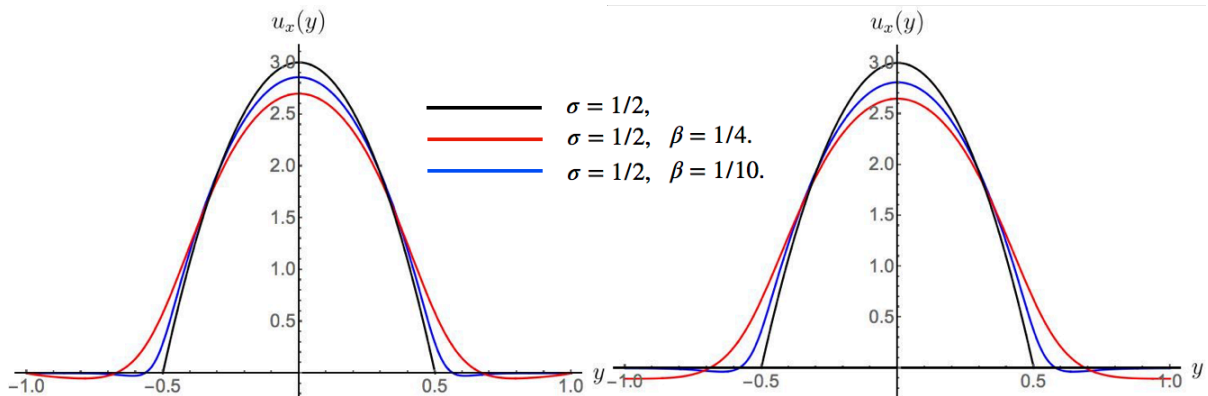
FIGURE 7. Flow velocity cuts at the center of the unit cell, $x = 0$, for no-slip (left) and no-stress (right) boundary conditions. The black lines correspond to Poiseuille flows for an effective center channel of width $\tilde{h} = 1/2 = 1 - \sigma$. Recall that we are in the low dissipation regime, $\Gamma = 1$. Note the similarity between the actual flow and the Poiseuille flow.

evolution of the velocity profile for different values of β, and as a function of the aperture parameter σ. In the top and middle panels of Fig. 8, the spatial dependence of the flow velocity is plotted for different parameters β and σ, concentrating particularly on small obstacles. For some combinations of these parameters the flow closely resembles the parabolic no-slip flow. Other combinations of parameters, corresponding to distantly spaced obstacles, yield flows differing considerably from classical Poiseuille.

In Fig. 8 (bottom panel), the velocity on the no-stress wall is plotted in red as a function of σ for β fixed. What can be seen is that when the velocity at the wall is not close to zero, the flow profile in the middle of the channel differs qualitatively from the parabolic Poiseuille flow. Based on that, a criterion indicating when the effective flow in the middle channel resembles a parabolic flow can be developed. The analysis of numerical data suggests, that in order to ensure that the velocity in the cavity is negligibly small the following condition needs to hold

$$\beta \lesssim \sigma,$$

i.e. it is important that the obstacles are not too far away from each other – the distance between them should be of order of obstacle length or smaller.

Note for example that for $\beta = 1/10$ (the parameter of the plots in Fig. 6), there is a large range of values of the σ parameter for which the velocity at the walls is very close to zero despite the no-stress boundary condition. This supports the idea that a series of obstacles can effectively change the slip parameter in a channel.

Also, note that mimicking no-slip boundary conditions reproduces more than just the simplest effects (such as parabolic Poiseuille flow). As a confirmation the above simulation is repeated in a time-dependent (AC) scenario with a periodic forcing.

The Stokes boundary layers emerge above a certain forcing frequency (see Fig. 9). This phenomenon, previously described for a flat channel[28], is also tied to the no-slip boundary condition, in the following way: for large frequencies, the fluid "cannot follow" the drive, and stops to be in phase with the rapidly oscillating force. The fluid in the middle of the channel oscillates uniformly, and only close to the boundary does the viscosity become important. This has to do with the frequency of forcing being too big for the viscosity to efficiently transport the momentum through the whole channel. As a consequence, a strong gradient is created near the boundary, on a distance that corresponds to the effective 'range' of viscous interaction under
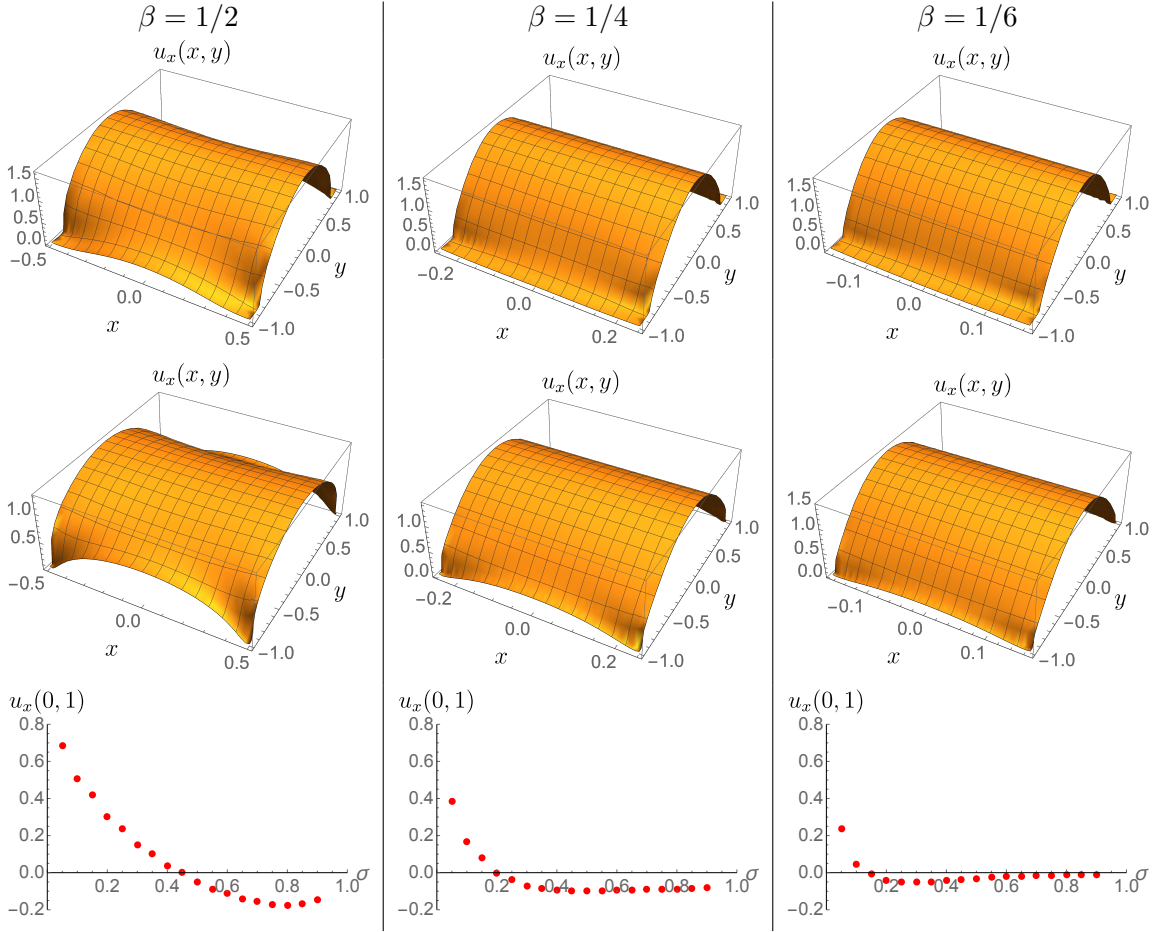
FIGURE 8. **T**op: Velocity profiles along the channel for the corresponding values of β and $\sigma = 1/5$, corresponding to small obstacles in comparison with the height of the channel. **M**iddle: Velocity profiles along the channel for the corresponding values of β and $\sigma = 1/20$, corresponding to very small obstacles in comparison with the height of the channel, $h = 2$ in our units. **B**ottom: Value of the flow velocity at the top wall, coordinates $(x, y) = (0, 1)$, of a unit channel cell as a function of σ and for three values of β.

periodic driving. This gradient of course only emerges if the fluid sticks to the boundary, i.e the velocity there is close to zero.

Also, much like in the AC forced channel flow of the previous section , fast forcing in our set-up results in the maximal velocity at some distance from the center, which further supports the conception of emulating no-slip condition with the mentioned, structured boundary set-up. This analysis also supplements previously existing literature on time dependent electronic flows [20, 52, 74].

2.2. Boundary conditions on curved geometry. The behavior of a fluid flow at the interface with other bodies (i.e. on the boundary of the sample) is a complicated one that crucially influences the solutions of the theory. Plenty of non-trivial physical phenomena governing this behavior are contained in effective descriptions in terms of a proper boundary condition [66, 75–79]. Indeed, various characteristics of the system modify the slip length. They include temperature and parameters related to the wall material and fluid composition, as well as mesoscopic and sub-mesoscopic components, in particular the wall curvature [53]. A quantitative understanding of the wall curvature in terms of an effective slip value was given by Einzel,

$$u_x(0, y, t)$$
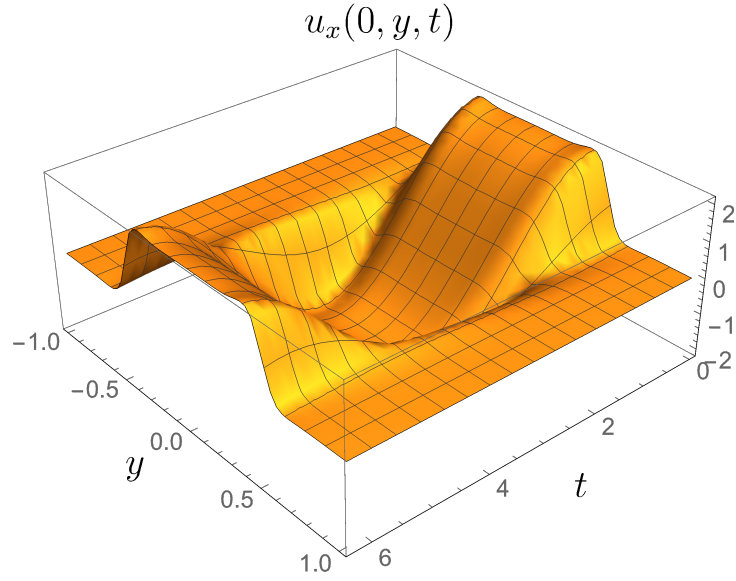
FIGURE 9. Spatiotemporal velocity cut profiles at $x = 0$, for high frequency driving over one period, $t \in [0, 2\pi]$. No-stress boundary conditions on walls and obstacles. Parameters: $\Lambda = 500\, i + 1$, $h = 2$, $\sigma = 1/2$ and $\beta = 1/10$.

Panzer and Liu[66]:

$$(4.25) \qquad\qquad \xi_{\text{eff}} = \left(\frac{1}{\xi_0} - \frac{1}{R} \right)^{-1},$$

where R is the curvature radius measured in such a way, that it is positive if the fluid domain is convex and negative otherwise, see Fig. 10.

$R < 0$ $R > 0$

Fluid domain
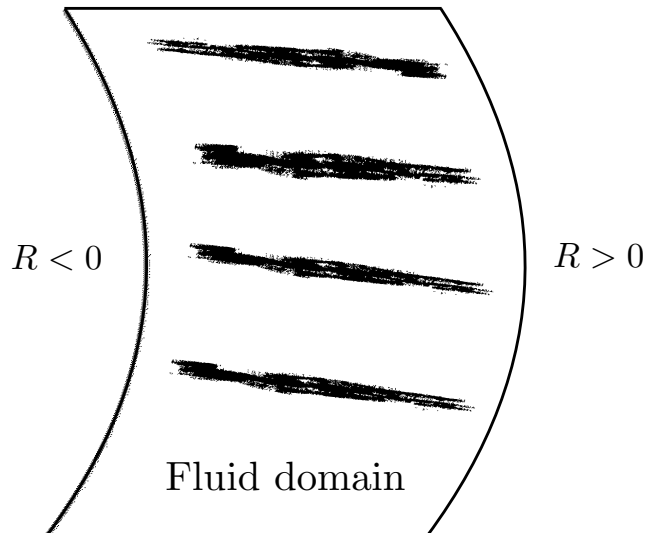
FIGURE 10. The conventions on boundary curvatue used in (4.25). $R > 0$ for convex domain boundary, $R < 0$ for concave.

2.3. Flow on disc domains. A interesting feature of the EPL slip length (4.25) is that for convex domains interplay between microscopic slip ξ_0 and boundary curvature R can render the effective slip infinite or negative. This motivates studies of simplest possible convex domain set-ups. A particularly appealing set-up of that kind is a disc domain with in- and outflow on the boundary. The simplifications come from high symmetry of the domain and the fact, that there is a single length-scale connected to the size of the system.

To solve the problem, equation (3.52) is re-written in radial coordinates. This is a simple task, as Ψ is a scalar function. In a coordinate system where r runs from 0 to 1 (so all the length scales are measured in units of R, the curvature radius), Laplacian reads

$$(4.26) \qquad \Delta\Psi(r,\theta) = \frac{\partial_\theta^2\Psi(r,\theta) + r\partial_r\Psi(r,\theta)}{r^2} + \partial_r^2\Psi(r,\theta).$$

For simplicity, the Ohmic coefficient γ is set to zero in this computation.

Making use of rotational symmetry of the domain a Fourier series solution is constructed from fundamental solutions of the biharmonic equation [80–85]

$$(4.27) \qquad \Psi(r,\theta) = a_0 + b_0 r^2 + \sum_{n=1}^{\infty}(a_n r^n + b_n r^{n+2})\cos(n\theta) + \sum_{n=1}^{\infty}(c_n r^n + d_n r^{n+2})\sin(n\theta).$$

The coefficients a_0, b_0, a_n, b_n, c_n, d_n are determined from the boundary conditions. These assume the following form

$$(4.28) \qquad \Psi(1) = f(\theta),$$

$$(4.29) \qquad \left.\frac{\partial^2\Psi}{\partial r^2}\right|_{r=1} = \frac{\xi-1}{\xi}\left.\frac{\partial\Psi}{\partial r}\right|_{r=1},$$

$$(4.30) \qquad \Psi(0) = 0.$$

The second condition above is (4.16) with the slip parameter being the microscopic slip expressed in terms of the curvature radius. Function $f(\theta)$ describes the inflow and outflow contacts and the angular separation between them. For one inflow and one outflow contacts with widths ϵ and ϵ', injecting uniform current, the function $f(\theta)$ is given by

$$(4.31) \qquad f(\theta) = \begin{cases} 1 + \frac{\theta-\alpha}{\epsilon'}, & \alpha - \epsilon' < \theta < \alpha + \epsilon' \\ 2, & \alpha + \epsilon' < \theta < \beta - \epsilon \\ 1 + \frac{\beta-\theta}{\epsilon}, & \beta - \epsilon < \theta < \beta + \epsilon \\ 0, & \beta + \epsilon < \theta < 2\pi + \alpha - \epsilon'. \end{cases}$$

In the following the inflow and outflow contacts have equal width $\epsilon = \epsilon'$. Imposing the derivative condition on the boundary fixes

$$(4.32) \qquad b_n = a_n \frac{n(1-n\xi)}{(n+2)[(n+2)\xi-1]},$$

$$(4.33) \qquad d_n = c_n \frac{n(1-n\xi)}{(n+2)[(n+2)\xi-1]}.$$

The condition (4.31) allows one to determine a_n and c_n using the orthogonality condition [86]

$$(4.34) \qquad a_n = -\frac{(n+2)[(n+2)\xi-1]\sin(n\epsilon)[\sin(\alpha n) - \sin(\beta n)]}{\pi n^2 \epsilon[2(n+1)\xi-1]},$$

$$(4.35) \qquad c_n = \frac{(n+2)[(n+2)\xi-1]\sin(n\epsilon)[\cos(\alpha n) - \cos(\beta n)]}{\pi n^2 \epsilon[2(n+1)\xi-1]}.$$

Finally the condition at the origin fixes $a_0 = 0$.[2] Note that for the most symmetric configurations with $\alpha = 0$, $\beta = \pi$ $a_n = b_n = 0$.

2.3.1. *Flow profiles.* The circular probe set-up was previously investigated in the ballistic regime, both experimentally and theoretically [87–89]. A striking feature that emerges in the ballistic regime is that the conductance exhibits characteristic irregular fluctuations as a function of Fermi momentum. It is therefore interesting, to compare this to the behavior of this system in the hydrodynamic regime. As a hydrodynamic setup a disc-shaped sample with two narrow contacts of width ϵ is chosen. The setup is presented in Fig. 11
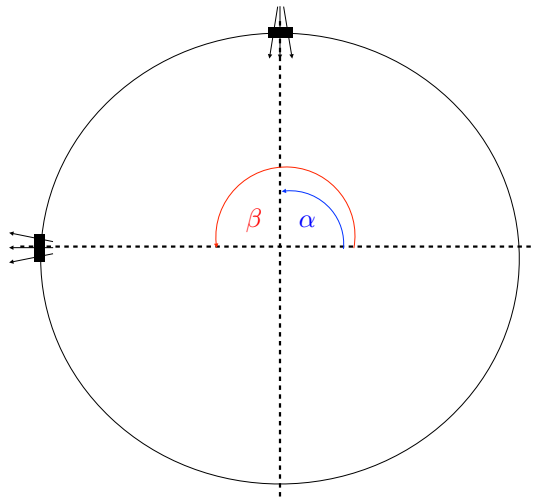
FIGURE 11. Inflow/outflow problem into a circular contact

Junctions possess a big advantage over the channels, namely that a relatively simple theoretical analysis may be possible in both ballistic and hydrodynamic regimes unveiling the distinctive features. The hydrodynamic flow through a confined geometry is smooth due to electron-electron interactions. To illustrate this fact (see Fig. 12) a stream pattern is plotted for two configurations of contacts. In one configuration the contacts are separated by an angle $\pi/2$ in the second by $\pi/8$. Note that the former configuration was studied in the ballistic regime, both semi-classically[89] and quantum-mechanically[88]. One can see that the hydrodynamic flow profile is smooth. Moreover, the closer the contacts are to each other, the less regions away from them participate in the flow.

In the ballistic regime only discrete values of the Fermi momentum, corresponding to the classical trajectories between the entry and the exit, contribute to the conductance. This is attributed to the fact that for some, 'resonant', values of the Fermi momentum of the injected electrons, there exist families of trajectories connecting source and sink contacts in a direct way. Existence of those trajectories sharply increases conductivity. As a result, the conductance, as a function of the Fermi momentum, jitters and has a form of plateaus with oscillating peaks at particular values of the Fermi momentum.

Combining these two behaviors would presumably lead to the disappearance of the plateaus and the suppression of oscillating peaks at a cross-over, which, in principle, could be observable experimentally. This set-up can serve as an exemplification of interaction enhanced conduction [25].

---

[2]Actually, this last condition does not influence the physics too much, as a constant can be added to the stream function without changing the physical velocity field.
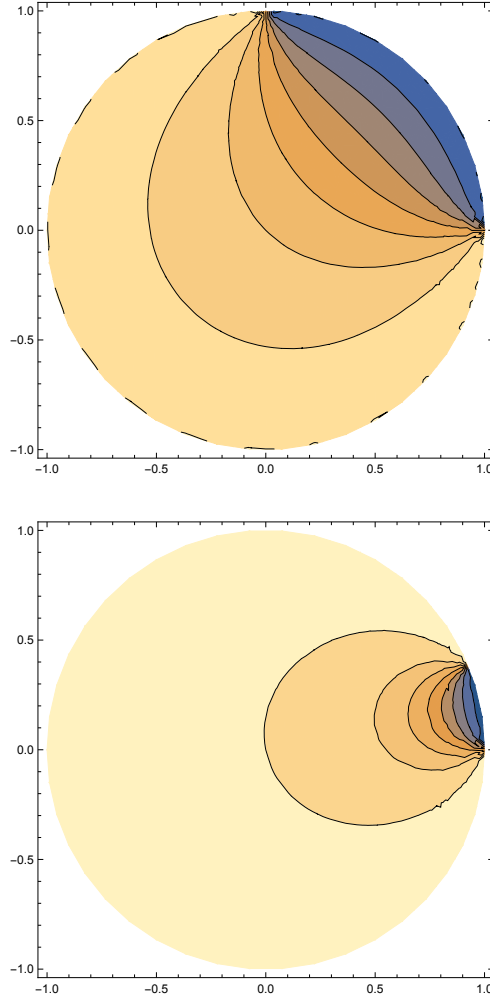
FIGURE 12. **Top:** Streamlines in a circular cavity between two contacts separated by an angle $\pi/2$ ($\alpha = 0$, $\beta = \pi/2$). See 11 for the conventions on angles α, β. **Bottom:** Streamlines between two contacts separated by an angle $\pi/8$ ($\alpha = 0$, $\beta = \pi/8$).

2.4. Slip Length extraction. The circular junction set-up has one additional attractive feature: as mentioned before, the curvature term and the microscopic slip-length in 4.25 have opposite signs. So, one may expect distinctive effects when the microscopic slip is of order of the sample radius. It turns out that one observable in which such an effect is visible is the boundary electrochemical potential profile, which can be computed from the stream function (see introductory section 3.4). This observable describes the local voltage drop along the boundary of the sample $\phi(\theta)$. In the case at hand its measurement allows to directly access the slip length experimentally.

The proposed set-up is presented on Fig. 11 with $\alpha = 0$, $\beta = \pi$. For computational convenience contact sizes are taken to be vanishing $\epsilon = \epsilon' \to 0$ (injecting current by point-like contacts). Remarkably, in this set up, the Fourier series can be summed up analytically and expressed in form of a rather complicated combination of hypergeometric functions for an arbitrary slip length.
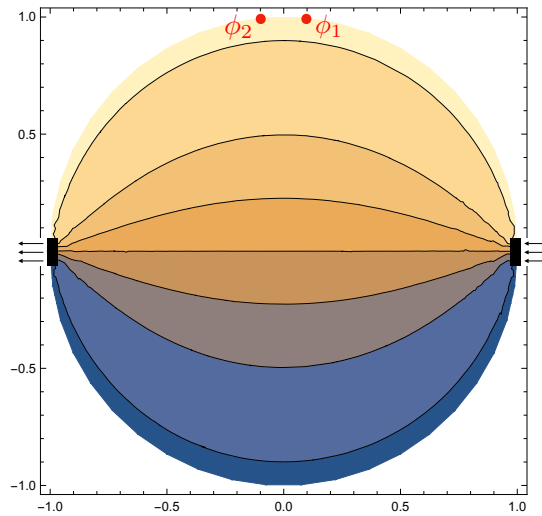
FIGURE 13. Experimental set-up proposed to extract the value of the microscopic slip-length. The current flows between a pair of contacts on opposite sides of circle diameter, and the electrochemical potential difference $\phi_2 - \phi_1$ is measured between two points

A salient feature of the boundary potential profile is that the curves are not too distinct for no-stress and no-slip conditions, but have pronouncedly smaller derivative at an intermediate value of the slip length (numerically found to be $\xi/R \approx 0.36$). This is displayed in Fig. 14 (a), which shows the value of angular derivative of the potential precisely in the middle between two contacts as a function of microscopic slip. This quantity undergoes significant changes (around 50%) upon changing microscopic slip from zero to infinity. based on that, an experimental method to measure the slip length would be to add to the set-up two measurement contacts located on the boundary around point $\theta = \pi/2$ (See fig. 13). Then one would vary external conditions such as temperature or background chemical potential and observe the values of potential at the probe contacts ϕ_1, ϕ_2. Such a set-up would effectively measure the angular derivative of the boundary electrochemical potential $\phi'(\pi/2)$.

Panel (b) of Fig 14 presents the predicted behavior of our observable as a function of temperature, assuming the slip length temperature dependence calculated in [68]. We consider a case of doped graphene at different chemical potentials. It should be noted here, that the Stokes equations which we solve to obtain those results, are strictly speaking valid only in the Fermi liquid regime, i.e if the background chemical potential is much larger than the temperature. The main simplification in that regime is that thermal effects are suppressed, i.e. local temperature is no longer a relevant degree of freedom for the dynamics, and the electric charge current is proportional to the particle number current. That in turn limits the number of independent variables and equations, thus allowing for a simple description. The results discussed above, for doped samples, should be directly comparable to experiment. It follows from the plots that the temperature dependence of the slip length can be measured using a series of such circular devices with different radii: for every radius R there should be a temperature in which potential difference between the electrodes (divided or multiplied by T^2 for charge neutral and doped cases respectively, to get rid of thermal viscosity dependence) is maximal. Then, the slip length is approximately equal $0.36R$ at this temperature.
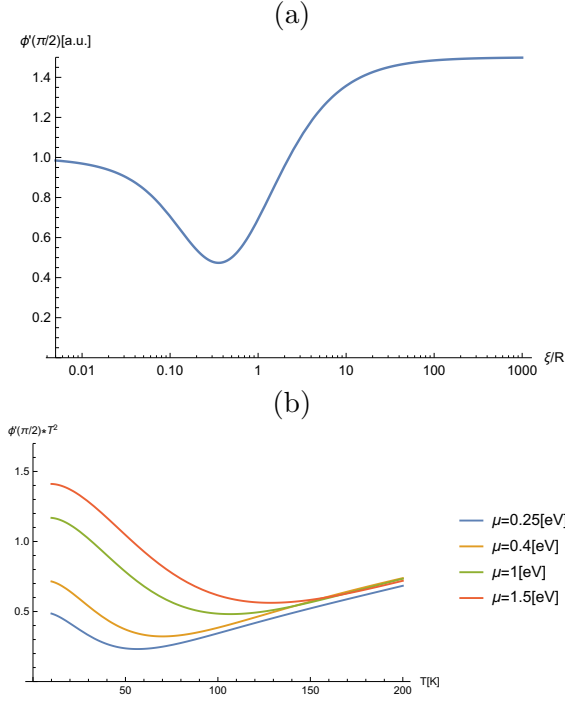
FIGURE 14. The proposed observable, boundary potential drop around $\pi/2$, is characterised by a strongly non-monotonic behavior. **Top (a):** the observable as a function of a slip to radius ratio, keeping all the other parameters fixed. The plot is normalized to its no-slip value. **Bottom (b):** predicted values of the observable times temperature squared (to account for the thermal dependence of viscosity [31]) for doped graphene with various chemical potentials μ. In the given range of doping, the temperatures at which peaks occur lie in the hydrodynamic regime for graphene[18], which makes it feasible to measure the effect. The values of parameters used to generate the plot coincide with [68], all the plots are normalized by the room-temperature value of the observable ($T = 293K$). The sample radius is 5μm

3. Summary and outlook: a handful of mesoscopic effects

This chapter provided some examples on how mesoscopic effects influence various aspects of electronic transport in the hydrodynamic regime. These included AC effects: boundary layer formation and appearance of the floating Drude peak. The former crucially influences the width-scaling of the AC conductance that changes from quadratic in slow forcing regime to asymptotically constant once the boundary layer develops. Apart from that, the development of the boundary layer causes local changes in the phase-shift of the current. In turn, the dissipation of energy happens mostly in this thin region around the boundary while the bulk of the flow is almost dissipation-less. The presence of the floating Drude peak, observed at frequency

$$(4.36) \qquad\qquad \omega_D \approx 9.89 \frac{\nu}{L^2}$$

opens a way to directly measure the viscosity of the electronic fluid. This effects exemplify how the AC measurements can be used in the study of hydrodynamic regime, but are by no means the only ones expected. Some other, very interesting effects are connected to higher harmonic generation by the hydrodynamic modes [90, 91]. Also, it turns out that the non-trivial local phase shift effects described in the first Section are a general phenomenon characteristic to the hydrodynamic regime of transport [92]. A interesting possible extension of the presented work

would be to investigate the AC response over the ballistic-to-hydrodynamic crossover. This would require solving the Boltzmann kinetic equation for the system, which may be technically challenging especially on non-trivial domains, but would deliver information on how 'deep' in the hydrodynamic regime must one be in order to observe the mentioned effects.

On the other hand, in the DC forcing scenario geometric effect was shown to modify the boundary condition (dictated by microscopic properties of the system) which in turn influenced the whole flow pattern. This can be used to control the boundary condition(see subsection 2.1), especially to ensure effective no-slip character of the boundary by a proper micro-structuring. This allows to eliminate one possible source of error from the experimental set-ups like the one presented in [18]. Apart from that, the interplay of microscopic and mesoscopic contributions to the boundary behavior of the fluid opens also a possibility to directly, experimentally access the microscopic slip-length and verify the theoretical computations of [68].

An interesting research avenue in the topic of Fermi liquids is including additional degrees of freedom. Examples of those are local spin that couples to the angular momentum or, in the case of graphene, the so-called valley index. Similar works, including local degrees of freedom [93, 94] indicate that new transport effects can be observed in such modified set-ups.

Finally, it should be mentioned that the situation with strong mesoscopic dependence of transport is not completely unique to the hydrodynamic regime as some similar effects are known for the ballistic conduction [88, 89]. The difference is, however, that the origin of these effects is radically different: in the ballistic regime the dependence stems from single particle effects like reflections from complicated-shaped boundary. In hydrodynamic realm on the other hand, the inter-carrier interactions allow the boundary effects to influence the flow in the bulk of the system.This results, as was presented in subsection 2.3, in a smooth dependence of mesoscopic effects on parameters like the temperature or chemical potential observed in hydrodynamic regime as opposed to irregular, 'resonant' behavior characteristic to the ballistic regime.

Odd transport in fluids subject to magnetic field.

Chapter based on [35]

The previous chapter focused on observable effects of viscous charge flow in the simplest case when the number of transport coefficients is limited to just one – shear viscosity. This simplification comes from the strong symmetry constrains, imposed by both continuous (rotational and translational invariance), and discreet symmetries (parity, time reversal invariance). However, relaxing those symmetry constraints a little by breaking just discrete symmetries, one can introduce a new and starkly different type of transport coefficients, called 'odd'.

Among those, the most famous is the Hall conductivity. Its effect is to induce a voltage transverse to the applied current, and in the simplest case it is direct consequence of the Lorentz force acting on charge carriers. For 2d quantum systems it exhibits a universal behavior, with the value of the Hall conductivity assuming form [29]

$$(5.1) \qquad \sigma_H = k\frac{e^2}{h},$$

where $\frac{e^2}{h}$ is the so-called quantum of conductance and k is the filling fraction. The filling fraction can take integer (integer QHE) or rational values (fractional QHE). Whereas the integer QHE can be understood in terms of free fermions subject to disorder, the fractional QHE is a consequence of strong correlations between electrons in partially filled Landau levels. Understanding the universal behavior of iQHE was one of the greatest achievements of condensed matter physics in the XXth century, and studies on nature of the fQHE are still one of the central problems of the field.

The Hall conductivity is, however, not the only odd transport coefficient allowed. Another quantity that appears in the hydrodynamic description is the Hall viscosity, linking the strain rate to stress-energy tensor. The observable consequences of the presence of that odd coefficient are not as straightforward as in the case of the Hall conductivity, but some intuitive understanding can be gained by analyzing the following example [95]: if a circular object is rotating in a viscous fluid, the viscous force stemming from even (shear) viscosity acts as friction hindering the rotation. Hall viscosity on the other hand induces a force *perpendicular* to the surface of the disc, therefore increasing pressure acting on that object. Conversely, an object with increasing volume (for example a swimmer breathing air in) would be subject to torque – see Figure 1.

That odd viscosity is going to be the central topic of this chapter, and the main result presented here is how the value of this coefficient for a strongly coupled system in magnetic field can be obtained using the holographic duality [35]. This Chapter is organized as follows: first Section 1 is introducing the concept of odd viscosity and presenting the known results. Then Section 2 introduces relativistic hydrodynamics in external magnetic field as well as so-called Kubo formulas that will be later used to compute transport coefficients. After that, in Section 1 the holographic duality is introduced as a method of computing transport coefficients. The following Section 2 presents the computations in the concrete case of strongly coupled magnetized 2d matter. The Chapter ends with a Summary.

Notational remark: in this and the following Chapters, various geometric objects in spaces of various dimensions are going to be introduced. To avoid confusions concerning these objects, the following convention applies: small Latin indices like a, i, j will be used as *spatial* indices
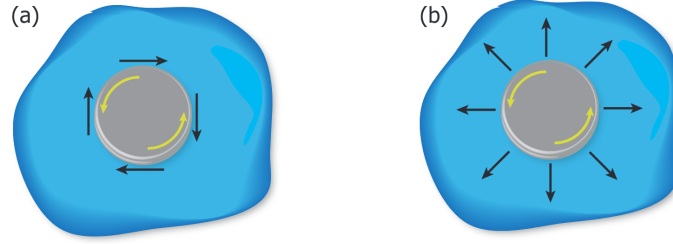
FIGURE 1. Effects of shear (a) versus odd (b) viscosity on a rotating circular body immersed in fluid. The odd viscosity is source of a force *perpendicular* to the body's surface, while the even coefficient is responsible for a tangnt force, acting as friction in that situation. Figure adopted from [95]

– either in non-relativistic description or as spatial parts of relativistic objects. Small Greek indices μ, ν ... will denote *relativistic* space-time objects. Time-like dimension is always $\mu = 0$. Finally, capital Latin letters A, B, N are used for objects in *higher-dimensional (bulk)* space-time introduced in the holographic framework. In the system that is a main focus of this chapter, namely 2+1 dimensional fluid $a \in [x, y]$,$\mu \in [t, x, y]$ and $A \in [t, r, x, y]$. Capital Greek letters are used in case if some other type of index is introduced.

1. Odd viscosity coefficient.

When a hydrodynamic description of a system is constructed, symmetries of the underlying microscopic theory play a twofold role (as already mentioned in chapter 1): first, based on the Nöther theorem, they dictate possible conserved quantities. Then, upon constructing the gradient expansion, symmetries limit the number of possible transport coefficients as the resulting equations need to be covariant[10].

When a theory is symmetric not only under continuous symmetries like translational or rotational invariance but also discrete symmetries (time reversal invariance, reflection invariance), the amount of possible transport coefficients is very limited – for example, the stress tensor, governing momentum conservation, can only have two independent components: *shear* and *bulk* viscosities. To see how the breaking of discrete symmetries can lead to the appearance of new transport coefficients it is instructive to analyze the non-relativistic hydrodynamic equations, as the analysis is technically less involved than the relativistic case.

In the non-relativistic case the stress tensor is given in terms of the hydrodynamic variables (up to first order in the gradients) as

$$(5.2) \qquad T_{ab} = p\delta_{ab} - 2\eta_{abcd}u_{(c,d)} - 2\lambda_{abcd}\xi_{(c,d)},$$

where p is pressure, u_a is local velocity and ξ_a is a local displacement field, $\xi_{(c,d)}$ and $u_{(c,d)}$ are symmetrized derivatives, eg. $\xi_{(c,d)} = 1/2(\partial_a\xi_b + \partial_b\xi_a)$. The local velocity and displacement fields are linked by the following, intuitive relation[96]

$$\partial_t\xi_a = u_a.$$

For a fluid, the tensor λ_{abcd} reduces to inverse compressibility $\kappa^{-1} = -u\frac{\partial p}{\partial V}$ as local displacement only results in change of local volume, and so $\lambda_{abcd} = \kappa^{-1}\delta_{ab}\delta_{cd}$ [96]. The coefficient η_{abcd} is called the viscosity tensor and describes how stress depends on local changes in velocity. By the virtue of the Onsager relations [97], if time reversal $\mathcal{T}$ is a symmetry of the system, the viscosity tensor must be symmetric with respect to the following exchange of pairs of indices

$$(5.3) \qquad \eta_{abcd} = \eta_{cdab}.$$

If the system is also rotationally symmetric, the tensor structure is largely constrained and reads

$$(5.4) \qquad \eta_{abcd}^{(S)} = \eta(\delta_{ac}\delta_{bd} + \delta_{ad}\delta_{bc}) + \left(\zeta - \frac{2}{d}\eta\right)\delta_{ab}\delta_{cd},$$

with the numeric coefficients η *shear viscosity* and ζ *bulk viscosity*.

However, if the system is not time reversal invariant, there is another possibility, namely the viscosity tensor can have an antisymmetric part $\eta_{abcd}^{(A)}$

$$(5.5) \qquad \eta_{abcd} = \eta_{abcd}^{(S)} + \eta_{abcd}^{(A)}, \ \ \eta_{abcd}^{(A)} = -\eta_{cdab}^{(A)},$$

that is also odd under time reversal [97, 98]

$$(5.6) \qquad \mathcal{T}(\eta_{abcd}^{(A)}) = -\eta_{abcd}^{(A)}.$$

In hydrodynamic systems (even) viscosity is a *dissipative* transport coefficient as it is directly linked to the entropy production. A striking feature of the odd viscosity is that it does not contribute to the dissipation. This can be seen straightforwardly by evaluating the time derivative of the entropy in the hydrodynamic theory. To do so, first one takes an infinitesimal change of energy density due to strain

$$(5.7) \qquad \delta\epsilon = -2T_{ab}\delta\xi_{(a,b)}.$$

The the first law of thermodynamics says that

$$(5.8) \qquad \delta\epsilon = T\delta s - p\delta V,$$

so, taking strain variation that preserves volume one arrives at $\partial_t\epsilon = T\partial_t s$, which implies

$$(5.9) \qquad T\partial_t s = -2T_{ab}\partial_t\xi_{(a,b)} = 4\eta_{abcd}u_{(a,b)}u_{(c,d)}.$$

Due to contraction with two copies of $u_{(a,b)}$ the antisymmetric part of η_{abcd} does not contribute to entropy production in and so it does not introduce dissipation in the system. Identity (5.9) also shows that the symmetric part of the viscosity tensor must vanish at zero temperature $T = 0$. This constraint does not apply to the Hall viscosity, which indicates that the physics encoded in the odd viscosity is starkly different than the one of the even part.

Now it is instructive to ask the question whether this antisymmetric viscosity tensor being non-zero is compatible with the other symmetries of the system. The answer depends on the dimensionality of the system: in two spatial dimensions it is enough to break another discrete symmetry – parity – even when isotropy of the space is preserved. In three dimensions on the other hand, one needs to introduce anisotropy in order to generate a no-zero value of antisymmetric viscosity tensor. As the main concern of this Thesis is hydrodynamics of two dimensional materials, let us focus on this case below. The following analysis is due to Avron [98], and has an analogue for 3d systems that can be found therein.

Since the viscosity tensor must be symmetric in first and second pair of indices (due to contraction with symmetric tensor in (5.2) and conditions (5.3),(5.5)), there is a convenient basis in which it can be written for a 2d system: a sub-set of 2x2 Pauli matrices

$$(5.10) \qquad \eta = \eta_{\Lambda\Omega}\sigma^\Lambda \otimes \sigma^\Omega,$$

or, in the index notation

$$(5.11) \qquad \eta_{abcd} = \eta_{\Lambda\Omega}\sigma_{ab}^\Lambda\sigma_{cd}^\Omega,$$

where $\sigma^\Lambda \in (\sigma^0 = Id, \sigma^x, \sigma^z)$, Id stands for the identity matrix and σ_x, σ_z are the two real Pauli matrices following the standard convention. Then symmetric and antisymmetric viscosities are given by the following:

$$(5.12) \qquad \eta_{abcd}^{(S)} = \eta_{\Lambda\Omega}^{(S)}(\sigma_{ab}^\Lambda\sigma_{cd}^\Omega + \sigma_{cd}^\Omega\sigma_{ab}^\Lambda), \ \ \eta_{abcd}^{(A)} = \eta_{\Lambda\Omega}^{(A)}(\sigma_{ab}^\Lambda\sigma_{cd}^\Omega - \sigma_{cd}^\Lambda\sigma_{ab}^\Omega).$$

The convenience of this basis becomes evident when one wants to investigate the behavior of $\eta^{(S)}$ and $\eta^{(A)}$ under a spatial rotation. Such a rotation is generated by $i\sigma^y$, and it's action on

4-th rank tensors is generated by $\sigma^y \otimes \sigma^y$. Since σ^y anticommutes with both σ^x and σ^z and commutes with σ^0, there is precisely one, invariant, antisymmetric tensor of form

$$(5.13) \qquad\qquad \eta^{(A)}_{abcd} = \eta_H(\sigma^x_{ab}\sigma^z_{cd} - \sigma^x_{cd}\sigma^z_{ab}).$$

So, even maintaining rotational symmetry one is allowed to introduce odd viscosity tensor. It has one independent component – η_H which is called 'Hall viscosity' (this term was coined in analogy to Hall conductivity and is used even if the odd viscosity is present in the absence of magnetic field). By an explicit calculation it can be shown that once Hall viscosity is introduced the theory can no longer admit spatial reflection symmetry. The same reasoning can be conducted for relativistic hydrodynamics where odd viscosity also turns out to be a single, non dissipative transport coefficient. Further details can be found in [96].

The value of the Hall viscosity can be topologically protected in some systems [96, 98–100]. An example of system in which Hall viscosity is nonzero are compressible states like two-dimensional metals, where it's presence can produce measurable effects in Hall transport in a hydrodynamic regime[22, 24, 31, 33]. Unfortunately in general computing the value of Hall viscosity from a microscopic theory is a very hard task, as it requires computation of the retarded correlation functions of stress-energy tensor. To obtain these correlators one must compute response of a theory to local strains or, in other words, perturbations of local geometry, which technically is as complicated as solving the microscopic theory on an arbitrary curved background. Since quantum theory in such set-up is very non-trivial even in the non-interacting regime, it is clear that similar computations for strongly coupled systems are out of reach so far.

Because of the technical limitations in extracting information from microscopic theories of strongly correlated electron states in condensed matter, one must try to understand this systems in other way. Some insight may be gained by studying other strongly coupled systems exhibiting similar properties. Typically they would be as hard to study as the original problem but, thanks to the AdS/CFT correspondence (or holographic duality) [101–103], a whole class of strongly coupled theories can be studied using much simpler classical theories of gravity. A more detailed discussion of these methods can be fund in Section 1.

As the aim of this chapter is computing Hall viscosity of a strongly coupled system due to magnetic field, the next section will be dedicated to equations of hydrodynamics in external magnetic fields. As the holographic description is most straightforwardly obtained for relativistic systems this case is presented here. Therefore, also the hydrodynamic equations will be introduced in a relativistically-invariant form.

2. Hydrodynamics with a magnetic field

Let us now revisit the hydrodynamic construction in the presence of an external magnetic field. The general form of relativistic, charged matter conservation equations reads

$$(5.14) \qquad\qquad \nabla_\alpha T^{\alpha\mu} = F^{\mu\beta}J_\beta, \quad \nabla_\mu J^\mu = 0,$$

where $T^{\mu\nu}$ is the energy-momentum tensor and J^μ the charge current. In the studied case a background magnetic field is turned on, so that parity is broken. This situation allows for various power counting schemes. The constitutive relations for this type of fluid in $2+1$ dimensions has been worked out in [104], however in their case the magnetic field was constrained to be much smaller than the temperature. Here, this assumption will be omitted and the background magnetic field will be of order zero in derivatives $B \sim \mathcal{O}(\nabla^0)$. This means allowing the thermodynamic potentials to depend on the magnetic field, at least in the employed hydrodynamic frame, referred to as "magnetovortical". With such power counting, terms that depend on gradients of the magnetic field are allowed in the constitutive relations. Their inclusion would yield very complicated magneto-hydrodynamic system. Since the primary interest of this work is investigation of the parity-breaking effects, only homogeneous and constant background magnetic field is considered here, as a minimal example of such physical situation, and the gradients of

magnetic field are ignored. A partial confirmation of the validity of our assumptions will be provided later by deriving linear response results using hydrodynamic equations and comparing with the holographic model. In the hydrodynamic analysis, some of the linear response coefficients are determined by thermodynamic quantities only. The fact that they match exactly analogues results derived from holography serves as a consistency check for hydrodynamics derived here.

Now the constitutive relations can be presented. The hydrodynamic variables are the fluid velocity u^μ, $u^\mu u_\mu = -1$, temperature T and chemical potential μ. The energy-momentum and current are expanded in derivatives of those and the background sources. Mind, that the magnetic field B is not a hydrodynamic variable, but only an external parameter that bares no space-time dependence. At zeroth order one finds the pressure p, energy density ε and magnetization M, all of which are functions of μ T and the background magnetic field B. In order to have covariant expressions, the magnetic field dependence will enter through the pseudoscalar

$$(5.15) \qquad \mathcal{B} = -\frac{1}{2}\varepsilon^{\mu\nu\lambda}u_\mu F_{\nu\lambda},$$

where $F_{\mu\nu}$ is the field strength of the background gauge field A_μ. The curly epsilon symbol is defined as a tensor, i.e with a factor of the metric determinant $\varepsilon^{012} = +\frac{1}{\sqrt{-g}}$. With these ingredients, the constitutive relations are

$$(5.16) \qquad T^{\mu\nu} = \varepsilon u^\mu u^\nu + (p - \mathcal{B}M)P^{\mu\nu} + T^{\mu\nu}_{(1)}, \quad J^\mu = nu^\mu + J^\mu_{(1)}.$$

Here $P^{\mu\nu} = g^{\mu\nu} + u^\mu u^\nu$ is the projector transverse to the velocity and $T^{\mu\nu}_{(1)}$, $J^\mu_{(1)}$ contain higher derivative terms and satisfy the frame condition

$$(5.17) \qquad J^\mu_{(1)}u_\mu = 0, \; T^{\mu\nu}_{(1)}u_\nu = 0.$$

The magnetization should satisfy

$$(5.18) \qquad M = \left(\frac{\partial p}{\partial \mathcal{B}}\right)_{T,\mu}.$$

The energy density, pressure, entropy density and charge satisfy the thermodynamic relations

$$(5.19) \qquad \varepsilon + p = Ts + \mu n, \quad s = \left(\frac{\partial p}{\partial T}\right)_{\mu,\mathcal{B}}, \quad n = \left(\frac{\partial p}{\partial \mu}\right)_{T,\mathcal{B}}.$$

At first order in the derivative expansion, the independent contributions allowed by the second law of thermodynamics are identical to the ones derived in [104][1]

$$(5.20) \qquad \begin{aligned} T^{\mu\nu}_{(1)} &= -\eta\Sigma^{\mu\nu} - \eta_H\tilde{\Sigma}^{\mu\nu} - \zeta P^{\mu\nu}\nabla_\alpha u^\alpha, \\ J^\mu_{(1)} &= \sigma_V V^\mu + \bar{\sigma}_H \tilde{E}^\mu - T\tilde{\sigma}_V \varepsilon^{\mu\nu\lambda}u_\nu\nabla_\lambda\frac{\mu}{T} + \tilde{\chi}_T\varepsilon^{\mu\nu\lambda}u_\nu\nabla_\lambda T. \end{aligned}$$

The expressions for each of the tensor objects appearing in the formulas above are

$$(5.21) \qquad \begin{aligned} \Sigma^{\mu\nu} &= P^{\mu\alpha}P^{\nu\beta}\left(\nabla_\alpha u_\beta + \nabla_\beta u_\alpha - g_{\alpha\beta}\nabla_\sigma u^\sigma\right), \\ V^\mu &= E^\mu - TP^{\mu\alpha}\nabla_\alpha\frac{\mu}{T}, \quad E^\mu = F^{\mu\alpha}u_\alpha, \\ \tilde{E}^\mu &= \varepsilon^{\mu\nu\lambda}u_\nu E_\lambda, \quad \tilde{\Sigma}^{\mu\nu} = \varepsilon^{(\mu|\alpha\beta}u_\alpha\Sigma_\beta^{\;\;\nu)}. \end{aligned}$$

The allowed transport coefficients are η (shear viscosity), η_H (Hall viscosity), ζ, σ_V, $\tilde{\sigma}_V$, $\bar{\sigma}_H$, $\tilde{\chi}_T$.

This completes the setup. For a flat background and constant magnetic field $\mathcal{B} = B$ the energy-momentum tensor and current are

$$(5.22) \qquad T^{00} = \varepsilon, \quad T^{ij} = (p - BM)\delta^{ij}, \quad J^0 = n, \quad J^i = 0.$$

---

[1]The differences between the equations here and in [104] are the following: terms proportional to the vorticity have been dropped, as those will not play a role in present analysis. Apart form that $\bar{\sigma}_H$ has been introduced, which is related with the susceptibility coefficient $\tilde{\chi}_E$ of [104] as $\bar{\sigma}_H = \tilde{\sigma}_V + \tilde{\chi}_E$.

3. Transport coefficients and correlation functions. Kubo formulas.

The hydrodynamic equations presented above describe the low-energy dynamics of a charged fluid subject to the external magnetic field. However to fully understand the physics implied by these equations one must know the values of the transport coefficients as functions of parameters of state (i.e. the magnetic field). In the following it will be shown how to link these transport coefficients to the *correlation functions* of the conserved currents – quantities that are natural observables in the microscopic quantum or statistical theories. The formulas linking the transport coefficient to the correlation functions go under the name of *Kubo formulas*.

The basic idea behind the computation is that the conserved currents of the hydrodynamic theory are, from the microscopic perspective, the one-point functions of conserved current operators of the microscopic (quantum) theory

$$(5.23) \qquad\qquad T^{\mu\nu} = \langle \hat{T}^{\mu\nu} \rangle, \ J^{\mu} = \langle \hat{J}^{\mu} \rangle,$$

In the expression above the brackets $\langle ... \rangle$ denote taking an expectation value in the microscopic theory, and the objects on the left hand side are the conserved currents from relations (5.14). According to the constitutive relations (5.16), the one-point function of conserved quantity a function of effective degrees of freedom and transport coefficients. To isolate the transport coefficients one must eliminate the effective degrees of freedom from the equations. This can be done by passing from one-point functions to two-point functions using the linear response formalism.

The general way of computing a two point correlator from a one-point function is to perform a variation of the latter with respect to a proper source. In the case at hand the procedure is the following: one introduces a formal perturbation of the background metric, which plays the role of a source for the stress-energy tensor, and the gauge field, as a source for the electromagnetic current. This method can be applied to the hydrodynamic theory. One introduces the perturbed metric and gauge field to the equations (5.14) and the constitutive relations (5.16).

In the next step the hydrodynamic equations are solved for u^{μ}, T and μ to the linear order in the perturbations. Then the constitutive relations for energy-momentum tensor and the current (5.16) are evaluated on the solutions. In that way one obtains expectation values of the energy-momentum tensor and conserved current as the functions of sources. The two-point functions are obtained by taking variations of these expressions with respect to the sources in the following way

$$
\begin{aligned}
G_{TT}^{\mu\nu,\alpha\beta} &= \frac{\delta T^{\mu\nu}}{\delta g_{\alpha\beta}}, \quad G_{JJ}^{\mu,\nu} = \frac{\delta J^{\mu}}{\delta A_{\nu}}, \\
G_{TJ}^{\mu\nu,\lambda} &= \frac{\delta T^{\mu\nu}}{\delta A_{\lambda}}, \quad G_{JT}^{\lambda,\mu\nu} = \frac{\delta J^{\lambda}}{\delta g_{\mu\nu}}.
\end{aligned}
$$

(5.24)

To extract the transport coefficients from the two-point functions presented above it is convenient to pass to the Fourier description. Let us present it on a concrete example in which, for simplicity, only homogeneous but time-dependent sources are considered. The metric and gauge field will be

$$(5.25) \qquad g_{\mu\nu} = \eta_{\mu\nu} + \epsilon\, h_{\mu\nu}(t), \quad A = \epsilon\, a(t)dt + \left(-\frac{B}{2}\epsilon_{ij}x^{j} + \epsilon\, a_{i}(t) \right) dx^{i}.$$

This should trigger response in the dynamic variables. For the sake of a linearized analysis, the following Ansatz is employed:

$$(5.26) \qquad u^{\mu} = (1, \epsilon\delta u^{x}(t), \epsilon\delta u^{y}(t)), \ \mu(x^{\nu}) = \mu + \epsilon\delta\mu(t), \ T(x^{\mu}) = T + \epsilon\delta T(t).$$

The parameter $\epsilon \ll 1$ is small in order to stay in the regime of linear response for the perturbations $h_{\mu\nu}$ and a_μ. The perturbations will be expanded in plane waves

$$(5.27) \qquad h_{\mu\nu}(t) = \int \frac{d\omega}{2\pi} \hat{h}_{\mu\nu}(\omega) e^{-i\omega t}, \quad a_\mu(t) = \int \frac{d\omega}{2\pi} \hat{a}_\mu(\omega) e^{-i\omega t}.$$

The same Fourier expansion is applied to the responses (5.26). Then, only the low frequency components are taken into account, in such a way that the equations for each Fourier component are expanded up to linear order in ω and higher orders are neglected. When solving the equations different sectors decouple according to representation of spatial rotations under which they transform. One can distinguish a tensor, vector and scalar sector related respectively to shear and Hall viscosities, conductivities and bulk viscosity.

After substituting Eqs. (5.16) into the conservation equations (5.14) and solving for the velocities, temperature and chemical potential perturbations (5.26) one obtains the following results for the two-point functions in the tensor sector,

$$(5.28) \qquad G_{TT}^{xy,xy} = \frac{1}{4} G_{TT}^{xx-yy,xx-yy} = -(p - BM) + i\omega\eta, \quad G_{TT}^{xy,xx-yy} = -G_{TT}^{xx-yy,xy} = -i\eta_H \omega$$

The scalar sector contains a term linear in the frequency proportional to the bulk viscosity ζ

$$(5.29) \qquad \frac{1}{4} G_{TT}^{xx+yy,xx+yy} \supset i\zeta\omega.$$

Equation (5.28) is the first and most important Kubo formula that will be used in this work, namely the one giving value of shear and Hall viscosities.

There is also a zero frequency contribution that is a fairly complicated combination of thermodynamic derivatives. This contribution is analogous to the inverse compressibility term appearing in non-relativistic systems [105]. At zero magnetic field the structure of the correlators does not change, one can use the expression above setting $B = 0$.

In the vector sector the current-current and current-momentum correlators are a bit more surprising

$$(5.30) \qquad G_{JJ}^{ij} = i\frac{n}{B}\omega\epsilon^{ij}, \quad G_{TJ}^{0i,j} = G_{JT}^{i,0j} = i\frac{\varepsilon + p - BM}{B}\omega\epsilon^{ij}.$$

The striking feature of this correlators is that they do not involve any of the transport coefficients introduced in the constitutive relations (5.20). In the same sector, the momentum-momentum correlator is

$$(5.31) \qquad G_{TT}^{0i,0j} = (p - BM + iK\sigma_V \omega)\delta^{ij} + iK\left(\frac{n}{B} - \bar{\sigma}_H\right)\omega\epsilon^{ij},$$

where

$$(5.32) \qquad K = \frac{(\varepsilon + P - BM)^2}{B^2\sigma_V^2 + (n - B\bar{\sigma}_H)^2}.$$

This function can be used to extract the transport coefficients σ_V and $\bar{\sigma}_H$.

The susceptibilities present in the constitutive relations (5.20) $\tilde{\chi}_E = \bar{\sigma}_H - \tilde{\sigma}$ and $\tilde{\chi}_T$ can be computed combining the zero frequency correlators $G_{JJ}^{x,t}(0, q_y)$ and $G_{JT}^{x,tt}(0, q_y)$, however, the explicit computation of these quantities will be omitted in the holographic regime, as they do not contribute to the actual transport, which will be shown below.

Let us analyze that sector with a bit more care. First, following [40], the heat current is defined as a combination of energy and charge currents $Q^i = T^{0i} - \mu J^i$,[2] and the measurable transport coefficients correspond to the linear response of the charge and heat current to electric fields and temperature gradients

$$(5.33) \qquad \begin{pmatrix} \vec{J} \\ \vec{Q} \end{pmatrix} = \begin{pmatrix} \sigma & \alpha \\ T\alpha & \bar{\kappa} \end{pmatrix} \begin{pmatrix} \vec{E} \\ -\vec{\nabla}T \end{pmatrix}.$$

---

[2]Recall that in a relativistic system energy current is the same as momentum density.

The conductivities (electrical and heat) are then defined by the identity above. This identity leads to the following Kubo formulas[3]

$$\sigma^{ij} = \lim_{\omega \to 0} \frac{1}{\omega} \text{Im} \, G^{ij}_{JJ},$$

(5.34)
$$T\alpha^{ij} = \lim_{\omega \to 0} \frac{1}{\omega} \text{Im} \left(G^{i,0j}_{JT} - \mu G^{ij}_{JJ} \right) + M\epsilon^{ij},$$

$$T\bar{\kappa}^{ij} = \lim_{\omega \to 0} \frac{1}{\omega} \text{Im} \left(G^{0i,0j}_{TT} - \mu G^{0i,j}_{TJ} - \mu G^{i,0j}_{JT} + \mu^2 G^{ij}_{JJ} \right) - 2\mu M\epsilon^{ij}.$$

The last terms in the Kubo formulas for thermoelectric (α) and heat ($\bar{\kappa}$) conductivities subtract the contributions from the magnetization current, which are not part of the transport by motion of charge carriers. Results obtained here agree with the literature [40, 106].

The combination of the Kubo formulas (5.34) and the hydrodynamic form of correlators (5.30) leads to a conclusion that the observable response coefficients, defined via (5.33), are different quantities than the ones present in the constitutive relations (5.20). For example, the transport coefficient σ_V that is a current-electric field coefficient in the constitutive relation (5.20) and could naively be called a 'conductivity' does not influence the physical conductivity, defined in (5.33) by examining the response of the on-shell current to a small electric field. In fact the latter response coefficient is fully determined by the thermodynamic properties of the system – the density n and the magnetic field B. This is a consequence of the relativistic invariance of the system.

The coefficients derived above describe the response of the system when one of the sources is absent, i.e the conductivity is the ration of the electric current and electric field when the temperature gradient is zero, etc. When it comes to the thermal transport, it is customary to study heat current in the absence of electric current, rather than in the absence of the electric field. In order to do that, one can define the thermal conductivity κ as the heat current produced by a temperature gradient, and thermoelectric response as the electric field in this situation $\vec{E} = -\vartheta \vec{\nabla} T$. The response coefficients are determined by

(5.35)
$$\kappa = \bar{\kappa} - T\alpha\sigma^{-1}\alpha, \quad \vartheta = -\sigma^{-1}\alpha.$$

Using the results obtained from the hydrodynamic equations, the values of the electric and thermoelectric conductivities are determined by the charge and entropy densities

(5.36)
$$\sigma^{ij} = \frac{n}{B}\epsilon^{ij}, \quad \alpha^{ij} = \frac{s}{B}\epsilon^{ij}.$$

The heat conductivity (in the absence of electric fields) is, for $B/T^2 \ll 1$,

(5.37)
$$\bar{\kappa}^{ij} = \frac{(\varepsilon + P)^2}{Tn^2}\sigma_V \delta^{ij} + \left(\frac{Ts^2}{nB} + \frac{(\varepsilon + P)^2}{Tn^2}\bar{\sigma}_H \right) \epsilon^{ij}.$$

While the thermal conductivity (for $B/T^2 \ll 1$) and Seebeck coefficients are

(5.38)
$$\kappa^{ij} = \frac{(\varepsilon + P)^2}{Tn^2} \left(\sigma_V \delta^{ij} + \bar{\sigma}_H \epsilon^{ij} \right), \quad \vartheta^{ij} = -\frac{s}{n}\delta^{ij}.$$

Therefore, the terms appearing in the constitutive relations of the charge current manifest themselves as contributions to the thermal conductivity, in particular the parity odd coefficient $\bar{\sigma}_H$, induces a thermal Hall conductivity that would otherwise be vanishing.

---

[3]Note sign difference in the Kubo formulas with respect to [40] because of conventions used here. The electric field has been defined as $E_i = F_{i0}u^0 = \partial_i A - \partial_t A_i$. Then, Ohm's law becomes $J^i = \sigma^{ij}E_j \simeq -\sigma^{ij}\partial_t A_j \sim +i\omega\sigma^{ij}A_j$. Hence the conductivity is extracted as proportional to the positive imaginary part of the correlator. More generally, with these conventions the spectral function is proportional to the imaginary part of the retarded correlator obtained through the linear response formulas.

Because of the subtleties encountered in the vector sector, it is interesting to note how the structure of correlators and transport coefficients changes when the magnetic field is set to zero. It turns out, that that it changes significantly. The current-current correlator becomes

$$(5.39) \qquad G_{JJ}^{ij} = \left(-\frac{n^2}{\varepsilon + p} + i\sigma_V \omega \right) \delta^{ij} + i\bar{\sigma}_H \omega \epsilon^{ij}.$$

While the current-momentum and momentum-momentum correlator take the simple form

$$(5.40) \qquad G_{TJ}^{0i,j} = G_{JT}^{i,0j} = -n\delta^{ij}, \quad G_{TT}^{0i,0j} = -\varepsilon\delta^{ij}.$$

For the sake of simplicity let us analyze the case of vanishing chemical potential μ (assuming, that the magnetization vanishes as well). Then the conductivities are the following

$$(5.41) \qquad \sigma^{ij} = \sigma_V \delta^{ij} + \bar{\sigma}_H \epsilon^{ij}, \quad \alpha^{ij} = \bar{\kappa}^{ij} = 0.$$

Now σ_V is the longitudinal electric conductivity, while $\bar{\sigma}_H$ enters as an (anomalous) Hall conductivity. So, the 'constitutive relation' definition of conductivity agrees with the 'linear response' one. At zero chemical potential the charged current in the system is produced by particle-antiparticles pair. The flow of those particles transport a net charge, but the total momentum flow is zero, because particles and antiparticles move in opposite directions. This fact explains the vanishing value for both the thermoelectric and thermal conductivities.

Let us recapitulate once more the most counter-intuitive result of this computation: the observable, linear response coefficients defined by (5.33) can, and in general are *different* than the transport coefficients entering the constitutive relations (5.16). It is especially striking in the case of electric conductivity: in the presence of the magnetic field the observable conductivity tensor σ^{ij} is purely antisymmetric and *independent* of the values of transport coefficients σ_V, σ_H (5.36) whereas in the case with no magnetic field (5.41) the coefficients σ_V, σ_H enter the expressions for conductivity in an intuitive way – as longitudinal and Hall conductivities respectively. This, however, shows that one must proceed with care when trying to interpret the physical meaning of the transport coefficients introduced in a constitutive relation for any hydrodynamic theory.

Once the link between the correlation functions and the transport coefficients is established a microscopic theory can be employed to obtain the latter quantities. Such a computation will be the subject of the next Chapter.

CHAPTER 6

Holographic computation of the transport coefficients

Chapter based on [35]

1. Holography and transport coefficients

The final result of the previous chapter is how the transport coefficients can be obtained by evaluating retarded correlation functions of the system. Unfortunately, these are not straightforward to compute for many systems, and especially for strongly coupled theories there is no universal prescription for computing them. One method to obtain the correlators for such system is the so-called holographic duality or AdS/CFT correspondence. The general idea behind the holography is that certain quantum theories in flat space are equivalent to theories of quantum gravity. The feature that makes this duality especially interesting is that it links the strongly coupled regime of one theory to the weakly coupled regime of the other. Historically, the first example of such a duality was the one between $\mathcal{N} = 4$ supersymmetric Yang-Mills (SYM) theory and type IIB superstring theory on $AdS_5 \times S^5$ space[101]. In that case, the strongly coupled regime of SYM theory (the so-called t'Hooft limit [107]) is linked to a *classical* theory of gravity – type II B supergravity with a negative cosmological constant. Due to the fact that it links conformal quantum field theory (CFT) with a gravity theory admitting anti de Sitter solutions (AdS) the term 'AdS/CFT correspondence' was coined.

Regardless of the fact, that a mathematically rigorous proof of the AdS/CFT conjecture is still missing, many checks where conducted on the original version of the duality (which consisted of computing observables using both frameworks) and similar dualities were constructed for different theories, including QFT in dimensions different than original 3+1. Among them there are some in which neither is the quantum theory conformal nor is the gravity solution AdS – some constructed to describe nuclear matter [108, 109] and others with condensed matter problems in mind [38, 110–112]. Nevertheless, the term AdS/CFT was adopted in general to describe the whole class of dualities conceptually originating from the original one.

The holographic theories vary a lot in the details of construction, but share one key feature: the gravity theory is formulated on a *larger-dimensional space-time* than the field theory. Although the original duality was proposed in high energy physics, already in the early 2000's attempts were made to use it for gaining insight on problems known from condensed matter theory. The motivation to use them for that purpose is the Wilsonian understanding of the renormalization group, according to which systems of different microscopic nature can yield the same long-wavelength behavior if they belong to the same universality class characterized by an IR fixed point of the renormalization group transformation. Therefore the theories with holographic duals, despite being be microscopically very different to a typical condensed matter system, can still be used as a playing ground to understand better the properties of strongly coupled electronic states as long as they share IR fixed point with the electronic system of interest. Some examples of phenomena studied in this framework are superconductivity and superfluidity [113, 114]. More recently much effort was put into studying holographic model of strange metal resistivity [115]. For a more complete review of holography and its applications for condensed matter problems see [116].

When it comes to odd transport physics, there have been many proposals for describing Quantum Hall states in 2+1 dimensions using holography [117–136]. Although some of these

models describe fractional filling fractions and features like transitions between Hall plateaus, the situation is not entirely satisfactory when the holographic models are examined in detail. In most cases the Hall conductivity is non-vanishing even in the absence of a magnetic field, thus these models have an "anomalous" Hall effect, rather than the usual Hall effect induced by a magnetic field. On the other hand, in 3+1 dimensional systems, application of the holographic methods was a key ingredient for understanding how the universal quantum properties of the microscopic system (the so-called *quantum anomalies*) can manifest themselves in the magneto-transport phenomena even at the semi-classical level [32, 137]. Therefore, constructing a model in which both Hall conductivity and viscosity are induced by the presence of magnetic field only is one of the goals of this Chapter.

1.1. Holography – basic description. As was already stated holography is a statement of equivalence between d-dimensional QFT and d+1-dimensional theory of gravity. So, there is an extra dimension in the gravitational description. To understand its role, it is very useful to refer to a schematic illustration of the AdS space that can be found on Figure 1 – which is taken from an excellent, short review [138]. Here, r represents the extra (*radial*) direction in
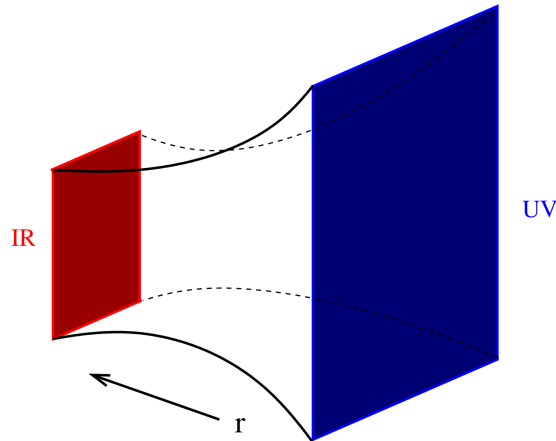
FIGURE 1. A cartoon of the AdS space from holographic perspective. Picture from [138]

d+1-dimensional space time (called *the bulk*). It's customary to refer to the gravity theory as the *bulk theory*. The blue plane described as UV is a d-dimensional Minkowski space-time – a conformal *boundary* of the AdS space. In many cases one says that the QFT degrees of freedom 'live' on this boundary, and the QFT itself is called the *boundary theory*. The radial direction in bulk (r) plays in this description the role of an *energy scale* understood in the spirit of Wilson renormalization group. With that interpretation one says, that the behavior 'far away' from the boundary, so at small r with the conventions that will be used here, describes long wavelength modes of the QFT (IR), while what happens close to the boundary describes the UV, or high energy behavior.

The way the duality relates bulk and boundary theories is by stating that the partition functions of both theories are identical

$$(6.1) \qquad\qquad\qquad\qquad Z_{QFT} = Z_{QG}.$$

The identification goes under the name of GKPW formula (named after Gubser, Klebanov, Polyakov and Witten) [138]. If one is interested in the partition function of a strongly coupled quantum system, thanks to the weak-strong nature of AdS/CFT, it is enough to evaluate the

quantum gravity partition function in the semiclassical limit. Then the saddle point approximation to the path integral can be involved

$$(6.2) \qquad\qquad Z_{QFT} \approx \exp\left(iS_{GR}\right),$$

and the partition function is just an exponential of the *on-shell action* S_{GR} of the classical gravity. On shell means here that the values of fields in the action obey the gravitational equations of motion.

1.2. Holographic dictionary. To extract information from the partition function mentioned above, one must make the connection between objects in the bulk and on the boundary more concrete. The prescription connecting the gravitational and quantum sides of the duality is called in the literature the "holographic dictionary" [138] or "field-operator map" [139]. The spirit is that fields in gravity theory (scalars, vectors, tensors) are related to operators of the quantum theory that have definite transformation properties under the conformal group – scalar, vector or tensor. To understand how the classical, gravitational fields encode properties of quantum operators one must make use of specific properties of asymptotically AdS spaces. In what follows, the Reader should assume that the bulk space time is 3+1 dimensional while the dimensionality of the boundary is 2+1, unless stated otherwise.

In an asymptotically AdS space time, as the one sketched on Figure 1, some restrictions are put on the form of matter fields. For example for a scalar field ϕ, the large-r, near-boundary expansion can be written

$$(6.3) \qquad\qquad \phi(r, x^\mu) = \left(\frac{r}{L}\right)^{\Delta_-} \phi_0(x^\mu) + \left(\frac{r}{L}\right)^{\Delta_+} \phi_1(x^\mu) + \dots$$

where $\Delta_- < \Delta_+$ are theory-dependent constants, characterizing the scaling properties of the field and $\phi_0(x^\mu)$, $\phi_1(x^\nu)$ are arbitrary functions on the Minkowski space-time.

From the gravity perspective ϕ_0 is a boundary condition for the scalar field – it determines the behavior of the field in the whole bulk space-time. In the quantum theory on the other hand, this function plays the role of the source for the dual scalar operator $\mathcal{O}$.

$$(6.4) \qquad\qquad Z_{QFT} = \int [D\psi] \exp i \left(S_{QFT} + \int dx^\mu \mathcal{O}(\psi) \phi_0(x^\mu) \right).$$

Integral over $[D\psi]$ is the path integral over fields in the theory.

Now, according to the GKPW formula (6.2), an expectation value of the operator $\mathcal{O}$ can be evaluated according to the standard prescription

$$(6.5) \qquad\qquad \langle \mathcal{O} \rangle = \frac{\delta}{\delta \phi_0(x^\mu)} Z_{QFT} \approx i \exp\left(iS_{GR}\right) \frac{\delta}{\delta \phi_0(x^\mu)} S_{GR}.$$

It turns out that the result of that variation is nothing else but the term ϕ_1 from the formula (6.3). This sub-leading term is therefore dual to the *expectation value* of the operator $\mathcal{O}$ in the presence of the source ϕ_0 [138]

$$(6.6) \qquad\qquad \phi_1(x) = \langle \mathcal{O} \rangle.$$

This result is a key idea of holographic computations: one solves the gravity equations in bulk, and reads off the expectation values of operators from the *subleading* behavior of fields near the conformal boundary.

As was mentioned before, the dictionary maps scalar fields to scalar operators, vector fields to vector operators and so on. There is, however, more to that identification. If a vector field in the bulk has a local gauge symmetry this poses additional constrains on the dual operator – it implies *conservation equation* for the boundary vector. So, a *bulk gauge field* is dual to a *conserved current operator* in field theory. One may of course be worried that a vector in the bulk space-time has more components than one in the boundary theory, but due to the gauge symmetry the radial component A_r that has no boundary interpretation can be always set to zero.

There is also another very special tensor field in any theory of gravity: the *metric*. That field is dual to the *stress-energy tensor* of the boundary theory. Again, diffeomorphism invariance of the metric ensures conservation equation for the stress energy tensor and allows one to get rid of spurious metric components.

Finally, it should be noted that an expectation value in the quantum theory is always taken with respect to a concrete quantum *state*. On the gravitational side what determines the expectation values is the space-time itself – every solution of gravitational equations corresponds to a state in the QFT. This solution is characterized by boundary conditions in the UV, that encode the sources but also by the behavior *in the IR* of the bulk. A particularly important example of two solutions that differ by the IR behavior despite identical UV boundary conditions are an empty AdS space and an asymptotically AdS black hole solution. The former corresponds to the vacuum state of the QFT, while the latter is dual to the thermal state.

The fact that a black hole solution corresponds to a thermodynamic equilibrium state can be understood invoking the connection between radial direction in bulk and renormalization group scale. From the RG perspective the thermal state is characterized by an energy scale (temperature) that provides a IR cut-off, blurring the information on low energy scales. This is reflected in the holographic description by introducing a horizon in the IR of the bulk space time. A horizon has an associated temperature and entropy density which directly correspond to the thermodynamic quantities of the QFT state. [1]

The holographic dictionary presented above is summarized in Table 1.

Quantum theory (*boundary*)	Gravity theory (*bulk*)
State of the theory	Particular solution of the equations of motion
Scalar with conformal dimension Δ	Scalar with asymptotic behavior $\sim (r/L)^{\Delta - (\Delta)}$
Conserved current	Gauge field
Stress-energy tensor	Metric tensor
Source of an operator	Boundary condition (ϕ_0 in (6.3))
Expectation value $\langle \mathcal{O} \rangle$	Sub-leading term around boundary (ϕ_1 in (6.3))
Thermal state	Metric with horizon (black hole)

TABLE 1. The dictionary of the holographic duality

As mentioned before, the well-established and studied models of holography connect highly symmetric QFTs with theories of supergravity, which are also rich in field content. These models certainly help understanding formal aspects of QFT but are not of much use for condensed matter physics. To study CMT problems one can however take a different approach: starting from a conformal theory represented by just Einstein gravity (conformal fixed point) and deforming it. This deformation means adding new terms to the bulk action. The type of terms to be included is determined by the symmetry of the quantum theory one wants to study. This approach is analogous to constructing an effective field theory for a given system, where action is constructed by including all possible terms allowed by symmetry up to a given order in derivatives. The role of derivative order in holographic action is much different to the hydrodynamic gradient expansion: the higher-derivative terms appear in action when one takes into account *quantum corrections* to the saddle-point approximation of string theory.

This "effective theory" type holography was used before to describe superconductivity and superlfuidity [113, 114] or anomalous transport in 3+1 dimensional QFT [32]. That is also

---

[1] It is worth noting here, that small perturbations of black hole solution in AdS space-time lead to perturbations of the 'shape' of horizon that are described by equations identical to those of relativistic hydrodynamics. This fact, known as fluid-gravity correspondence [140] is now understood as a consequence of hydrodynamics being a universal, low-energy description of quantum theory[141, 142].

the approach that will be presented here for studying anomalous transport in 2+1 dimensions. Constructing a proper model will be the starting point of the analysis in Section 2.

1.3. Correlation functions and transport coefficients. The holographic dictionary 1 relates the near-boundary behavior of fields with the expectation value of corresponding operators. However, to make use of Kubo formulas (5.28, 5.34) and compute transport coefficients one needs to compute two-point functions instead of just one-point that are directly given by the dictionary. To compute those, one makes use of the following general identity for the correlation functions

$$(6.7) \qquad \frac{\delta}{\delta\phi_0(y^\nu)} \langle \mathcal{O}(x^\mu)\rangle \left[\phi_0(y^\nu)\right]\Big|_{\phi_0=0} = \langle \mathcal{O}(x^\mu)\mathcal{O}(y^\nu)\rangle.$$

This identity is just a consequence of the definition of correlation functions by differentiating the generating functional. A straightforward use of this identity to access two-point functions would be by computing the dependence of the expectation value on the source. In the language of the bulk theory that would mean computing the sub-leading behavior ϕ_1 (see 6.3) as a function of the source ϕ_0 – which in practice means solving the full gravity system for an arbitrary boundary condition. However, one can simplify this task a lot by realizing that what matters in the formula above (6.7) is only the part that is *linear* in the source ϕ_0. This means that one only needs to compute the full solution for the fields to the linear order in sources, i.e analyze the linear perturbations of the gravitational theory around a given background solution. From the QFT perspective, this corresponds to a linear response analysis conducted in a thermodynamic equilibrium state. In the case presented, this will be the thermal state so perturbations around a black hole solutions will be considered.

If one is only interested in the zero-frequency values of transport coefficients, there is yet another simplification, stemming from the nature of formulas (5.28, 5.34). Since the coefficients appear as terms *linear in frequency*, it is enough to restrict analysis to linear order in frequency only. Technically, this leads to a major simplification of computations.

To summarize the strategy of obtaining transport coefficients from holography is the following:

(1) Construct a gravity action using symmetries as a guiding principle.
(2) Construct a solution of the equations of motion that captures the desired properties of the QFT state under consideration – for example a black hole for a thermal state.
(3) Find equations for linear perturbations around the given background solution.
(4) Linearize the equations from the point above in frequency.
(5) Find the solutions, and read the two-point functions (up to first order in frequency) from the near-boundary expansion.
(6) Use the Kubo formulas to extract the transport coefficients.

1.3.1. *An example computation.* As an example let us present how this procedure works for a classical computation – values of the even transport coefficients of the of a strongly coupled theory. The gravitational action of interest is then

$$(6.8) \qquad S_0 = \frac{1}{2\kappa^2} \int d^4x \sqrt{-g} \left[R + \frac{6}{L^2} - \frac{L^2}{4} F^{MN} F_{MN}\right].$$

The fields present in the action are metric and a $U(1)$ gauge field, which allows to compute stress-energy tensor and conserved current correlation functions, from which *shear viscosity* and *electric conductivity* can be extracted. From this action a well-known set of equations of motion (so called Einstein-Maxwell equations) follows

$$(6.9) \qquad R_{MN} - \frac{L^2 R + 3}{2L^2} g_{MN} - \frac{L^2}{2} F_{(M|P|} F_{N)}{}^P + \frac{L^2}{4} g_{MN} F_{PQ} F^{PQ} = 0,$$

$$(6.10) \qquad \nabla_M F^{MP} = 0.$$

Above R_{MN} is the Ricci curvature tensor. The first equation is the Einstein equation modified by the presence of the electromagnetic field, while the second one is the covariant Maxwell equation.

The following solution

$$(6.11) \qquad \frac{ds^2}{L^2} = g_{MN}dx^M dx^N = \frac{1}{r^2 f(r)}dr^2 + r_0^2 r^2 \left(-f(r)dt^2 + \left(dx^2 + dy^2\right)\right),$$

$$f(r) = \frac{(r-1)\left(-B^2 - \mu^2 r_0^2 + 4r\left(r^2 + r + 1\right)r_0^4\right)}{4r^4 r_0^4},$$

$$(6.12) \qquad F_{MN} = \partial_{[M}A_{N]}, \ A_N dx^N = \mu\left(1 - \frac{1}{r}\right)dt + Bxdy,$$

is dual to the thermodynamic equilibrium state with chemical potential μ, finite temperature (determined by the value of the constant r_0) and subject to external magnetic field B. The relation between the coefficient r_0 and the temperature T can be obtained by continuing the geometry to Euclidean signature and imposing regularity at the horizon, yielding the Hawking temperature of the black hole

$$(6.13) \qquad \frac{\left(-B^2 - \mu^2 r_0^2 + 12r_0^4\right)}{4r_0^3} = 4\pi T.$$

The chemical potential μ serves as a source for the 0-th component of the conserved current, i.e.the density, and is encoded in the boundary value of the bulk gauge field

$$(6.14) \qquad \mu = \lim_{r \to \infty} a(r).$$

To make use of the Kubo formulas one must take variations of the on-shell action, i.e. expand action (6.8) around the solution (6.11,6.12). Performing these variations will result in the formulas for the one-point functions in terms of the gravitational fields. For example, the variation of the gauge field gives the following

$$(6.15) \quad \frac{\delta S_0}{\delta A_C}\delta A_C = \frac{1}{2\kappa^2}\int d^4x\sqrt{-g}\left[-L^2 F^{MC}(\nabla_M \delta A_C)\right] =$$

$$\frac{1}{2\kappa^2}\int d^4x\sqrt{-g}\left[-L^2\nabla_M F^{MC}\delta A_C + L^2\nabla_M(F^{MC}\delta A_C)\right].$$

While the first term vanishes on-shell as it is essentially the equation of motion, the second is a total derivative that can be integrated by parts using the Stokes theorem

$$(6.16) \qquad \frac{1}{2\kappa^2}\int d^4x\sqrt{-g}\left[L^2\nabla_M(F^{MC}\delta A_C)\right] = \frac{1}{2\kappa^2}\int_{\Sigma} d^3\Sigma\left[L^2(F^{MC}\delta A_C)\right]n_M.$$

Above Σ denotes the boundary of the space and n_M – the outward pointing unit normal vector. The surface that contributes to the integral above is the conformal boundary of the space-time, located at $r \to \infty$, so the variation is due to the boundary value of the gauge field

$$(6.17) \qquad \frac{\delta S_0}{\delta A_C}\delta A_C = -\lim_{r \to \infty}\int d^3x L^2\frac{\sqrt{-g}}{2\kappa}F^{rM}\delta A_M.$$

It follows, that the one point function of the current defined as variation of the on-shell action with respect to the boundary value of the field assumes the following form

$$(6.18) \qquad J^i = \frac{\delta S_0}{\delta A_i} = -\lim_{r \to \infty}\int d^3x L^2\frac{\sqrt{-g}}{2\kappa}F^{ri}.$$

For the case of the stress tensor T^{ij} an analogues construction can be realized. Since is technically much more involved – a special counter-term is needed to regularize the variational problem for

the Einstein-Hilbert action [143] – the full derivation is omitted here. The result is

$$(6.19) \qquad T^{ij} = - \lim_{r \to \infty} L^2 r^2 \frac{\sqrt{-\gamma}}{\kappa^2} \left(K^{ij} - K\gamma^{ij} + \frac{2}{L}\gamma^{ij} \right),$$

and $\gamma^{ij}, \gamma, K^{ij}, K$ denote objects induced on a $r = constant$ hypersurface – metric, its determinant, extrinsic curvature and its trace respectively. With those formulas at hand one can compute the one point functions for arbitrary values of sources which, according to prescription (6.7), allow to read off two-point correlators.

To do so let us write perturbations around the background solution. Using formulas (5.28) and (5.34) one can infer that it ts not needed to take the most general form of perturbations to metric and the gauge field. The perturbations can then be simplified in the following way: first, they depend only on time and radial direction t, r while being homogeneous in the spatial directions. Also, the time dependence of the perturbations can be readily assumed to be in a Fourier form. Apart from that, only some components of the original metric (6.11) and gauge field (6.12) need to be perturbed, which yields the following form

(6.20a)
$$\frac{ds_\epsilon^2}{L^2} = \frac{ds^2}{L^2} + \epsilon L^2 r_0^2 r^2 \left[h_x(r)e^{-i\omega t} \left(dx^2 - dy^2 \right) + 2h_y(r)e^{-i\omega t}dxdy + 2\left(\frac{r_0 r}{L}\right) w_j(r)e^{-i\omega t}dtdx^j \right],$$
(6.20b)
$$A_{(\epsilon)} = A_N dx^N + \epsilon \left[b_x(r)e^{-i\omega t}dx + b_y(r)e^{-i\omega t}dy \right].$$

Above the perturbations have been classified according to their transformation properties under the O(2) rotational invariance of the boundary theory (since the fluctuations are spatially homogeneous, the equations remain symmetric under rotations). The classification is similar to the one presented in [144], although there a spatial momentum is introduced. The terms h_x, h_y are tensor modes that can be used to compute viscosities, while the terms w_j, b_j are vector modes that are related to the conductivities.

Now, the perturbative Ansatz (6.20) is inserted into the equations of motion (6.9, 6.10) and the equations are expanded in the small parameter ϵ to the linear order. As a result one obtains equations of motion for the small perturbations. The equations belonging to different sectors decouple, but in each sector mixing is allowed – i.e. equations for b_x can depend on b_y but not on h_x.

The equations of motion for the tensor perturbations h_i are the following

$$(6.21) \qquad \left(r^4 f(r)h_k'(r)\right)' + \omega^2 \frac{1}{r_0^2 f(r)}h_k(r) = 0$$

while in the vector sector a more complicated set is obtained

$$(6.22a) \qquad f(r)(r^4 w_i'(r))' - \frac{B^2 L^8}{r^2 r_0^4}w_i(r) + \frac{L^4 r^2 f(r)a'(r)}{r_0^2}b_i'(r) - \frac{iBL^8\omega}{r^2 r_0^4}\epsilon_{ij}b_j(r) = 0,$$

$$(6.22b) \qquad a'(r)w_i(r) + f(r)b_i'(r) + \epsilon_{ij}\frac{\omega}{iB}\left(a'(r)b_j(r) + \frac{r^2 r_0^2}{L^4}w_j'(r) \right) = 0.$$

For the sake of simplicity, in the following example only the solutions of the tensor sector equations, leading to the value of the shear viscosity will be presented. For the vector part the procedure is similar, albeit involves some technical difficulties which makes it less pedagogical.

Equations (6.21) have a singular point: the horizon of the space-time metric, where the function f vanishes. To regularize the behavior one must make the following substitutions:

$$(6.23) \qquad h_k(r) = f(r)^{-\frac{i\omega}{4\pi T}}p_k(r)$$

Then demanding functions p_k to be regular at the horizon $r = 1$ enforces the so-called *infalling boundary condition* which, from the duality point of view, ensures that the bulk fields encode the *retarded correlation functions*.

As the relevant regime is the hydrodynamic limit of the response functions, which means that ω/T is small, one can now expand the fluctuations and equations to linear order in the small parameter $\omega/(4\pi T)$

$$(6.24) \qquad p_k(r) = p_k^{(0)}(r) + \frac{\omega}{4\pi T}p_k^{(1)}(r) + \mathcal{O}\left(\frac{\omega}{4\pi T}\right)^2.$$

A key feature that makes this example especially simple is that the equations for different tensor modes decouple, so the p_x solution is independent of the p_y one. Already now one can infer that the model given by (6.8) does not support a non-zero value of the Hall viscosity.

The fluctuation equations of motion expanded to the first order in frequency form the following set

$$(6.25a) \qquad \left(r^4 f(r)p'^{(0)}(r)\right)' = 0,$$

$$(6.25b) \qquad \left(r^4 f(r)p'^{(1)}(r)\right)' - 2ir^4 f'(r)p'^{(0)}(r) - i\left(r^4 f'(r)\right)' p^{(0)}(r) = 0.$$

The general solution to the first one (6.25a) is

$$(6.26) \qquad p^{(0)}(r) = c_1 + c_2 \int (r^4 f(r))dr,$$

and since the part proportional to c_2 is singular at the horizon only the constant solution $p^{(0)}(r) = c_1$ is allowed. Then the first order equation can be readily integrated (6.25b) to yield

$$(6.27) \qquad p'^{(1)}(r) = ic_1\frac{f'(r) + c_2 r^{-4}}{f(r)},$$

which leads to the following regular solution

$$(6.28) \qquad p^{(1)}(r) = ic_1 \int\limits_\infty^r \frac{f'(s) - f'(1)r^{-4}}{f(r)}.$$

The solution for the metric perturbation takes than the following form

$$(6.29) \qquad h_k(r) \approx f(r)^{-\frac{i\omega}{4\pi T}}c_k\left(1 + \frac{i\omega}{4\pi T}i\int\limits_\infty^r \frac{f'(s) - f'(1)r^{-4}}{f(r)}\right).$$

Now, it is enough to evaluate formula (6.19) using perturbed metric (6.20) and the form of perturbation given above (6.29)

$$(6.30) \qquad G_T^{ij} = \begin{pmatrix} c_x\left(-L^2 M_{bh}r_0^3 + \frac{ir_0^2\omega}{L^4}\right) & c_y\left(-L^2 M_{bh}r_0^3 + \frac{ir_0^2\omega}{L^4}\right) \\ c_y\left(-L^2 M_{bh}r_0^3 + \frac{ir_0^2\omega}{L^4}\right) & -c_x\left(-L^2 M_{bh}r_0^3 + \frac{ir_0^2\omega}{L^4}\right) \end{pmatrix}.$$

Above M_{bh} denotes the mass of the black hole solution, which can be defined by expansion coefficient of the function f around the boundary

$$(6.31) \qquad f(r) \approx 1 - \frac{M_{bh}}{r^3} + \mathcal{O}(r^{-4}),$$

and for the solution (6.11) reads

$$(6.32) \qquad M_{bh} = \frac{B^2 + 4r_0^4 + \mu^2 r_0^2}{4r_0^4}.$$

To use the Kubo formulas (5.28) one needs 2-point functions, which can be extracted according to the prescription (6.7). Differentiation of (6.30) with respect to sources directly yields

$$(6.33) \qquad G_{TT}^{xy,xy} = \frac{\delta}{\delta c_y} G_T^{xy} = \left(L^2 M_{bh} r_0^3 + \frac{i r_0^2 \omega}{L^4} \right),$$

$$(6.34) \qquad G_{TT}^{xy,xx-yy} = \frac{\delta}{\delta c_x} G_T^{xy} = 0.$$

Comparing the result above with the Kubo formulas (5.28), one arrives at the following

$$(6.35) \qquad - L^2 M_{bh} r_0^3 + \frac{i r_0^2 \omega}{L^4} = -(p - BM) + i\omega\eta, \ \ -i\eta_H \omega = 0,$$

that implies

$$(6.36) \qquad (p - BM) = L^2 M_{bh} r_0^3,$$

$$(6.37) \qquad \eta = \frac{r_0^2}{L^4},$$

$$(6.38) \qquad \eta_H = 0.$$

In that way, the value of the transport coefficients is obtained. It is also shown, that the mass of the black hole determines thermodynamic quantity $p - BM$ (a combination of pressure and magnetic field), which is in accordance with the statement that the background space-time encodes the state of the system. Also, in agreement with the previous statement, the Hall viscosity of this toy model is zero.

Finally, the combination $\frac{r_0^2}{L^4}$ is the horizon surface element that encodes the Hawking entropy density s, resulting in the famous formula for the shear viscosity to entropy ratio [36]

$$(6.39) \qquad \eta = \frac{s}{4\pi}.$$

The next Section presents implementation of that scheme in order to obtain transport coefficients of a strongly coupled, magnetized fluid.

2. Transport coefficients for strongly coupled magnetised fluid

2.1. Gravitational model. The simplest holographic model that is incorporating magnetic fields is the Einstein-Maxwell theory, which admits dyonic black hole solutions dual to states of a strongly coupled theory at nonzero temperature, charge density and magnetic field [106]. When both charge and magnetic field are present, there is a nonzero Hall conductivity, but the Hall viscosity vanishes, even though it is not forbidden by symmetries and it is generated by a magnetic field in other cases, such as Quantum Hall systems. The first goal is to identify the ingredients necessary in a holographic model such that a Hall viscosity will be induced upon applying a magnetic field.

As was shown before in the example computation, a simple model (6.8) does not yield a non-zero value value of the Hall viscosity. From an effective theory point of view it is natural to look for a model with higher amount of derivatives. Also, higher-derivative actions have been successfully used in holographic description of the anomalous transport in 3+1 space-time dimensions [32].

The action of interest should involve coupling between the Riemann curvature tensor R_{ABCD} and electromagnetic field strength F_{MN} and the extra terms should introduce breaking the parity invariance of the system. In the following terms involving four derivatives will be considered. For simplicity all the four derivative terms that are parity even will be ignored and the terms with three derivatives (such as $\sim F^3$) or more than four derivatives will also not be taken into

account.[2] The most general action compatible with this requirements is

$$(6.40) \quad S = \frac{1}{2\kappa^2} \int d^4x \sqrt{-g} \left[R + \frac{6}{L^2} - \frac{L^2}{4} F^{MN} F_{MN} + \lambda_0 L^2 \mathcal{L}_0 + \sum_{i=1}^{5} \lambda_i L^4 \mathcal{L}_i \right] + S_{GH} + S_{CT} ,$$

where

$$(6.41) \qquad \mathcal{L}_0 = \epsilon^{MNPQ} F_{MN} F_{PQ} , \qquad \mathcal{L}_1 = \epsilon^{MNPQ} F_{MN} F_B^A R_{APQ}^B ,$$

$$(6.42) \qquad \mathcal{L}_2 = \epsilon^{MNPQ} R_{SRPQ} F_M^S F_N^R , \qquad \mathcal{L}_3 = \epsilon^{MNRP} R_{ARBP} F_M^A F_N^B ,$$

$$(6.43) \qquad \mathcal{L}_4 = \epsilon^{MNPQ} \nabla_A F_{MN} \nabla^A F_{PQ} , \qquad \mathcal{L}_5 = \frac{1}{2} \epsilon^{MNPQ} R^A{}_{BMN} R^B{}_{APQ} ,$$

where $\epsilon^{trxy} = -\frac{1}{\sqrt{-g}}$.

The term $\mathcal{L}_0$ introduces an anomalous Hall conductivity, while the term $\mathcal{L}_5$ in principle does not affect to the first order transport coefficients. In the literature $\mathcal{L}_0$ [104], and $\mathcal{L}_5$ [145] have also been considered including a coupling to an axion field. In this case, the last can produce a non-zero Hall viscosity. However, as the axion would count as a different source of parity breaking not related to the magnetic field, the approach presented here is to keep the coefficients of these terms constant and drop $\mathcal{L}_5$ from the subsequent analysis. On top of this, it can be shown that among the $\mathcal{L}_1, \ldots, \mathcal{L}_5$ only two of them are independent. Therefore, only λ_0, λ_1, and λ_3 are taken non-vanishing in present analysis. It is straightforward to derive the equations of motion for this action, but as they are not very illuminating, they are presented in Appendix B. The most apparent change that the new terms introduce is that the electric flux is not necessarily the same at the black hole horizon and the boundary (as it is in standard Einstein-Maxwell theory), which will be discussed in depth later.

2.2. Background solutions and thermodynamics. In the absence of higher derivative terms $\lambda_1 = \lambda_3 = 0$, the action (6.40) admits dyonic black hole solutions with non-zero charge and magnetic field, presented in the example before (6.11, 6.12). Assuming that in a consistent truncation of supergravity the couplings λ_1 and λ_3 should come as subleading corrections in the dual large-N, strong coupling expansions, and to avoid all the subtleties associated to having a higher derivative theory of gravity, one can treat those parameters perturbatively. In that way the black hole solution shall be similar to the dyonic black hole and the following Ansatz that generalizes the known black hole solutions can be taken as a starting point

$$(6.44) \qquad \frac{ds^2}{L^2} = \frac{1}{r^2 f(r)} dr^2 + r_0^2 r^2 \left(-f(r) dt^2 + C(r) \left(dx^2 + dy^2 \right) \right) , \quad A = a(r) dt + Bx dy ,$$

where again the factor r_0 comes from a convenient re-scaling of the equations such that the black hole horizon is located at $r = 1$. Functions $f(r)$, $C(r)$, $a(r)$ are assumed to be Taylor series in λ parameters that are assumed to be of the same order. Note that the coordinate r is dimensionless, but r_0 has dimensions of energy. Regularity of the Euclidean solution demands the following boundary conditions

$$(6.45) \qquad\qquad\qquad\qquad f(1) = a(1) = 0.$$

The chemical potential, as it was in the example case (6.14), is the source for the conserved current operator and is therefore determined by the value of the gauge potential at the boundary

$$(6.46) \qquad\qquad\qquad\qquad \mu = \lim_{r \to \infty} a(r).$$

Considering that the solutions are lengthy and not particularly enlightening, for the general case of $\mu \neq 0$ they are relegated (the explicit formulas for the solutions along with their associated thermodynamic quantities) to the appendix 2. Remarkably, the black hole is electrically charged

---

[2]For a discussion of the possible connection between parity-odd, 4-th order in derivatives holographic actions and effective actions for quantum Hall systems, see [35]

even in the absence of a chemical potential $\mu = 0$ –a peculiar consequence of the presence of λ_1 and λ_3 (see Eq. (B.12)). Actually, without chemical potential, the black hole solution takes the simple form of the electrically neutral dyonic black hole, but with a non vanishing electric field. For $\mu = 0$ the metric and gauge field are (to linear order in λ's)

$$(6.47) \qquad f(r) \;\; = \;\; 1 - \frac{B^2 + 4r_0^4}{4r_0^4 r^3} + \frac{B^2}{4r_0^4 r^4}, \qquad C(r) = 1,$$

$$(6.48) \qquad a(r) \;\; = \;\; (4\lambda_1 - \lambda_3)\left(\frac{20r_0^4 - 3B^2}{20rr_0^5} - \frac{(B^2 + 4r_0^4)}{4r^4 r_0^5} + \frac{2B^2}{5r^5 r_0^5} \right) B.$$

The solution given above allows to study the thermodynamic properties of the state in the dual theory. The temperature of the dual theory equals to the Hawking temperature of the black hole and reads

$$(6.49) \qquad\qquad T = \frac{r_0}{4\pi} f'(1),$$

notice that r_0 is a function of μ, B and T, which can be obtained by solving Eq. (6.49), also notice that the underlining conformal invariance implies that $r_0 = g(B/T^2, \mu/T)T$. The energy and charge densities are computed following the standard AdS/CFT dictionary (see table 1) and applying holographic renormalization methods (more details can be found in Appendix A). The following expressions are obtained

$$(6.50)\;\; \varepsilon = 2(p - MB) = \frac{2c_T r_0^3}{3} \lim_{r\to\infty} r^4 f'(r) \quad, \quad n = 8c_T B(2\lambda_1 + \lambda_3 - \lambda_0) + r_0 c_T \lim_{r\to\infty} r^2 a'(r),$$

where $c_T = L^2/2\kappa^2$ [3], p is the pressure and M is the magnetization $M = \frac{\partial p}{\partial B}$. The relation between the energy density and $p - MB$ follows from conformal invariance of the theory, but we have checked that it is satisfied by explicitly computing the expectation value of the stress tensor.

The entropy density is normally defined as the area of the black hole in Planck units, however, in the presence of higher derivative terms, there are additional contributions that can be computed using Wald's formula for the entropy [147]. In particular, for a static background the formula reads

$$(6.51) \qquad\qquad S = \frac{2\pi}{\kappa^2} \int_\Sigma Q^{ABCD} \nabla_A \chi_B \nabla_C \chi_D \sqrt{\sigma} dx^2 \equiv \int_\Sigma s\, dx^2,$$

with $Q^{ABCD} = -\frac{\partial \mathcal{L}}{\partial R_{ABCD}}$, χ the killing field generating the isometry of the horizon and $\sqrt{\sigma}$ being the determinant of the induced metric on the horizon. Upon evaluating the above, we get that total entropy density takes the form

$$(6.52) \qquad s = 4\pi c_T \frac{d\mathrm{Vol}_{2d}}{L^2} - 4\pi c_T \lambda_1 L^2 \,{}^\star F^{tr} F^{tr} = 4\pi c_T \left(r_0^2 C(1) + Ba'(1)\frac{4\lambda_1}{r_0} \right).$$

As can be seen in Eq. (6.52), the usual formula formula for the entropy as the area of the horizon gets modified by the λ_1 term. Actually the correction is proportional to the product of the magnetic field and electric flux evaluated at the horizon.

Particularizing the formulas above for the $\mu = 0$ geometry (6.48), the temperature and entropy density take the same form as in the dyonic black hole

$$(6.53) \qquad\qquad T = \frac{12r_0^4 - B^2}{16\pi r_0^3}, \qquad s = 4\pi c_T r_0^2.$$

---

[3]If the dual is a large-N gauge theory, $c_T \sim N^{3/2}$ [146] roughly counts the number of microscopic degrees of freedom.
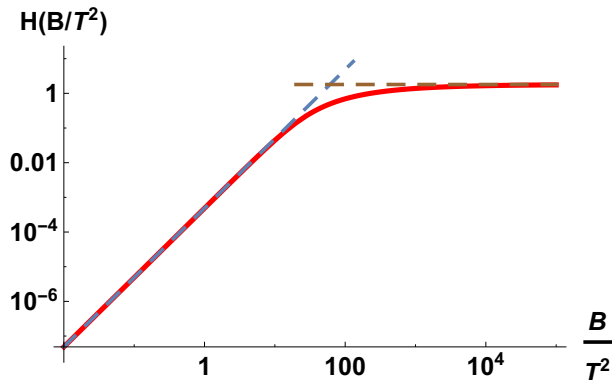
FIGURE 2. Temperature dependence of H in (6.54) as a function of the dimensionless parameter B/T^2. H interpolates between a power-law $\sim (B/T^2)^2$ at high temperatures $B/T^2 \ll 1$ and a constant at low temperatures $B/T^2 \gg 1$. Dashed lines show the asymptotic behavior.

It should be stressed here that the electric flux at the horizon is $O(\lambda)$, so the correction to the entropy density vanishes to leading order but there can be subleading corrections that have not been computed.

The charge density is non-zero, and takes the form

$$(6.54) \qquad n_B = c_T(4\lambda_1 - \lambda_3)H\left(\frac{B}{T^2}\right)B + c_T(12\lambda_1 + 9\lambda_3 - 8\lambda_0)B,$$

where the dimensionless function H is represented in Figure 2. In the plot one can observe two well defined asymptotic regions at high and low temperatures. At high temperatures the contribution proportional to H goes to zero and the density is determined by the second term in (6.54). At low temperatures H goes to a constant and both terms in the density contribute at the same order. In both cases the density has a linear dependence with B at leading order, but different proportionality constant.

The energy density, pressure and magnetization of the system take the form

$$(6.55) \qquad \varepsilon = c_T\frac{\left(B^2 + 4r_0^4\right)}{2r_0}, \qquad p = c_T\frac{\left(4r_0^4 - 3B^2\right)}{4r_0}, \qquad M = -c_T\frac{B}{r_0}.$$

As can be checked from Eqs. (6.55) the system obeys the condition $T^\mu_\mu = 0$ coming from conformal invariance.

2.3. Transport coefficients. According to the prescription mentioned in the introduction to this Chapter, to obtain the transport coefficients, one studies linear response around the equilibrium state described by the black hole Eq. (6.44). Linear response in the context of holography corresponds to solving the problem of small perturbations propagating on such black hole geometry. As was done in he example before, a small parameter $\epsilon \ll 1$ is introduced and the equations are then expanded to linear order in this parameter. The perturbed form of the metric and gauge field again is

$$ds_\epsilon^2 = ds_{(0)}^2 + \epsilon\, L^2 r_0^2 r^2 C(r)\left[h_x(r,t)\left(dx^2 - dy^2\right) + 2h_y(r,t)dxdy + 2w_j(r,t)dtdx^j\right] + \mathcal{O}(\epsilon^2),$$
(6.56)

$$A = a(r)dt + B\,x\,dy + \epsilon b_j(r,t)dx^j + \mathcal{O}(\epsilon^2).$$

The classification of the perturbations according to their transformation properties under the $O(2)$ rotational invariance of the boundary theory is the same as in the example studied before: the terms h_x, h_y are tensor modes that can be used to compute viscosities, while the terms w_j, b_j are vector modes that are related to the conductivities. The remaining components form

the scalar sector, that contains the bulk viscosity. Since the dual theory is conformal, the bulk viscosity vanishes $\zeta = 0$, which was confirmed by explicit calculation but but is omitted here, as it is straightforward but quite lengthy, and not particularly interesting since no other transport coefficients belong to this sector.

2.3.1. *Viscosities.* Since the main goal of this work is to investigate the Hall viscosity in a strongly couple magnetized plasma, the discussion begins with the perturbations in the tensor sector, that encodes this response coefficient. This sector is constituted by the fluctuations $h_x(r,t)$, $h_y(r,t)$ and responsible for the shear and Hall viscosities. In particular, after Fourier transforming the fields $h_i \to h_i(r)e^{-i\omega t}$, the equations of motions can be written as follows

$$(6.57) \qquad \left(r^4 F_1(r)f(r)h_k'(r)\right)' + i\omega\epsilon_{kj}F_2'(r)h_j(r) + \omega^2 F_3(r)h_k(r) = 0\,,$$

where

$$(6.58) \qquad F_1 \;=\; C(r) + (2\lambda_1 - \lambda_3)\frac{2Ba'(r)}{r^2 r_0^3}\,,$$

$$(6.59) \qquad F_2 \;=\; \frac{1}{r_0^3}(4\lambda_1 - \lambda_3)\left(\frac{B^2}{r^2 r_0^2 C(r)} - r^2 C(r)a'(r)^2\right)\,,$$

$$(6.60) \qquad F_3 \;=\; \frac{C(r)}{r_0^2 f(r)} + (2\lambda_1 - \lambda_3)\frac{2Ba'(r)}{r_0^5 r^2 f(r)}\,.$$

Remarkably, the simple structure of the tensor sector equations from the example 6.21 gets only slightly modified by the presence of the λ terms and the equations above can be obtained without exactly. Therefore a general solution is presented, and only at the end a perturbative background solution is used to read the concrete dependence of viscosities on temperature and magnetic field. Mind, that unlike the dyonic case (6.21), the equation above (6.57) introduces mixing between different tensor components $h_x(r,t)$ and $h_y(r,t)$. This mixing will result in a non-zero value of the Hall viscosity.

As the holographic dictionary establishes, one must find solutions satisfying an infalling boundary condition, which we guarantee by redefining the fields

$$(6.61) \qquad h_k(r) = f(r)^{-\frac{i\omega}{4\pi T}}p_k(r)\,,$$

and then requiring regularity at the horizon for $p_k(r)$. As before, it is only necessary to know of the fields up to linear order in the frequency ω. Therefore, a perturbative expansion in frequency is done, such that $p_k(r) = p_k^0(r) + \frac{\omega}{4\pi T}p_k^1(r)$. After doing so, the equations of motion read

$$(6.62) \qquad \left(r^4 F_1(r)f(r)p_k^{s\prime}(r)\right)' = S_k^s(r),$$

with

$$(6.63) \qquad S_k^0 = 0\,, \quad S_k^1 = i\frac{r^4 f'(r)}{f(r)}F_1(r)p_k^{0\prime}(r) + i\left(\frac{r^4 f'(r)}{f(r)}F_1(r)p_k^0(r)\right)' - 4i\pi T F_2'(r)\epsilon_{kj}p_j^0(r)\,.$$

A set of two linearly independent solutions can be constructed imposing regularity at the horizon, and considering independent boundary values h_y^0 and h_x^0 which are dual to sources for the stress tensor components $T^{xy}, T^{xx} - T^{yy}$. The system can be solved in terms of the background solution coefficients without doing any additional approximations, the result being

$$(6.64) \qquad p_k = h_k^0 + \frac{\omega}{4\pi T}\int_\infty^r \frac{g_k(x) - g_k(1)}{x^4 f(x)F_1(x)}\,dx\,, \quad g_k = i\frac{r^4 f'(r)}{f(r)}F_1(r)h_k^0 - 4i\pi T F_2(r)\epsilon_{kj}h_j^0\,.$$
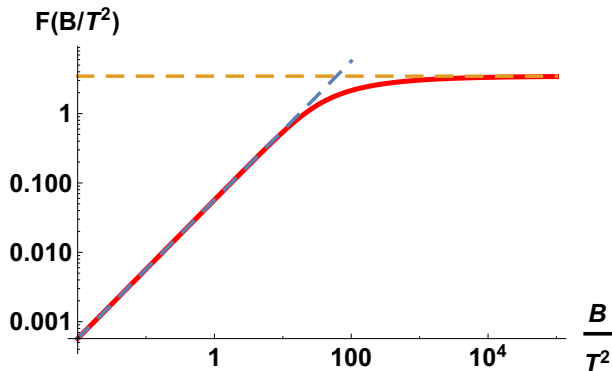
FIGURE 3. Hall viscosity ($\eta_H \sim F\left(\frac{B}{T^2}\right) B$) at zero chemical potential as a function of B/T^2 (red continuous line). Dashed lines show the asymptotic power laws. In particular blue dashed line corresponds to $F = \frac{9B}{16\pi^2 T^2}$, on the other hand orange dashed line corresponds with the fitting $F = 2\sqrt{3}$.

Which, after being plugged in Eq. (A.18) and combined with the Kubo relations Eq. (5.28), gives the values for the viscosities of the model

$$(6.65) \qquad \eta = \left(\frac{s}{4\pi} + \frac{2c_T\lambda_3}{r_0}Ba'(1)\right) \approx c_T r_0^2 \left[1 - (20\lambda_1 - 3\lambda_3)\frac{\mu B}{3r_0^3}\right] + \mathcal{O}(\lambda^2)$$

$$(6.66) \qquad \eta_H = (4\lambda_1 - \lambda_3)\left(C(1)a'(1)^2 - \frac{B^2}{C(1)r_0^2}\right) \approx c_T(4\lambda_1 - \lambda_3)r_0^{-2}\left((r_0\mu)^2 - B^2\right) + \mathcal{O}(\lambda^2)$$

Note that the Hall viscosity is not zero even at $\mu = 0$ as long as the magnetic field does not vanish,

$$(6.67) \qquad\qquad\qquad \eta_H = c_T(\lambda_3 - 4\lambda_1)F\left(\frac{B}{T^2}\right)B,$$

where, due to the underlying conformal invariance of the system, the function F depends only on the dimensionless combination B/T^2. In Fig. 3 the dependence of F as a function of the ratio B/T^2 is shown, from which one concludes that for small values of B/T^2 the Hall viscosity grows quadratically with B, while for large values the Hall viscosity grows linearly with the magnetic field and becomes independent of the temperature.

The shear viscosity at zero chemical potential satisfies the Kovtun-Son-Starinets (KSS) formula [36], but when $\mu \neq 0$, higher derivative corrections change the viscosity to entropy ratio, with the sign of the correction depending on the details of the model. In particular, the correction to the KSS formula is proportional to the coefficient λ_3, while the correction to the entropy density, Eq. (6.52), was proportional to λ_1.

2.3.2. *Conductivities.* This sector is given by the fields $w_i(r,t), b_i(r,t)$, that are responsible for the charge and thermal conductivities. The analysis is similar to the tensor modes, but the system of equations remains higher order in derivatives. In order to avoid the issue of having to solve higher order derivative equations, a perturbative expansion of the fluctuations in the couplings $\lambda_1 \sim \lambda_3 \sim \delta \ll 1$, as well as in the frequency $\omega/T \ll 1$ is done. The fluctuations $\Phi_i = (w_i, b_i)$ are expanded in the following way

$$(6.68) \qquad\qquad \Phi_i = \phi_i^{00}(r) + \delta\phi_i^{01} + \frac{\omega}{4\pi T}\left(\phi_i^{10} + \delta\phi_i^{11}\right) + \text{higher order terms},$$

where the first upper index refers to the order in the frequency and the second to the order in the higher derivative couplings. An explicit factor of the parameter δ was left to help follow the expansion, it should be noted that at the end of the calculation its value will be fixed to $\delta = 1$. Using this expansion yields a set of second order equations, as all the higher derivative

terms in the original equations are already of order δ, and so they all contribute only to source terms in the expanded equations. So, technically, the higher derivative terms are turned to higher derivatives of lower (in δ) order solutions present in source terms. After imposing ingoing boundary conditions in the following way applicable to vector perturbations

$$(6.69) \qquad w_j(r) = f(r)^{1-\frac{i\omega}{4\pi T}} v_j, \ b_k = f(r)^{-\frac{i\omega}{4\pi T}} q_k(r) \,,$$

the system of equations takes the form

$$(6.70) \qquad \left(r^4 f^2(r) \partial_r v_j^{\alpha\beta}\right)' = S_j^{\alpha\beta} \,,$$

$$(6.71) \qquad \partial_r q_j^{\alpha\beta} + \mu v_j^{\alpha\beta} = \tilde{S}_j^{\alpha\beta} \,,$$

where $S^{\alpha\beta}, \tilde{S}^{\alpha\beta}$ are source terms, that can depend on all the lower order perturbations and their derivatives up to order 3, which we show in the appendix 3. In contrast to the tensor sector, the vector perturbations are mixed by the equations of motion and yield odd transport coefficients also for $\lambda_1 = \lambda_3 = 0$ [106]. On the technical level this means that the source terms S_v, S_q are in general quite complicated even within this perturbative scheme and their integration is difficult. However, setting $\mu = 0$ significantly simplifies the system without trivializing the transport coefficients. Therefore only zero chemical potential case is treated here, and understood as the leading contribution in an expansion for small μ/T. The Eqs. (6.70) and (6.71) have the same form as the equations found in [106], therefore the same strategy to find the solutions can be followed. Finally, after solving these equations, their solutions are inserted into into the definition for the one point functions Eqs. (A.19) and (A.18) to extract the two point functions. In this sector the current-current and current-momentum correlators satisfy the relations predicted by hydrodynamics Eqs. (5.30). The momentum-momentum correlator reads

$$(6.72) \quad G_{TT}^{0i,0j} = \left(16\pi^2 c_T \frac{r_0^4 T^2}{B^2} i\omega + \frac{\varepsilon}{2}\right)\delta^{ij} - \frac{3\pi c_T T}{20 B^2 r_0^3}(4\lambda_1 - \lambda_3)\left(B^2 + 4r_0^4\right)\left(7B^2 + 60r_0^4\right) i\omega \epsilon^{ij} \,,$$

from which the heat conductivity $\bar{\kappa}$ can be obtained

$$(6.73) \qquad T\bar{\kappa}^{ij} = 16\pi^2 c_T \frac{r_0^4 T^2}{B^2}\delta^{ij} - \frac{3\pi c_T T}{20 B^2 r_0^3}(4\lambda_1 - \lambda_3)\left(B^2 + 4r_0^4\right)\left(7B^2 + 60r_0^4\right)\epsilon^{ij} \,.$$

In fact, by comparing the expression for the heat conductivity with Eq. (5.31), one can fix the values for the transport coefficients σ_V and $\bar{\sigma}_H$, which read

$$(6.74) \qquad \sigma_V = 9 c_T \frac{(r_0 - \pi T)^2}{\pi^2 T^2} \,,$$

and

$$(6.75) \qquad \bar{\sigma}_H = (4\lambda_1 - \lambda_3)\frac{3B^2 c_T}{20 r_0^4}\left[\frac{16\pi r_0^3 T \sigma_V^2}{9 B^2 c_T^2}\frac{9r_0 - 7\pi T}{r_0 - \pi T} + 1\right] + c_T(12\lambda_1 + 9\lambda_3 - 8\lambda_0).$$

The previous expression can be conveniently written as

$$(6.76) \qquad \bar{\sigma}_H = c_T(4\lambda_1 - \lambda_3)\sigma_t\left(\frac{B}{T^2}\right) + c_T\left(6(4\lambda_1 + \lambda_3) - 8\lambda_0\right) \,.$$

In Fig. 4 the functional dependence of σ_t at $\mu = 0$ is shown. For small values of B/T^2 σ_t grows quadratically, while at large values $\bar{\sigma}_H \sim \left(B/T^2\right)^{3/2}$. In the limit $B/T^2 \to 0$ σ_t vanishes, but there is a nonzero contribution to $\bar{\sigma}_H$, corresponding to an anomalous Hall conductivity.
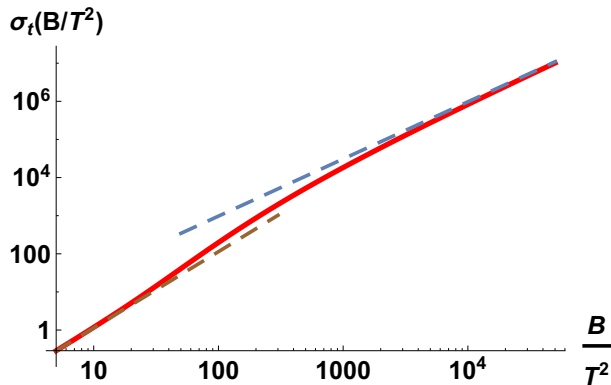
FIGURE 4. Function σ_t in (6.76) as a function of B/T^2 (continuous red line). Brown dashed line shows the high T behaviour $\sigma_t = B^2/T^4$. Blue dashed line represents $\sigma_t = \left(B/T^2\right)^{3/2}$.

2.3.3. *Anomalous Hall conductivity.* It follows from Eq. (6.76) that the presented system will in general have a non-vanishing anomalous Hall conductivity.

$$(6.77) \qquad\qquad \sigma_H^{\rm an} = c_T \left(6(4\lambda_1 + \lambda_3) - 8\lambda_0\right),$$

However, do notice that the value of the anomalous conductivity can be arbitrarily tuned by changing λ_0. From the point of view of the effective dual field theory the presence of this coupling corresponds to the addition of a Chern-Simons term (see action Eq. (6.40)). This modification only affects the definition of the field theory $U(1)$ current, e.g. Eq. (A.19), and consequently the charge density Eq. (6.54) and Hall conductivity (6.76). Interestingly, upon setting λ_0 to the value such that the anomalous Hall conductivity vanishes $\sigma_H^{\rm an} = 0$, i.e.

$$(6.78) \qquad\qquad \lambda_0 = \frac{3}{4}(4\lambda_1 + \lambda_3),$$

all odd transport coefficients and the charge density become proportional to the combination $(4\lambda_1 - \lambda_3)$ at $\mu = 0$. In particular, the charge density (6.54) reduces to

$$(6.79) \qquad\qquad n = c_T(4\lambda_1 - \lambda_3)\frac{3B\left(B^2 - 20r_0^4\right)}{20r_0^4}.$$

Even more interestingly, at large values of the magnetic field, the Hall viscosity becomes then proportional to the charge density

$$(6.80) \qquad\qquad \frac{\eta_H}{n} = \frac{5}{\sqrt{3}} + \mathcal{O}(T/\sqrt{B}).$$

This is similar to what happens in Quantum Hall states, with the difference that in known cases, such as Laughlin states, the coefficient is a fractional number.

3. Discussion of the results

Let us now comment a bit on the properties of transport coefficients and thermodynamics in the deformed dyonic black hole solution. For simplicity, only the case with no anomalous Hall conductivity (6.78) and $\mu = 0$ will be presented, although expressions for the thermodynamic quantities and viscosities at nonzero μ and other values of the coefficient λ_0 can also be found in the appendices 2. Since the theory is conformal, scaling arguments determine the dependence on the temperature/magnetic field with coefficients that can depend non-trivially on the dimensionless ratio B/T^2. It is thus equivalent to discuss low and high temperatures or large and small magnetic fields respectively. It should be mentioned that although the results at large magnetic field are found to be consistent with hydrodynamics, they are valid only as long as one

considers small enough spacetime derivatives of the thermodynamic variables – such that terms appearing at higher orders in the constitutive relations are suppressed.

At high temperatures $B/T^2 \ll 1$ thermodynamics is dominated by neutral degrees of freedom and the system behaves like a weakly magnetized conformal plasma

$$(6.81) \qquad \varepsilon \simeq \frac{128\pi^3}{27}c_T T^3\,, \qquad P \simeq \frac{\varepsilon}{2}\,, \qquad M \simeq -\frac{3c_T}{4\pi}\frac{B}{T}.$$

At low temperatures $B/T^2 \gg 1$ there is a "vacuum" contribution to the energy density

$$(6.82) \qquad \varepsilon \simeq \Lambda_B = \frac{2\sqrt{2}B^{3/2}c_T}{3^{3/4}}\,, \qquad P \simeq -\Lambda_B + Ts_B + O(\sqrt{B}),$$

where the entropy is proportional to the magnetic field

$$(6.83) \qquad s_B = \frac{2\pi B c_T}{\sqrt{3}}.$$

The magnetization is determined to leading order by the vacuum contribution $M \sim -\sqrt{B}$.

The charge density varies little between high and low temperatures, becoming a $2/5$ factor smaller at low temperatures

$$(6.84) \qquad \begin{aligned} &\frac{B}{T^2} \ll 1, \;\; n \simeq 3c_T(\lambda_3 - 4\lambda_1)B, \\ &\frac{B}{T^2} \gg 1, \;\; n \simeq \frac{6}{5}c_T(\lambda_3 - 4\lambda_1)B. \end{aligned}$$

The Hall conductivity then remains finite, with a change given by the same factor. Charge transport then remains largely independent of the temperature. The Hall viscosity however is more sensitive to the temperature. Taking the ratio with respect to the charge density

$$(6.85) \qquad \begin{aligned} &\frac{B}{T^2} \ll 1, \;\; \frac{\eta_H}{n} \simeq \frac{3}{16\pi^2}\frac{B}{T^2}, \\ &\frac{B}{T^2} \gg 1, \;\; \frac{\eta_H}{n} \simeq \frac{5}{\sqrt{3}}. \end{aligned}$$

In contrast to Hall charge transport, at high temperatures Hall viscous transport is strongly suppressed. Thermal and thermoelectric conductivities involve both charged and neutral degrees of freedom, so they are expected to be more sensitive to the particulars of the dyonic black hole geometry, such as the non-zero entropy density at zero temperature. It is worth noting that for small values of the higher derivative coefficients, the Hall thermal conductivity κ_H and the Seebeck coefficient $S = -\vartheta_{xx}$ are enhanced

$$(6.86) \qquad \begin{aligned} &\frac{B}{T^2} \ll 1, \;\; \frac{\kappa_H}{T} \simeq -\frac{(4\pi)^6}{3^5}\frac{c_T T^4}{B^2}\frac{1}{(\lambda_3 - 4\lambda_1)}, \;\; S \simeq \frac{64\pi^3}{27(\lambda_3 - 4\lambda_1)}\frac{T^2}{B}, \\ &\frac{B}{T^2} \gg 1, \;\; \frac{\kappa_H}{T} \simeq -\frac{10c_T\pi^2}{9}\frac{1}{(\lambda_3 - 4\lambda_1)}, \;\; S \simeq \frac{5\pi}{3\sqrt{3}(\lambda_3 - 4\lambda_1)}. \end{aligned}$$

Note that although these quantities depend on the inverse of the higher derivative couplings, they have been derived from a perturbative calculation of the transport coefficients obtained through the Kubo formulas, and applying formulas (5.38). As can be seen from those formulas, at zero density those transport coefficients diverge, which is consistent with the $1/\lambda$ behavior in the zero chemical potential regime presented above.

4. Summary and outlook

The chapter presented the way to obtain a non-zero Hall viscosity induced by a magnetic field in a holographic model via the introduction of higher derivative terms in the gravity action.

The key result of the computations – the Hall viscosity, as given in (6.65), receives two kinds of contributions, one proportional to the electric flux at the horizon produced by the charge

inside the black hole $a'(1)$ and another one independent of it. The charge inside the horizon has been associated with "fractionalized" or deconfined degrees of freedom [148, 149], while other contributions to transport have been dubbed confined, "mesonic" or "cohesive" [150]. Cohesive transport is present for instance in holographic superfluids [151–153], where some of the charge is carried by fields outside the horizon.

The fact that Hall transport is produced in part by the dynamics of the theory outside the horizon strongly suggests that similar behavior will also be possible in a geometry without horizons, *including holographic duals to gapped states.* This opens up the possibility of studying systems resembling much more Quantum Hall states, or at least some relativistic version. It should be noted that there is no obvious quantization of the coefficients of higher derivative terms, so there is no reason to expect Hall transport coefficients will be quantized even in the gapped systems. For the Hall conductivity, it is uncertain whether this is because we have not identified the right unit of conductance, it is a feature of the large-N limit, or there is no intrinsic quantization in strongly coupled relativistic systems, further work would be needed to explore this issue.

It would be interesting to understand better the meaning of the higher derivative terms from the point of view of the dual theory. Their structure suggests that they could be related to contributions in vacuum to the three point function of the energy-momentum tensor with two currents that are time-reversal and parity breaking. This could correspond to some type of explicit breaking by terms appearing at higher orders in a derivative expansion of the effective theory, or maybe an anomaly, although these are not topological terms. A weak coupling calculation could shed light on some of these questions.

Another interesting generalization of the presented work would be to construct the solutions of the holographic model at zero temperature – an extremal black hole solution. This is a non-trivial task, since the extremal solutions are known for causing problems bout in numerical and analytical treatment due to the presence of the asymptotic $\text{AdS}_2 \times \text{R}^2$ 'neck' as a near-horizon geometry. The zero-temperature behavior of the Hall viscosity is especially interesting since in this regime many other transport coefficients (i.e. shear viscosity) are suppressed. Apart from that a direct comparison of the holographic model with other models exhibiting odd transport, like Quantum Hall states would be possible at $T = 0$, as these models are usually under better analytical control in that regime.

Variational Principle and renormalization

As it generically happens, also in the presented case the higher derivative nature of the action (6.40) spoils the variational principle. So, in this appendix the possible boundary terms that can be added to 'regularize' the variational problem and to renormalize the theory are studied. First, the following ADM-style decomposition is performed

$$(A.1) \qquad ds^2 = dr^2 + \gamma_{ij} dx^i dx^j \,,$$

with the gauge condition $A_r = 0$, and the epsilon tensor defined as $\epsilon_{rtxy} = -\sqrt{-\gamma}$. The non vanishing components of the Christoffel symbols (and the extrinsic curvature) are

$$(A.2) \qquad -\Gamma^r_{ij} = K_{ij} = \frac{1}{2}\dot{\gamma}_{ij} \,,$$

$$(A.3) \qquad \Gamma^i_{jr} = K^i_j \,,$$

and $\hat{\Gamma}^i_{jk}$ are three dimensional Christoffel symbols computed with γ_{ij}. Dot denotes differentiation respect r. Another useful table of formulas is

$$(A.4) \qquad \dot{\hat{\Gamma}}^l_{ki} \;\; = \;\; D_k K^l_i + D_i K^l_k - D^l K_{ki} \,,$$

$$(A.5) \qquad R^r{}_{irj} \;\; = \;\; -\dot{K}_{ij} + K_{il} K^l_j \,,$$

$$(A.6) \qquad R^k{}_{rjr} \;\; = \;\; -\dot{K}^k_j - K^k_l K^l_j \,,$$

$$(A.7) \qquad R^r{}_{ijk} \;\; = \;\; D_k K_{ij} - D_j K_{ik} \,,$$

$$(A.8) \qquad R^l{}_{kri} \;\; = \;\; D_k K^l_i - D^l K_{ik} \,,$$

$$(A.9) \qquad R^i{}_{jkl} \;\; = \;\; \hat{R}^i{}_{jkl} - K^i_k K_{jl} + K^i_l K_{jk} \,,$$

with D_i the three dimensional covariant derivative compatible with γ_{ij}. Note that indices are now raised and lowered with γ_{ij}, e.g. $K = \gamma^{ij} K_{ij}$, and intrinsic three dimensional objects are denoted with a hat, so $\hat{R}^i{}_{jkl}$ is the intrinsic three dimensional Riemann tensor on the $r = $ const surface. Finally the Ricci scalar is

$$(A.10) \qquad R = \hat{R} - 2\dot{K} - K^2 - K_{ij} K^{ij} \,.$$

Now, upon writing the action, it is useful to divide it up in three terms. The first one is the Einstein-Maxwell part with the usual Gibbons-Hawking term included

$$(A.11) \qquad \mathcal{L}_{EM} = \frac{1}{2\kappa^2} \left(\hat{R} + 2\Lambda + K^2 - K_{ij} K^{ij} - \frac{1}{2} E_i E^i - \frac{1}{4} \hat{F}_{ij} \hat{F}^{ij} \right) \,,$$

where $E_i = \dot{A}_i$. The contributions to the action parametrized by λ_1 and λ_3 are

$$\mathcal{L}_1 = -\frac{2L^4}{\kappa^2} \epsilon^{ijk} \left(E_l \left[2 E_i D_k K^l_j - \hat{F}_{ij} K^l_m K^m_k + E_i \hat{F}_l{}^s \left(\hat{R}^l{}_{sjk} \; + 2 K^l_{[k} K_{j]s} \right) + 2 \hat{F}_{ij} \hat{F}^{ls} D_{[s} K_{l]k} \right] + \right.$$

$$(A.12) \qquad \left. -\hat{F}_{ij} E^l \dot{K}_{lk} \right) \,,$$

$$\mathcal{L}_3 = \frac{L^4}{\kappa^2} \epsilon^{ijk} \left(E_m \hat{F}_i{}^l \hat{R}^m{}_{jlk} + E_m \hat{F}_i{}^l K^m_k K_{jl} - E_m E_i D_j K^m_k + \hat{F}_i{}^l \hat{F}_j{}^s D_s K_{lk} + \hat{F}_{il} E_j K^l_s K^s_k + \right.$$

$$(A.13) \qquad \left. - \hat{F}_i{}^l E_j \dot{K}_{lk} \right) \,.$$

Taking variations of the action, the last terms in Eqs. (A.12) and (A.13) which are proportional to $\dot{K}_{lk}$ will produce a boundary contribution of the type $\sim \delta K_{ij} \sim \delta \dot{\gamma}_{ij}$, suggesting we can regularize the problem by adding the boundary term

$$(A.14) \qquad \delta S_{GH} = -\frac{1}{\kappa^2} \int d^3x \sqrt{\gamma} \epsilon^{ijk} \left(2\lambda_1 F_{ij} E^l - \lambda_3 F_i{}^l E_j \right) K_{lk} \,.$$

However, δS_{GH} would cancel the terms proportional to δK_{ij} at the price of introducing a new term proportional to δE_i. Therefore, Dirichlet boundary conditions can be fixed either for the metric or for the gauge field, but not simultaneously for both. This fact resemble the case in AdS_5 with the mixed gauge-gravitational Chern-Simons term [154–156], where a Gibbons-Hawking like term can be added but nonetheless, the regularity of the variational problem is not resolved. From a practical point of view, and in the context of this work, adding or not δS_{GH} does not affect the observables because the near boundary behaviour of the fields in an asymptotically locally AdS space is such that this boundary term always vanishes, as is discussed below.

On top of having a regular variational problem, the on-shell action needs to be finite, and so the proper counterterm which removes possible singularities needs to be found. However notice that the counterterm renormalizing Einstein-Maxwell theory has been previously computed [143], therefore the boundary action must have the following structure

$$(A.15) \qquad S_{CT} = -\frac{L}{2\kappa^2} \int d^3x \sqrt{\gamma} \left(\frac{4}{L^2} - \hat{R} \right) + \delta S_{CT}$$

where δS_{CT} is the contribution necessary to renormalize the parity odd terms in the action. Having applications to holography in mind one can however impose the boundary condition that the metric has an asymptotically locally AdS expansion of the form

$$(A.16) \qquad \gamma_{ij} = e^{2r} \left(g_{ij}^{(0)} + e^{-r} g_{ij}^{(1)} + \cdots \right) , \qquad A_i = A_i^{(0)} + e^{-r} A_i^{(1)} + \cdots ,$$

by inspection it is possible to conclude that δS_{GB}, $\mathcal{L}_1$ and $\mathcal{L}_3$ vanish fast enough on space-times with such asymptotic behaviour. Therefore,

$$(A.17) \qquad \delta S_{CT} = 0 \,.$$

Having studied the counterterms it is straightforward to compute the holographic one point functions of the $U(1)$ current and the stress energy tensor which read

$$(A.18) \qquad T^{ij} = -\lim_{r \to \infty} L^2 r^2 \frac{\sqrt{-\gamma}}{\kappa^2} \left(K^{ij} - K \gamma^{ij} + \frac{2}{L} \gamma^{ij} \right) ,$$

$$(A.19) \qquad J^i = -\lim_{r \to \infty} \frac{\sqrt{-g}}{2\kappa^2} \left(L^2 F^{ri} + H_1^{ri} + H_3^{ri} + 4\lambda_0 L^2 \epsilon^{ijk} F_{jk} \right) .$$

APPENDIX B

Equations of motion and solutions of the gravitiational theory

1. The full equations of motion

The structure of the equations of motion is the following

$$\text{(B.1)} \quad R_{MN} - \frac{L^2 R + 3}{2L^2} g_{MN} - \frac{L^2}{2} F_{(M|P|} F_{N)}^{\;P} + \frac{L^2}{4} g_{MN} F_{PQ} F^{PQ} + T_{1\;MN} + T_{3\;MN} = 0,$$

$$\text{(B.2)} \quad \nabla_M \left[L^2 F^{MP} + H_1^{MP} + H_3^{MP} \right] = 0.$$

where

$$\text{(B.3)} \quad T_1^{GS} = \lambda_1 L^4 \left(2\nabla_A \left(\nabla_L F^{A(G} \star F^{S)L} \right) + R_{PQ}^{B(G} F_B^{\;S)} \star F^{PQ} \right),$$

$$\text{(B.4)} \quad H_1^{MN} = -2\lambda_1 L^4 F_{AB} \left[R_{PQ}^{BA} \epsilon^{MNPQ} - R_{PQ}^{MN} \epsilon^{ABPQ} \right],$$

$$\text{(B.5)} \quad T_3^{GB} = \lambda_3 L^4 \left(F^{(GN} F_A^M \epsilon_{MNQP} R^{AQPB)} - \nabla_L \nabla_R \left[F_N^{\;L} \epsilon^{MNR(B} F_M^{\;G)} \right] \right),$$

$$\text{(B.6)} \quad H_3^{MN} = 4\lambda_3 L^4 \epsilon^{APQ[M|} R^{|N]}_{\;\;PBL} F_A^{\;B},$$

above $\star F^{SL} = \epsilon^{SLMN} F_{MN}$ stands for the Hodge dual of F_{MN}. Note, that due to the Lagrangian being fourth order in derivatives the given equations are in principle third order.

2. Background solutions

In this section the background solution for arbitrary chemical potential is shown, but only up linear order in the odd couplings λ_1, λ_3. The black hole Ansatz reads

$$\text{(B.7)} \quad \frac{ds^2}{L^2} = \frac{1}{r^2 f(r)} dr^2 + r_0^2 r^2 \left(-f(r) dt^2 + C(r) \left(dx^2 + dy^2 \right) \right), \quad A = a(r) dt + Bx dy.$$

After evaluating Eqs. (B.1) and (B.2) on it, linearizing the equations and solving them, the following solution for the background metric and gauge field is obtained

$$\text{(B.8)} \quad f(r) = \frac{(r-1)\left(-B^2 - \mu^2 r_0^2 + 4r \left(r^2 + r + 1 \right) r_0^4 \right)}{4r^4 r_0^4} +$$

$$- \frac{B\mu(8\lambda_1 + 3\lambda_3) \left(B^2 \left(r^4 - 1 \right) + \mu^2 \left((3 - 2r)r^4 - 1 \right) r_0^2 \right)}{60 r^8 r_0^7} +$$

$$\frac{B\mu(r-1)(4\lambda_1 - 3\lambda_3) \left(B^2 \left(r^4 - 2 \right) + \mu^2 \left(r^4 - 2 \right) r_0^2 + 4r(r(r(2-3r)+2)+2)r_0^4 \right)}{24 r^8 r_0^7},$$

$$\text{(B.9)} \quad C(r) = 1 + \frac{B\mu(8\lambda_1 + 3\lambda_3)}{3r^4 r_0^3},$$

$$\text{(B.10)} \quad a(r) = \mu \left(1 - \frac{1}{r} \right) - \frac{B \left(\mu^2 r_0^2 (68\lambda_1 + 3\lambda_3) + 3(4\lambda_1 - \lambda_3) \left(3B^2 - 20 r_0^4 \right) \right)}{60 r r_0^5} +$$

$$+ \frac{B \left(6B^2(4\lambda_1 - \lambda_3) + \mu^2 r_0^2(32\lambda_1 - 3\lambda_3) \right)}{15 r^5 r_0^5} - \frac{B(4\lambda_1 - \lambda_3) \left(B^2 + \mu^2 r_0^2 + 4 r_0^4 \right)}{4 r^4 r_0^5}.$$

The knowledge of the background allows to compute the temperature T, and the one point functions of the current and stress-energy tensor after evaluating (6.50)

(B.11)
$$T \approx \frac{12r_0^4 - B^2 - \mu^2 r_0^2}{16\pi r_0^3} + \frac{\mu B \left(3B^2(28\lambda_1 + 3\lambda_3) + \mu^2 r_0^2(52\lambda_1 - 3\lambda_3) + 60r_0^4(3\lambda_3 - 4\lambda_1)\right)}{480\pi r_0^6}$$

(B.12)
$$\rho \approx c_T r_0 \mu + \left(\frac{3B^2}{20r_0^4}(4\lambda_1 - \lambda_3) + \frac{\mu^2}{60r_0^2}(68\lambda_1 + \lambda_3) + 3(4\lambda_1 + 3\lambda_3) - 8\lambda_0\right) c_T B.$$

(B.13)
$$\varepsilon \approx \frac{c_T \left(B^2 + 4r_0^4 + \mu^2 r_0\right)}{2r_0} + \frac{c_T \mu B \left(5 \left(B^2 - 12r_0^4\right)(4\lambda_1 - 3\lambda_3) + \mu^2 r_0(52\lambda_1 - 3\lambda_3)\right)}{60r_0^4},$$

(B.14)
$$M \approx c_T \left(-\frac{B}{r_0} - \frac{\mu^2(r_0 - 1)}{2B}\right) - \frac{4c_T \mu \left(6 \left(5\lambda_0 - 16\lambda_1 - 6\lambda_3\right) r_0 + \pi \left(68\lambda_1 + 3\lambda_3\right) T\right)}{15r_0} + \mathcal{O}(\mu^3),$$

and the pressure satisfy the relation $p = \frac{\varepsilon}{2} + BM$. Finally, also the entropy can be evaluated

(B.15)
$$s \approx 4\pi c_T r_0^2 \left(1 - \frac{\mu B(4\lambda_1 - 3\lambda_3)}{3r_0^3}\right) + O\left(\lambda^2\right).$$

Interestingly, although the density (B.12) at zero chemical potential is non-zero and a function of magnetic field (6.54), the first order term in entropy density in (B.15) is proportional to the chemical potential, and therefore vanishes when $\mu = 0$. So, the presented holographic action describes a theory in which at zero chemical potential some charge density is induced by the presence of magnetic field, but this charge density *does not contribute to the total entropy*.

3. Sources for the perturbative equations in the vectors sector

The explicit form of the sources introduced in Sec. 2.3.2 are presented below. For simplicity the chemical potential is set to zero $\mu = 0$ and the previous order solutions are evaluated in

some of them.

(B.16)

$$S_j^{00} = 0$$

(B.17)

$$\tilde{S}_j^{00} = 0$$

(B.18)

$$S_j^{10} = -\frac{i\left(B^4\left(r\left(r^2+r-8\right)+20\right)-8B^2r(5r(r+1)+14)r_0^4+144r^2(r+1)r_0^8\right)}{(r-1)r^2\left(B^2-4r\left(r^2+r+1\right)r_0^4\right)^2}w_j^0$$

(B.19)

$$\tilde{S}_j^{10} = \frac{i(r+1)\left(B^2-12r_0^4\right)\left(B^2(3r-4)+12rr_0^4\right)}{4Brr_0\left(B^2-4r\left(r^2+r+1\right)r_0^4\right)}w_j^0$$

(B.20)

$$S_j^{01} = 0$$

(B.21)

$$\tilde{S}_j^{01} = -\frac{B(4\lambda_1-\lambda_3)\left(B^2\left(3r^4+20r-40\right)-20r\left(r^3-4\right)r_0^4\right)}{20r^6r_0^5}w_j^0$$

$$S_j^{11} = \frac{(4\lambda_1-\lambda_3)\epsilon_{ji}w_i^0}{r^{11}r_0^{12}f_0(r)^2}\left(ir^{10}r_0^8\left(B^2-12r_0^4\right)f_0'(r)^2+\right.$$

$$-\frac{1}{80}ir^5r_0^4\left(B^2-12r_0^4\right)f_0'(r)\left(B^2\left(3r^4+20r-50\right)-240r^4r_0^4f_0(r)+20r\left(5r^3+4\right)r_0^4\right)+$$

$$3ir^8r_0^8\left(B^2-12r_0^4\right)f_0(r)^2-\frac{1}{4}ir^4r_0^4\left(B^2-12r_0^4\right)f_0(r)\left(B^2+12r^4r_0^4\right)+$$

(B.22)

$$\frac{1}{320}i\left(B^2-12r_0^4\right)\left(B^4\left(7r^5-12r^4-20r+32\right)-8B^2r\left(\left((3r-10)r^3+10\right)r_0^4-720r^5r_0^8\right)\right)$$

$$\tilde{S}_j^{11} = -\frac{B(4\lambda_1-\lambda_3)v_i^{10}(r)\left(B^2\left(3r^4+20r-40\right)-20r\left(r^3-4\right)r_0^4\right)}{20r^6r_0^5}+$$

$$\frac{iw_i^0(r-1)}{320Br^{10}f_0(r)r_0^9}(4\lambda_1-\lambda_3)\left(B^6\left(r\left(r\left(r\left(r\left(3r\left(r^2+r-6\right)+76\right)-12\right)-12\right)+48\right)-128\right)+$$

$$-4B^4r(r(r(r(r(23r(r+1)+26)+264)-56)-56)-176)r_0^4+$$

(B.23)

$$+48B^2r^2(r(r(r(19r(r+1)+70)+100)-20)-20)r_0^8-2880r^5\left(r^2+r-2\right)r_0^{12}\right)$$

Bibliography

[1] C. Fefferman, "Existence and smoothness of the Navier–Stokes Equation." Clay mathematics institute, 2000.
`http://www.claymath.org/sites/default/files/navierstokes.pdf`.

[2] M. Vogelsberger, S. Genel, V. Springel, P. Torrey, D. Sijacki, D. Xu, G. Snyder, S. Bird, D. Nelson, and L. Hernquist, "Properties of galaxies reproduced by a hydrodynamic simulation," *Nature* **509** no. 7499, (May, 2014) 177–182.
`http://dx.doi.org/10.1038/nature13316`.

[3] B. P. Moster, A. V. Macciò, and R. S. Somerville, "Numerical hydrodynamic simulations based on semi-analytic galaxy merger trees: method and Milky Way-like galaxies," *Monthly Notices of the Royal Astronomical Society* **437** no. 2, (Nov, 2013) 1027–1044.
`http://dx.doi.org/10.1093/mnras/stt1702`.

[4] O. M. Blaes, "Physics fundamentals of luminous accretion disks around black holes," *Les Houches Lect. Notes* **78** (2004) 137–185, `arXiv:astro-ph/0211368`.

[5] J. D. Bjorken, "Highly relativistic nucleus-nucleus collisions: the central rapidity region," *Physical Review D* **27** (Jan, 1983) 140–151.
`https://link.aps.org/doi/10.1103/PhysRevD.27.140`.

[6] S. Chatrchyan, V. Khachatryan, A. Sirunyan, A. Tumasyan, W. Adam, E. Aguilo, T. Bergauer, M. Dragicevic, J. Erö, C. Fabjan et al., "Observation of long-range, near-side angular correlations in pPb collisions at the LHC," *Physics Letters B* **718** no. 3, (Jan, 2013) 795–814. `http://dx.doi.org/10.1016/j.physletb.2012.11.025`.

[7] W. Florkowski and R. Ryblewski, "Highly anisotropic and strongly dissipative hydrodynamics for early stages of relativistic heavy-ion collisions," *Physical Review C* **83** no. 3, (Mar, 2011). `http://dx.doi.org/10.1103/PhysRevC.83.034907`.

[8] J. L. Nagle, R. Belmont, K. Hill, J. O. Koop, D. V. Perepelitsa, P. Yin, Z.-W. Lin, and D. McGlinchey, "Minimal conditions for collectivity in e+e- and p+p collisions," *Physical Review C* **97** no. 2, (Feb, 2018). `http://dx.doi.org/10.1103/PhysRevC.97.024909`.

[9] F. Jülicher, S. W. Grill, and G. Salbreux, "Hydrodynamic theory of active matter," *Reports on Progress in Physics* **81** no. 7, (Jun, 2018) 076601.
`https://doi.org/10.1088%2F1361-6633%2Faab6bb`.

[10] L. Landau and E. Lifshitz, *Fluid mechanics*, vol. 6 of *Landau and Lifshitz Course of Theoretical Physics*. Elsevier Science, 2013.
`https://books.google.pl/books?id=eOBbAwAAQBAJ`.

[11] S. J. Putterman, *Superfluid hydrodynamics*, vol. 3 of *North-Holland Series in Low Temperature Physics*. Amsterdam, North-Holland Publishing Co.; New York, American Elsevier Publishing Co., Inc., 1974.

[12] C. Cao, E. Elliott, J. Joseph, H. Wu, J. Petricka, T. Schafer, and J. E. Thomas, "Universal quantum viscosity in a unitary Fermi gas," *Science* **331** no. 6013, (Dec, 2010) 58–61. `http://dx.doi.org/10.1126/science.1195219`.

[13] D. Forster, *Hydrodynamic fluctuations, broken symmetry, and correlation functions*. CRC Press, 2018.

[14] R. N. Gurzhi, "Minimum of resistance in impurity-free conductors," *Soviet Physics – JETP* **44** no. 2, (1963) 771–772.

[15] R. N. Gurzhi, "Hydrodynamic effects in solids at low temperature," *Soviet Physics Uspekhi* **11** no. 2, (Feb, 1968) 255–270.

[16] L. Molenkamp and M. de Jong, "Observation of Knudsen and Gurzhi transport regimes in a two-dimensional wire," *Solid-State Electronics* **37** no. 4-6, (Apr, 1994) 551–553.

[17] L. Levitov and G. Falkovich, "Electron viscosity, current vortices and negative nonlocal resistance in graphene," *Nature Physics* **12** no. 7, (Feb, 2016) 672–676.

[18] D. A. Bandurin, I. Torre, R. K. Kumar, M. B. Shalom, A. Tomadin, A. Principi, G. H. Auton, E. Khestanova, K. S. Novoselov, I. V. Grigorieva, L. A. Ponomarenko, A. K. Geim, and M. Polini, "Negative local resistance caused by viscous electron backflow in graphene," *Science* **351** no. 6277, (Feb, 2016) 1055–1058.

[19] P. Alekseev, "Negative magnetoresistance in viscous flow of two-dimensional electrons," *Physical Review Letters* **117** no. 16, (Oct, 2016).
https://doi.org/10.1103/physrevlett.117.166601.

[20] P. S. Alekseev, "Magnetic resonance in a high-frequency flow of a two-dimensional viscous electron fluid," *Physical Review B* **98** no. 16, (Oct, 2018).
https://doi.org/10.1103/physrevb.98.165440.

[21] A. P. Mackenzie, "The properties of ultrapure delafossite metals," *Reports on Progress in Physics* **80** no. 3, (Jan, 2017) 032501.

[22] I. Matthaiakakis, D. Rodríguez Fernández, C. Tutschku, E. M. Hankiewicz, J. Erdmenger, and R. Meyer, "Functional dependence of Hall viscosity induced transverse voltage in two-dimensional Fermi liquids," *Physical Review B* **101** no. 4, (Jan, 2020). http://dx.doi.org/10.1103/PhysRevB.101.045423.

[23] K. A. Guerrero-Becerra, F. M. D. Pellegrino, and M. Polini, "Magnetic hallmarks of viscous electron flow in graphene," *Physical Review B* **99** no. 4, (Jan, 2019).
http://dx.doi.org/10.1103/PhysRevB.99.041407.

[24] A. I. Berdyugin, S. G. Xu, F. M. D. Pellegrino, R. Krishna Kumar, A. Principi, I. Torre, M. Ben Shalom, T. Taniguchi, K. Watanabe, I. V. Grigorieva, M. Polini, A. K. Geim, and D. A. Bandurin, "Measuring Hall viscosity of graphene's electron fluid," *Science* **364** no. 6436, (2019) 162–165, arXiv:1806.01606.
https://science.sciencemag.org/content/364/6436/162.

[25] H. Guo, E. Ilseven, G. Falkovich, and L. S. Levitov, "Higher-than-ballistic conduction of viscous electron flows," *Proceedings of the National Academy of Sciences* **114** no. 12, (Mar, 2017) 3068–3073. https://doi.org/10.1073/pnas.1612181114.

[26] R. K. Kumar, D. A. Bandurin, F. M. D. Pellegrino, Y. Cao, A. Principi, H. Guo, G. H. Auton, M. B. Shalom, L. A. Ponomarenko, G. Falkovich, K. Watanabe, T. Taniguchi, I. V. Grigorieva, L. S. Levitov, M. Polini, and A. K. Geim, "Superballistic flow of viscous electron fluid through graphene constrictions," *Nature Physics* (Aug, 2017).
https://doi.org/10.1038/nphys4240.

[27] J. Crossno, J. K. Shi, K. Wang, X. Liu, A. Harzheim, A. Lucas, S. Sachdev, P. Kim, T. Taniguchi, K. Watanabe, T. A. Ohki, and K. C. Fong, "Observation of the Dirac fluid and the breakdown of the Wiedemann-Franz law in graphene," *Science* **351** no. 6277, (Feb, 2016) 1058–1061.

[28] R. Moessner, P. Surówka, and P. Witkowski, "Pulsating flow and boundary layers in viscous electronic hydrodynamics," *Physical Review B* **97** no. 16, (Apr, 2018).
https://doi.org/10.1103/physrevb.97.161112.

[29] K. v. Klitzing, G. Dorda, and M. Pepper, "New method for high-accuracy determination of the fine-structure constant based on quantized Hall resistance," *Physical Review Letters* **45** (Aug, 1980) 494–497.
https://link.aps.org/doi/10.1103/PhysRevLett.45.494.

[30] J.-i. Wakabayashi and S. Kawaji, "Hall effect in silicon MOS inversion layers under strong magnetic fields," *Journal of the Physical Society of Japan* **44** no. 6, (1978)

1839–1849. `https://doi.org/10.1143/JPSJ.44.1839`.

[31] B. N. Narozhny and M. Schütt, "Magnetohydrodynamics in graphene: shear and Hall viscosities," *Physical Review B* **100** no. 3, (Jul, 2019). `http://dx.doi.org/10.1103/PhysRevB.100.035125`.

[32] K. Landsteiner, "Notes on anomaly induced transport," *Acta Physica Polonica B* **47** no. 12, (Jan, 2016) 2617, `arXiv:1610.04413 [hep-th]`.

[33] T. Scaffidi, N. Nandi, B. Schmidt, A. P. Mackenzie, and J. E. Moore, "Hydrodynamic electron flow and Hall viscosity," *Physical Review Letters* **118** no. 22, (Jun, 2017). `https://doi.org/10.1103/physrevlett.118.226601`.

[34] F. M. D. Pellegrino, I. Torre, and M. Polini, "Nonlocal transport and the Hall viscosity of two-dimensional hydrodynamic electron liquids," *Physical Review B* **96** (Nov, 2017) 195401.

[35] C. Hoyos, F. Peña-Benitez, and P. Witkowski, "Hall viscosity in a strongly coupled magnetized plasma," *Journal of High Energy Physics* **2019** no. 8, (Aug, 2019) 146. `https://doi.org/10.1007/JHEP08(2019)146`.

[36] P. Kovtun, D. T. Son, and A. O. Starinets, "Viscosity in strongly interacting quantum field theories from black hole physics," *Physical Review Letters* **94** (2005) 111601, `arXiv:hep-th/0405231 [hep-th]`.

[37] E. Shuryak, "Strongly coupled quark-gluon plasma in heavy ion collisions," *Reviews of Modern Physics* **89** (Jul, 2017) 035001. `https://link.aps.org/doi/10.1103/RevModPhys.89.035001`.

[38] C. Charmousis, B. Goutéraux, B. Soo Kim, E. Kiritsis, and R. Meyer, "Effective holographic theories for low-temperature condensed matter systems," *Journal of High Energy Physics* **2010** no. 11, (Nov, 2010). `http://dx.doi.org/10.1007/JHEP11(2010)151`.

[39] O. DeWolfe, S. S. Gubser, and C. Rosen, "A holographic critical point," *Physical Review D* **83** no. 8, (Apr, 2011). `http://dx.doi.org/10.1103/PhysRevD.83.086005`.

[40] S. A. Hartnoll, P. K. Kovtun, M. Muller, and S. Sachdev, "Theory of the Nernst effect near quantum phase transitions in condensed matter, and in dyonic black holes," *Physical Review* **B76** (2007) 144502, `arXiv:0706.3215 [cond-mat.str-el]`.

[41] L. P. Kadanoff and P. C. Martin, "Hydrodynamic equations and correlation functions," *Annals of Physics* **281** no. 1, (2000) 800 – 852. `http://www.sciencedirect.com/science/article/pii/S0003491600960238`.

[42] A. Lucas, "Stokes paradox in electronic Fermi liquids," *Physical Review B* **95** no. 11, (Mar, 2017). `https://doi.org/10.1103/physrevb.95.115425`.

[43] P. Romatschke and U. Romatschke, *Relativistic fluid dynamics in and out of equilibrium – ten years of progress in theory and numerical simulations of nuclear collisions.* Cambridge University Press, 2019 `https://doi.org/10.1017/9781108651998`, `arXiv:1712.05815 [nucl-th]`.

[44] D. H. Rischke, "Fluid dynamics for relativistic nuclear collisions," *Lecture Notes in Physics* (1999) 21–70. `http://dx.doi.org/10.1007/BFb0107310`.

[45] B. Withers, "Short-lived modes from hydrodynamic dispersion relations," *Journal of High Energy Physics* **2018** no. 6, (Jun, 2018) 59. `https://doi.org/10.1007/JHEP06(2018)059`.

[46] S. c. v. Grozdanov, P. K. Kovtun, A. O. Starinets, and P. Tadić, "Convergence of the gradient expansion in hydrodynamics," *Physical Review Letters* **122** (Jun, 2019) 251601. `https://link.aps.org/doi/10.1103/PhysRevLett.122.251601`.

[47] D. Tong, "Kinetic theory." On-line, `http://www.damtp.cam.ac.uk/user/tong/kinetic.html`, 2012. Lecture notes.

[48] P. Romatschke, "Relativistic (lattice) Boltzmann equation with nonideal equation of state," *Physical Review D* **85** no. 6, (Mar, 2012).

`http://dx.doi.org/10.1103/PhysRevD.85.065012`.

[49] A. Lucas and K. C. Fong, "Hydrodynamics of electrons in graphene," *Journal of Physics: Condensed Matter* **30** no. 5, (Jan, 2018) 053001.
`https://doi.org/10.1088/1361-648x/aaa274`.

[50] J. A. Sulpizio, L. Ella, A. Rozen, J. Birkbeck, D. J. Perello, D. Dutta, M. Ben-Shalom, T. Taniguchi, K. Watanabe, T. Holder et al., "Visualizing Poiseuille flow of hydrodynamic electrons," *Nature* **576** no. 7785, (Dec, 2019) 75–79.
`http://dx.doi.org/10.1038/s41586-019-1788-9`.

[51] I. Torre, A. Tomadin, A. K. Geim, and M. Polini, "Nonlocal transport and the hydrodynamic shear viscosity in graphene," *Physical Review B* **92** no. 16, (Oct, 2015).

[52] A. Tomadin, G. Vignale, and M. Polini, "Corbino disk viscometer for 2D quantum electron liquids," *Physical Review Letters* **113** no. 23, (Dec, 2014).
`https://doi.org/10.1103/physrevlett.113.235901`.

[53] R. L. Panton, *Incompressible flow.* Wiley, 2013.

[54] P. J. W. Moll, P. Kushwaha, N. Nandi, B. Schmidt, and A. P. Mackenzie, "Evidence for hydrodynamic electron flow in PdCoO2," *Science* **351** no. 6277, (Feb, 2016) 1061–1064.

[55] B. N. Narozhny, I. V. Gornyi, A. D. Mirlin, and J. Schmalian, "Hydrodynamic approach to electronic transport in graphene," *Annalen der Physik* **529** no. 11, (2017) 1700043.

[56] E. Banks, A. Donos, J. P. Gauntlett, T. Griffin, and L. Melgar, "Thermal backflow in CFTs," *Physical Review D* **95** no. 2, (Jan, 2017).
`http://dx.doi.org/10.1103/PhysRevD.95.025022`.

[57] R. Shankar, "Renormalization-group approach to interacting fermions," *Reviews of Modern Physics* **66** no. 1, (Jan, 1994) 129–192.
`http://dx.doi.org/10.1103/RevModPhys.66.129`.

[58] J. González, F. Guinea, and M. Vozmediano, "Non-Fermi liquid behavior of electrons in the half-filled honeycomb lattice (A renormalization group approach)," *Nuclear Physics B* **424** no. 3, (Aug, 1994) 595–618. `http://dx.doi.org/10.1016/0550-3213(94)90410-3`.

[59] J. González, F. Guinea, and M. A. H. Vozmediano, "Marginal-Fermi-liquid behavior from two-dimensional Coulomb interaction," *Physical Review B* **59** no. 4, (Jan, 1999) R2474–R2477. `http://dx.doi.org/10.1103/PhysRevB.59.R2474`.

[60] D. E. Sheehy and J. Schmalian, "Quantum critical scaling in graphene," *Physical Review Letters* **99** no. 22, (Nov, 2007). `http://dx.doi.org/10.1103/PhysRevLett.99.226803`.

[61] I. Torre, L. Vieira de Castro, B. Van Duppen, D. Barcons Ruiz, F. M. Peeters, F. H. L. Koppens, and M. Polini, "Acoustic plasmons at the crossover between the collisionless and hydrodynamic regimes in two-dimensional electron liquids," *Physical Review B* **99** no. 14, (Apr, 2019). `http://dx.doi.org/10.1103/PhysRevB.99.144307`.

[62] A. Lucas and S. Das Sarma, "Electronic sound modes and plasmons in hydrodynamic two-dimensional metals," *Physical Review B* **97** no. 11, (Mar, 2018).
`http://dx.doi.org/10.1103/PhysRevB.97.115449`.

[63] T. Holder, R. Queiroz, and A. Stern, "Unified description of the classical Hall viscosity," *Physical Review Letters* **123** no. 10, (Sep, 2019).
`http://dx.doi.org/10.1103/PhysRevLett.123.106801`.

[64] E. G. Richardson and E. Tyler, "The transverse velocity gradient near the mouths of pipes in which an alternating or continuous flow of air is established," *Proceedings of the Physical Society* **42** no. 1, (Dec, 1929) 1–15.
`https://doi.org/10.1088/0959-5309/42/1/302`.

[65] R. Moessner, N. Morales-Durán, P. Surówka, and P. Witkowski, "Boundary-condition and geometry engineering in electronic hydrodynamics," *Physical Review B* **100** no. 15, (Oct, 2019). `http://dx.doi.org/10.1103/PhysRevB.100.155115`.

[66] D. Einzel, P. Panzer, and M. Liu, "Boundary condition for fluid flow: curved or rough surfaces," *Physical Review Letters* **64** (May, 1990) 2269–2272.

[67] E. Lauga, M. Brenner, and H. Stone, *Microfluidics: the no-slip boundary condition*, 1219–1240. Springer Berlin Heidelberg, Berlin, Heidelberg, 2007. `https://doi.org/10.1007/978-3-540-30299-5_19`.

[68] E. I. Kiselev and J. Schmalian, "Boundary conditions of viscous electron flow," *Physical Review B* **99** no. 3, (Jan, 2019). `https://doi.org/10.1103/physrevb.99.035430`.

[69] H. K. Moffatt, "Viscous and resistive eddies near a sharp corner," *Journal of Fluid Mechanics* **18** no. 01, (Jan, 1964) 1. `https://doi.org/10.1017/s0022112064000015`.

[70] F. Pan and A. Acrivos, "Steady flows in rectangular cavities," *Journal of Fluid Mechanics* **28** no. 04, (Jun, 1967) 643. `https://doi.org/10.1017/s002211206700237x`.

[71] A. M. J. Davis, "Periodic blocking in parallel shear or channel flow at low Reynolds number," *Physics of Fluids A: Fluid Dynamics* **5** no. 4, (Apr, 1993) 800–809. `https://doi.org/10.1063/1.858628`.

[72] M. Branicki and H. K. Moffatt, "Evolving eddy structures in oscillatory Stokes flows in domains with sharp corners," *Journal of Fluid Mechanics* **551** (Mar, 2006) 63. `https://doi.org/10.1017/s002211200500827x`.

[73] C. Y. Wang, "Stokes flow through a transversely finned channel," *Journal of Fluids Engineering* **119** no. 1, (1997) 110. `https://doi.org/10.1115/1.2819095`.

[74] M. Semenyakin and G. Falkovich, "Alternating currents and shear waves in viscous electronics," *Physical Review B* **97** no. 8, (Feb, 2018). `https://doi.org/10.1103/physrevb.97.085127`.

[75] S. Richardson, "On the no-slip boundary condition," *Journal of Fluid Mechanics* **59** no. 04, (Aug, 1973) 707. `https://doi.org/10.1017/s0022112073001801`.

[76] L. M. Hocking, "A moving fluid interface on a rough surface," *Journal of Fluid Mechanics* **76** no. 04, (Aug, 1976) 801. `https://doi.org/10.1017/s0022112076000906`.

[77] P. Panzer, M. Liu, and D. Einzel, "The effects of boundary curvature on hydrodynamic fluid flow: calculation of slip lengths," *International Journal of Modern Physics B* **06** no. 20, (Oct, 1992) 3251–3278. `https://doi.org/10.1142/s0217979292001420`.

[78] E. O. Tuck and A. Kouzoubov, "A laminar roughness boundary condition," *Journal of Fluid Mechanics* **300** (Oct, 1995) 59. `https://doi.org/10.1017/s0022112095003600`.

[79] K. Sarkar and A. Prosperetti, "Effective boundary conditions for Stokes flow over a rough surface," *Journal of Fluid Mechanics* **316** (Jun, 1996) 223. `https://doi.org/10.1017/s0022112096000511`.

[80] L. Rayleigh, "On the flow of viscous liquids, especially in two dimensions," *Philosophical Magazine* **36** no. 221, (Oct, 1893) 354–372. `https://doi.org/10.1080/14786449308620489`.

[81] D. G. Mabey, "Slow viscous flow within circular cylinders," *Journal of the Royal Aeronautical Society* **61** no. 556, (Apr, 1957) 281–283. `https://doi.org/10.1017/s0368393100129049`.

[82] S. C. R. Dennis, *Application of the series truncation method to two-dimensional internal flows.* Springer-Verlag, 1974. `https://doi.org/10.1007/bfb0019741`.

[83] R. D. Mills, "Computing internal viscous flow problems for the circle by integral methods," *Journal of Fluid Mechanics* **79** no. 03, (Mar, 1977) 609. `https://doi.org/10.1017/s0022112077000342`.

[84] S. Dennis, M. Ng, and P. Nguyen, "Numerical solution for the steady motion of a viscous fluid inside a circular boundary using integral conditions," *Journal of Computational Physics* **108** no. 1, (Sep, 1993) 142–152. `https://doi.org/10.1006/jcph.1993.1169`.

[85] A. N. Tikhonov and A. A. Samarskii, *Equations of mathematical physics.* Dover Publications, 2011.

[86] M. A. Pinsky, *Partial differential equations and boundary-value problems with applications.* American Mathematical Society, 2011.

[87] C. M. Marcus, A. J. Rimberg, R. M. Westervelt, P. F. Hopkins, and A. C. Gossard, "Conductance fluctuations and chaotic scattering in ballistic microstructures," *Physical Review Letters* **69** no. 3, (Jul, 1992) 506–509. https://doi.org/10.1103/physrevlett.69.506.

[88] H. Ishio and J. Burgdörfer, "Quantum conductance fluctuations and classical short-path dynamics," *Physical Review B* **51** no. 3, (Jan, 1995) 2013–2016. https://doi.org/10.1103/physrevb.51.2013.

[89] C. D. Schwieters, J. A. Alford, and J. B. Delos, "Semiclassical scattering in a circular semiconductor microstructure," *Physical Review B* **54** no. 15, (Oct, 1996) 10652–10668. https://doi.org/10.1103/physrevb.54.10652.

[90] D. Forcella, J. Zaanen, D. Valentinis, and D. van der Marel, "Electromagnetic properties of viscous charged fluids," *Physical Review B* **90** (Jul, 2014) 035143. https://link.aps.org/doi/10.1103/PhysRevB.90.035143.

[91] R. Toshio, K. Takasan, and N. Kawakami, "Nonlocal optical responses of ultrapure metals in the hydrodynamic regime," *arXiv e-prints* (2019) arXiv:1905.11698 [cond-mat.mes-hall].

[92] M. Chandra, G. Kataria, D. Sahdev, and R. Sundararaman, "Hydrodynamic and ballistic AC transport in two-dimensional Fermi liquids," *Physical Review B* **99** no. 16, (Apr, 2019). http://dx.doi.org/10.1103/PhysRevB.99.165409.

[93] D. T. Son, "Chiral metric hydrodynamics, Kelvin circulation theorem, and the fractional quantum Hall effect," *arXiv e-prints* (2019) arXiv:1907.07187 [cond-mat.str-el].

[94] E. V. Gorbar, V. A. Miransky, I. A. Shovkovy, and P. O. Sukhachov, "Hydrodynamic electron flow in a Weyl semimetal slab: role of Chern-Simons terms," *Physical Review B* **97** no. 20, (May, 2018). http://dx.doi.org/10.1103/PhysRevB.97.205119.

[95] M. F. Lapa and T. L. Hughes, "Swimming at low Reynolds number in fluids with odd, or Hall, viscosity," *Physical Review E* **89** no. 4, (Apr, 2014). http://dx.doi.org/10.1103/PhysRevE.89.043019.

[96] C. Hoyos, "Hall viscosity, topological states and effective theories," *International Journal of Modern Physics B* **28** no. 15, (Mar, 2014) 1430007, arXiv:1403.4739 [cond-mat.mes-hall].

[97] L. Onsager, "Reciprocal relations in irreversible processes. I." *Physical Review* **37** (Feb, 1931) 405–426. https://link.aps.org/doi/10.1103/PhysRev.37.405.

[98] J. E. Avron, "Odd viscosity," *Journal of Statistical Physics* **92** (1998) 543–557 physics/9712050, arXiv:physics/9712050 [physics.flu-dyn].

[99] J. E. Avron, R. Seiler, and P. G. Zograf, "Viscosity of quantum Hall fluids," *Physical Review Letters* **75** (Jul, 1995) 697–700. https://link.aps.org/doi/10.1103/PhysRevLett.75.697.

[100] N. Read, "Non-Abelian adiabatic statistics and Hall viscosity in quantum Hall states and $p_x + ip_y$ paired superfluids," *Physical Review B* **79** (Jan, 2009) 045308. https://link.aps.org/doi/10.1103/PhysRevB.79.045308.

[101] J. M. Maldacena, "The large N limit of superconformal field theories and supergravity," *Advances in Theoretical and Mathematical Physics* **2** (1998) 231–252, arXiv:9711200 [hep-th].

[102] S. S. Gubser, I. R. Klebanov, and A. M. Polyakov, "Gauge theory correlators from noncritical string theory," *Physics Letters* **B428** (1998) 105–114, arXiv:hep-th/9802109 [hep-th].

[103] E. Witten, "Anti-de Sitter space and holography," *Advances in Theoretical and Mathematical Physics* **2** (1998) 253–291, arXiv:hep-th/9802150 [hep-th].

[104] K. Jensen, M. Kaminski, P. Kovtun, R. Meyer, A. Ritz, and A. Yarom, "Parity-violating hydrodynamics in 2+1 dimensions," *Journal of High Energy Physics* **05** (2012) 102, arXiv:1112.4498 [hep-th].

[105] B. Bradlyn, M. Goldstein, and N. Read, "Kubo formulas for viscosity: Hall viscosity, Ward identities, and the relation with conductivity," *Physical Review* **B86** (2012) 245309, `arXiv:1207.7021 [cond-mat.stat-mech]`.

[106] S. A. Hartnoll and P. Kovtun, "Hall conductivity from dyonic black holes," *Physical Review* **D76** (2007) 066001, `arXiv:0704.1160 [hep-th]`.

[107] G. Hooft, "A planar diagram theory for strong interactions," *Nuclear Physics B* **72** no. 3, (1974) 461 – 473.
`http://www.sciencedirect.com/science/article/pii/0550321374901540`.

[108] U. Gürsoy and E. Kiritsis, "Exploring improved holographic theories for QCD: part I," *Journal of High Energy Physics* **2008** no. 02, (Feb, 2008) 032.
`http://dx.doi.org/10.1088/1126-6708/2008/02/032`.

[109] U. Gürsoy, E. Kiritsis, and F. Nitti, "Exploring improved holographic theories for QCD: part II," *Journal of High Energy Physics* **2008** no. 02, (Feb, 2008) 019.
`http://dx.doi.org/10.1088/1126-6708/2008/02/019`.

[110] B. Goutéraux and E. Kiritsis, "Generalized holographic quantum criticality at finite density," *Journal of High Energy Physics* **2011** no. 12, (Dec, 2011).
`http://dx.doi.org/10.1007/JHEP12(2011)036`.

[111] L. Huijse, S. Sachdev, and B. Swingle, "Hidden Fermi surfaces in compressible states of gauge-gravity duality," *Physical Review B* **85** no. 3, (Jan, 2012).
`http://dx.doi.org/10.1103/PhysRevB.85.035121`.

[112] X. Dong, S. Harrison, S. Kachru, G. Torroba, and H. Wang, "Aspects of holography for theories with hyperscaling violation," *Journal of High Energy Physics* **2012** no. 6, (Jun, 2012). `http://dx.doi.org/10.1007/JHEP06(2012)041`.

[113] G. T. Horowitz, *Introduction to holographic superconductors*, vol. 828, 313–347. Springer-Verlag Berlin Heidelberg, 2011.

[114] C. P. Herzog, "TOPICAL REVIEW: Lectures on holographic superfluidity and superconductivity," *Journal of Physics A Mathematical General* **42** no. 34, (Aug, 2009) 343001, `arXiv:0904.1975 [hep-th]`.

[115] J. Zaanen, "Planckian dissipation, minimal viscosity and the transport in cuprate strange metals," *SciPost Physics* **6** no. 5, (May, 2019) 061, `arXiv:1807.10951 [cond-mat.str-el]`.

[116] J. McGreevy, "Holographic duality with a view toward many-body physics," *Advances in High Energy Physics* (2010) 723105, `arXiv:0909.0518 [hep-th]`.

[117] E. Keski-Vakkuri and P. Kraus, "Quantum Hall effect in AdS/CFT," *Journal of High Energy Physics* **09** (2008) 130, `arXiv:0805.4643 [hep-th]`.

[118] J. L. Davis, P. Kraus, and A. Shah, "Gravity dual of a quantum Hall plateau transition," *Journal of High Energy Physics* **11** (2008) 020, `arXiv:0809.1876 [hep-th]`.

[119] M. Fujita, W. Li, S. Ryu, and T. Takayanagi, "Fractional quantum Hall effect via holography: Chern-Simons, edge states and hierarchy," *Journal of High Energy Physics* **06** (2009) 066, `arXiv:0901.0924 [hep-th]`.

[120] Y. Hikida, W. Li, and T. Takayanagi, "ABJM with flavors and FQHE," *Journal of High Energy Physics* **07** (2009) 065, `arXiv:0903.2194 [hep-th]`.

[121] S. Kawamoto and F.-L. Lin, "Holographic anyons in the ABJM theory," *Journal of High Energy Physics* **02** (2010) 059, `arXiv:0910.5536 [hep-th]`.

[122] A. Belhaj and A. Segui, "Engineering of quantum Hall effect from type IIA string theory on the K3 surface," *Physics Letters* **B691** (2010) 261–267, `arXiv:1002.2067 [hep-th]`.

[123] O. Bergman, N. Jokela, G. Lifschytz, and M. Lippert, "Quantum Hall effect in a holographic model," *Journal of High Energy Physics* **10** (2010) 063, `arXiv:1003.4965 [hep-th]`.

[124] K. Goldstein, N. Iizuka, S. Kachru, S. Prakash, S. P. Trivedi, and A. Westphal, "Holography of dyonic dilaton black branes," *Journal of High Energy Physics* **10** (2010)

027, `arXiv:1007.2490 [hep-th]`.

[125] A. Bayntun, C. P. Burgess, B. P. Dolan, and S.-S. Lee, "AdS/QHE: towards a holographic description of quantum Hall experiments," *New Journal of Physics* **13** (2011) 035012, `arXiv:1008.1917 [hep-th]`.

[126] M. Fujita, "M5-brane defect and QHE in AdS4 x N(1,1)/N=3 SCFT," *Physical Review* **D83** (2011) 105016, `arXiv:1011.0154 [hep-th]`.

[127] N. Jokela, M. Jarvinen, and M. Lippert, "A holographic quantum Hall model at integer filling," *Journal of High Energy Physics* **05** (2011) 101, `arXiv:1101.3329 [hep-th]`.

[128] M. Fujita, M. Kaminski, and A. Karch, "SL(2,Z) action on AdS/BCFT and Hall conductivities," *Journal of High Energy Physics* **07** (2012) 150, `arXiv:1204.0012 [hep-th]`.

[129] M. Blake, S. Bolognesi, D. Tong, and K. Wong, "Holographic dual of the lowest Landau level," *Journal of High Energy Physics* **12** (2012) 039, `arXiv:1208.5771 [hep-th]`.

[130] D. Melnikov, E. Orazi, and P. Sodano, "On the AdS/BCFT approach to quantum Hall systems," *Journal of High Energy Physics* **05** (2013) 116, `arXiv:1211.1416 [hep-th]`.

[131] C. Kristjansen and G. W. Semenoff, "Giant D5 brane holographic Hall state," *Journal of High Energy Physics* **06** (2013) 048, `arXiv:1212.5609 [hep-th]`.

[132] N. Jokela, G. Lifschytz, and M. Lippert, "Holographic anyonic superfluidity," *Journal of High Energy Physics* **10** (2013) 014, `arXiv:1307.6336 [hep-th]`.

[133] M. Lippert, R. Meyer, and A. Taliotis, "A holographic model for the fractional quantum Hall effect," *Journal of High Energy Physics* **01** (2015) 023, `arXiv:1409.1369 [hep-th]`.

[134] Y. Bea, N. Jokela, M. Lippert, A. V. Ramallo, and D. Zoakos, "Flux and Hall states in ABJM with dynamical flavors," *Journal of High Energy Physics* **03** (2015) 009, `arXiv:1411.3335 [hep-th]`.

[135] J. Lindgren, I. Papadimitriou, A. Taliotis, and J. Vanhoof, "Holographic Hall conductivities from dyonic backgrounds," *Journal of High Energy Physics* **07** (2015) 094, `arXiv:1505.04131 [hep-th]`.

[136] A. Mezzalira and A. Parnachev, "A holographic model of quantum Hall transition," *Nuclear Physics* **B904** (2016) 448–469, `arXiv:1512.06052 [hep-th]`.

[137] D. T. Son and P. Surówka, "Hydrodynamics with triangle anomalies," *Physical Review Letters* **103** (Nov, 2009) 191601.
`https://link.aps.org/doi/10.1103/PhysRevLett.103.191601`.

[138] D. Tong, "Holographic conductivity." *Acta Physica Polonica B* **44** no. 12, (2013) .

[139] M. Ammon and J. Erdmenger, *Gauge/gravity duality: foundations and applications.* Cambridge University Press, 2015.

[140] S. Bhattacharyya, S. Minwalla, V. E. Hubeny, and M. Rangamani, "Nonlinear fluid dynamics from gravity," *Journal of High Energy Physics* **2008** no. 2, (Feb, 2008) 045, `arXiv:0712.2456 [hep-th]`.

[141] M. Rangamani, "Gravity and hydrodynamics: lectures on the fluid-gravity correspondence," *Classical and Quantum Gravity* **26** no. 22, (Nov, 2009) 224003, `arXiv:0905.4352 [hep-th]`.

[142] V. E. Hubeny, S. Minwalla, and M. Rangamani, "The fluid/gravity correspondence," *arXiv e-prints* (Jul, 2011) arXiv:1107.5780, `arXiv:1107.5780 [hep-th]`.

[143] V. Balasubramanian and P. Kraus, "A stress tensor for anti-de Sitter gravity," *Commun. Math. Phys.* **208** (1999) 413–428, `arXiv:hep-th/9902121 [hep-th]`.

[144] P. K. Kovtun and A. O. Starinets, "Quasinormal modes and holography," *Physical Review D* **72** no. 8, (Oct, 2005) 086009, `arXiv:hep-th/0506184 [hep-th]`.

[145] O. Saremi and D. T. Son, "Hall viscosity from gauge/gravity duality," *Journal of High Energy Physics* **04** (2012) 091, `arXiv:1103.4851 [hep-th]`.

[146] C. P. Herzog, P. Kovtun, S. Sachdev, and D. T. Son, "Quantum critical transport, duality, and M-theory," *Physical Review* **D75** (2007) 085020, `arXiv:hep-th/0701036`

[hep-th].

[147] V. Iyer and R. M. Wald, "Some properties of the Noether charge and a proposal for dynamical black hole entropy," *Physical Review D* **50** no. 2, (Jul, 1994) 846–864, `arXiv:gr-qc/9403028 [gr-qc]`.

[148] S. Sachdev, "Holographic metals and the fractionalized Fermi liquid," *Physical Review Letters* **105** (2010) 151602, `arXiv:1006.3794 [hep-th]`.

[149] S. A. Hartnoll, "Horizons, holography and condensed matter," in *Black holes in higher dimensions*, G. T. Horowitz, ed., 387–419. 2012. `arXiv:1106.4324 [hep-th]`.

[150] S. A. Hartnoll and D. Radicevic, "Holographic order parameter for charge fractionalization," *Physical Review* **D86** (2012) 066001, `arXiv:1205.5291 [hep-th]`.

[151] S. A. Hartnoll, C. P. Herzog, and G. T. Horowitz, "Building a holographic superconductor," *Physical Review Letters* **101** (2008) 031601, `arXiv:0803.3295 [hep-th]`.

[152] S. A. Hartnoll, C. P. Herzog, and G. T. Horowitz, "Holographic superconductors," *Journal of High Energy Physics* **12** (2008) 015, `arXiv:0810.1563 [hep-th]`.

[153] N. Iqbal and H. Liu, "Luttinger's theorem, superfluid vortices and holography," *Classical and Quantum Gravity* **29** (2012) 194004, `arXiv:1112.3671 [hep-th]`.

[154] K. Landsteiner, E. Megias, L. Melgar, and F. Pena-Benitez, "Holographic gravitational anomaly and chiral vortical effect," *Journal of High Energy Physics* **09** (2011) 121, `arXiv:1107.0368 [hep-th]`.

[155] C. Copetti, J. Fernández-Pendás, K. Landsteiner, and E. Megías, "Anomalous transport and holographic momentum relaxation," *Journal of High Energy Physics* **09** (2017) 004, `arXiv:1706.05294 [hep-th]`.

[156] C. Copetti and J. Fernández-Pendás, "Membrane paradigm and RG flows for anomalous holographic theories," *Journal of High Energy Physics* **04** (2018) 134, `arXiv:1712.06628 [hep-th]`.

Versicherung

Hiermit versichere ich, Piotr Witkowski, dass ich die vorliegende Arbeit ohne unzulässige Hilfe Dritter und ohne Benutzung anderer als der angegebenen Hilfsmittelangefertigt habe; die aus fremden Quellen direkt oder indirekt übernommenen Gedanken sind als solche kenntlich gemacht. Die Arbeit wurde bisher weder im Inland noch im Ausland in gleicher oder ähnlicher Form einer anderen Prüfungsbehörde vorgelegt. Diese Arbeit wurde unter der wissenschaftlichen Betreuung von Prof. Dr. Roderich Mössner und Dr. Piotr Surówka am Max-Planck Institut für Physik komplexer Systeme in Dresden angefertigt. Ich erkläre hiermit, dass keine früheren erfolglosen Promotionsverfahren stattgefundenhaben. Ich erkenne die Promotionsordnung der Bereich Mathematik und Naturwissenschaften der Technische Universität Dresden an.

_____

Unterschrift
Dresden, Februar 2020